DOCTOR OF PHILOSOPHY

The structural analysis of histone H3 lysine 56 acetylation and related histone chaperone complexes

Hammond, Colin

Award date:
2013

DOCTOR OF PHILOSOPHY

The structural analysis of histone H3 lysine 56 acetylation and related histone chaperone complexes

Colin Hammond

2013

University of Dundee

The structural analysis of histone H3 lysine 56 acetylation and related histone chaperone complexes

Colin Mark Hammond

A thesis submitted for the degree of Doctor of Philosophy

University of Dundee

September 2013

Declarations

I hereby declare that the following thesis is based on the results of work conducted by myself and that the thesis is of my own composition. Work other than my own is clearly indicated in the text by reference to the relevant researchers or their publications. This thesis has not in whole, or in part, been presented for a higher degree.

…….

Colin M. Hammond

I certify that Colin Hammond has spent at least nine terms in research in the Wellcome Trust Centre for Gene Regulation and Expression, University of Dundee and that he has fulfilled the conditions of Ordinance General No. 39 of the University of Dundee and is qualified to submit the accompanying thesis in application for the degree of Doctor of Philosophy.

…….

Prof. Tom Owen-Hughes

Professor of Chromatin Structure and Function

University of Dundee

Abstract

Access to the genetic information of eukaryotic organisms is regulated in part by the assembly and disassembly of chromatin. Key regulators of these processes are histone binding proteins known as histone chaperones. The histone chaperone complex Chromatin Assembly Factor 1 (CAF-1) is responsible for depositing H3.1/H4 tetramers in a DNA synthesis dependent manner. During replication independent assembly H3.3/H4 is deposited by Histone Regulator (Hir) complex. In both instances nascent histone H3/H4 dimers are supplied by Anti-Silencing Factor 1 (Asf1).

In yeast, newly synthesised H3 is acetylated at multiple sites in complex with H4 by the histone acetyl transferase (HAT) Regulator of Ty1 Transposition (Rtt109). The activity of Rtt109 towards H3 tail residues and H3 lysine 56 (K56) is stimulated by the histone chaperones Vacuolar Protein Sorting 75 (Vps75) and Asf1 respectively. In this study, acetylation of K56, located at the C-terminus of the H3 αN helix, was found to promote secondary structure formation in this region by Circular Dichroism. Furthermore, Pulsed Electron Double Resonance experiments demonstrate that the acetylation mimic K56Q stabilises the αN helix in an alternate conformation than observed in the histone octamer. This may have implications in the handover of histones between chaperones or at other stages of *de novo* nucleosome assembly.

Vps75 is a member of the Nucleosome Assembly Protein 1 (Nap1) chaperone family. Nap1 family chaperones adopt a characteristic homo-dimeric 'headphone' fold and are capable of binding H2A/H2B and H3/H4, the latter in its tetrameric conformation. Experiments described here reveal Vps75 and Nap1 form ring-like tetramers which sequester the highly acidic, putative histone binding, surfaces of the chaperones. Cross-linking analysis shows a H3/H4 tetramer can accommodate two Vps75 dimers. The tetramerisation of Nap1 family chaperones may have an important role in the cooperative assembly or recognition of H3/H4 tetramers allowing the conservation of H3/H4 tetramers evicted from chromatin during nucleosome reassembly. Vps75 and Nap1 were also shown to bind H3/H4 in the presence of Asf1 demonstrating that a Nap1 fold dimer indeed binds a histone fold dimer. These homogeneous complexes are good candidates for future structural analysis of the mode of interaction of Vps75 and Nap1 with H3/H4.

Acknowledgements

Prior to starting my PhD I had limited experience of molecular biology and biochemistry based lab work as I had graduated with a degree in chemistry. As such I would like to thank my rotation projects supervisors Professor Kees Weijer, Dr Ruth Brenk and Professor Tom Owen-Hughes (TOH) who enabled me to quickly adapt to new subject areas whilst being enthusiastic mentors. During these rotation projects my lab work was in part supervised by three fellow Wellcome Trust PhD programme students, Grzegorz Sobczyk, Peter Daldrop and Andrew Bowman whom I would like to thank for their integral role in this training and development. I would also like to thank the members of the Wellcome Trust PhD programme committee, namely Dr Arno Muller, Professor Paul Crocker and TOH, who shaped the first year of my PhD programme.

I would like to thank a few key people that have provided technical expertise in some of the biophysical techniques I have learned whilst in Dundee they include: Dr Jane Potter from St Andrews for getting me up and running with Circular Dichroism and helping me troubleshoot problems with the Spectropolarimeter; Dr Hassane El Mkami for running lots and lots of PELDOR experiments in St Andrews; Michael Stevens of Dr David Norman's laboratory for shuttling many of these samples over to St Andrews; and David who has been hugely supportive during my time as a PhD student in the TOH lab, being generally positive about my research whilst offering constructive advice.

Of course I have to thank my supervisor TOH for providing a supportive and fun environment to work in. The TOH lab has been a great place to do a PhD. I would like to thank Subbu (Ramasubramanian Sundaramoorthy) for helping me out with crystallography experiments and generally teaching me a lot about crystallography. I am confident that this will reap its rewards in future postdoc positions. I would also like to thank Andrew Bowman from whom I inherited my PhD project; it's been great following on from Andy who has contributed a lot of resources to the area of study. Asides from that the rest of the TOH lab members have been great to be around and have provided lots of support in their own ways. I would like to extend thanks to all the friends I have met along the way for their support and the laughs. Last but not least, I would like to thank my wife Julie, family and friends for their continued support throughout my education.

Abbreviations

^{14}C	Carbon-14
3,4-Bis-MTSL	3,4-Bis-(methanethiosulfonylmethyl)-2,2,5,5-tetramethyl-2,5-dihydro-1H-pyrrol-1-yloxy Radical
acetyl-CoA	Acetyl-coenzyme A
Ada2	Transcriptional ADAptor 2
Ada3	Transcriptional ADAptor 3
Asf1	Anti-silencing factor 1
ATAC	Ada2/Gcn5/Ada3 transcription activator complex
ATM	Ataxia Teleangiectasia Mutated
ATP	Adenosine triphosphate
B_0	External magnetic field
bp	Base pairs
Bre1	BREfeldin A sensitivity 1
BS_2G	Bis(sulfosuccinimidyl) glutarate
BS3	Bis(sulfosuccinimidyl) suberate
Cac1	p150 subunit of CAF-1
Cac2	p60 subunit of CAF-1
Cac3	p48 subunit of CAF-1
CAF-1	Chromtin assembly factor 1
CBP	CREB-binding protein
CD	Circular Dichroism
CENP-A	Centromere Protein A
cf.	Latin for compare
Chz1	Chaperone for Htz1/H2A-H2B dimer 1
Cse4	Chromosome SEgregation 4
D	Deuterium
D_2O	Deuterium oxide
Daxx	Death domain-associated protein 6
DIM-5	H3 lysine-9 specific dim-5
DNA	Deoxyribonucleic acid
Dot1	Disrupter of telomere silencing protein 1
dRI	Differential Refractive Index
DSB	Double strand break
DTSSP	3,3'-Dithiobis(sulfosuccinimidyl propionate)
E. coli	*Escherichia coli*
Eaf3	Esa1p-Associated Factor 3
EDTA	Ethylenediaminetetraacetic acid
EPR	Electron paramagnetic resonance
Esa1	Catalytic subunit of NuA4

FACT	Facilitates chromatin transcription complex
FRET	Förster resonance energy transfer
Fun30	Function Unknown Now 30
Gcn5	General Control Nonderepressible 5
GNAT	Gcn5 related N-acetyltransferase family
H2A	Histone H2A
H2AX	Histone H2AX
H2AZ	Histone H2AZ
H2B	Histone H2B
H3	Histone H3
H3.1	Histone H3.1
H3.3	Histone H3.3
H4	Histone H4
HAT	Histone acetyl transferases
HEPES	4-(2-hydroxyethyl)-1-piperazineethanesulfonic acid
Hir	Histone Regulator
Hir1	Component of the HIRA complex
Hir2	Component of the HIRA complex
Hir3	Component of the HIRA complex
HIRA	Histone Regulator A complex
HJURP	Holliday Junction Recognition Protein
HKMT	Histone Lysine Methyl Transferase
HP1α	Hetrochromatin Protein 1α
Hpc2	Component of the HIRA complex
Hst3	Homolog of SIR Two 3
Hst4	Homolog of SIR Two 4
K56	Histone H3 lysine 56
K56Ac	Histone H3 acetylated at lysine 56
K56Q	Histone H3 lysine 56 to glutamine mutation
kDa	Kilodalton
KOH	Potassium Hydroxide
LS	Light Scattering
macroH2A	Histone macroH2A
MALDI	Matrix-assisted laser desorption/ionization
MDa	Megadalton
MTSL	S-(2,2,5,5-tetramethyl-2,5-dihydro-1H-pyrrol-3-yl)methyl methanesulfonothioate
MWCO	Molecular weight cut off
MYST	HAT family named after founding members: MOZ, Ybf2 (Sas3), Sas2, and Tip60
NaCl	Sodium chloride
NAD	Nicotinamide adenine dinucleotide
Nap1	Nucleosome assembly protein 1
NRMSD	Normalised root mean squared deviation
NuA4	Nucleosomal acetyltransferases of H3 and H4

NURD	Nucleosome remodelling and histone deacetylase complex
NURF	Nucleosome-remodelling factor complex
Nurf55	Nucleosome-remodelling factor subunit 55
p300	E1A binding protein p300
PAGE	Polyacrylamide gel electrophoresis
PCNA	Proliferating Cell Nuclear Antigen
PCR	Polymerase Chain Reaction
pdb	Protein Data Bank
PELDOR	Pulsed Electron Double Resonance
PHPH	Double pleckstrin homology domain
Pob3	Subunit of the FACT complex
Pol δ	DNA polymerase delta
PRC-2	Polycomb repressor complex 2
PTM	post translational modification
Py	Cysteine side chain labelled with N1-(pyrene)maleimide
R1	Cysteine side chain labelled with MTSL
Rad6	RADiation sensitive 6
RbAp46/48	Cac3 subunit of CAF-1
RMSD	Root mean squared deviation
RNA	Ribonucleic acid
Rpd3	Reduced Potassium Dependency 3
Rtt106	Repressor of Ty1 transposition 106
Rtt109	Repressor of Ty1 transposition 109
RX2	Two cysteine side chains cross-linked with 3,4-Bis-MTSL
S. cerevisiae	Saccharomyces cerevisiae
SAGA	Spt/Ada/Gcn5 acetyltransferase
Scm3	Suppressor of Chromosome Missegregation 3
SDS	Sodium dodecyl sulphate
SEC-MALS	Size Exclusion Chromatography coupled to Multi Angle Light Scattering
SET	Su(var)3-9, Enhancer-of-zeste and Trithorax
Set2	SET domain-containing 2
Spt16	Subunit of the FACT complex
T_2 *or* T_m	Traverse relaxation
TBE	Tris/Borate/EDTA
TFE	2,2,2-trifluoroethanol
TFTC	TBP-free TAF-containing complex
Tip60	TAT-interactive protein 60
Trap1	TNF Receptor-Associated Protein 1
Vps75	Vacuolar Protein Sorting 75
WD40	40 amino acids repeat terminating in a tryptophan-aspartic acid dipeptide
WT	Wild type
X. leavis	*Xenopus laevis*
Xist	X-inactive specific transcript

Yaf9	Yeast homolog of the human leukemogenic protein AF9
α	alpha helix
αC	C-terminal alpha helix
αN	Histone H3 N-terminal alpha helix
γH2AX	Histone H2AX phosphorylated at serine 139

Figures

Contents

Introduction

1.1 The Nucleosome

The term chromatin was first penned in 1880 by Walter Flemming to describe material within nuclei that readily absorbed basophilic dyes. We now know this material to be made up of individual chromosomes which are a complex of DNA packaged with basic proteins called histones and other associated factors. The fundamental subunit of chromatin is the nucleosome; the canonical nucleosome consists of ~146 base pairs of DNA wrapped around an octamer of histones. A beads-on-a-string array of nucleosomes forms the first level of packaging of DNA in the nucleus and is termed euchromatin, further packaging leads to heterochromatin and higher order chromatin structures which are finally compressed following DNA replication to form the metaphase chromosome for meiosis and mitosis. Chromatin forms a barrier to processes which necessitate access to the underlying DNA sequence such as DNA replication, repair and transcription. As such, in addition to the compaction of the eukaryotic genome, access to the genetic information encoded in DNA is regulated in part by the assembly and disassembly of chromatin.

The crystal structure of the histone octamer was first solved at atomic resolution (Arents, Burlingame et al. 1991) and was subsequently followed by the atomic resolution crystal structure of the nucleosome (Luger, Mäder et al. 1997). Remarkably, many years prior to these molecular insights, the composition of the nucleosome had been correctly identified as a histone octamer with equimolar amounts of histone H2A, H2B, H3 and H4 (Albright, Nelson et al. 1979) that wraps ~146 bp of DNA (Bryan, Wright et al. 1979; Lutter 1979). Sub-octameric particles of histones H2A/H2B and H3/H4 dimers were also identified with inter-particle contacts made between H2A/H2B-H4, H2A-H3 and H3-H3 in the histone octamer, the latter governing H3/H4 tetramerisation (D'Anna and Isenberg 1974).

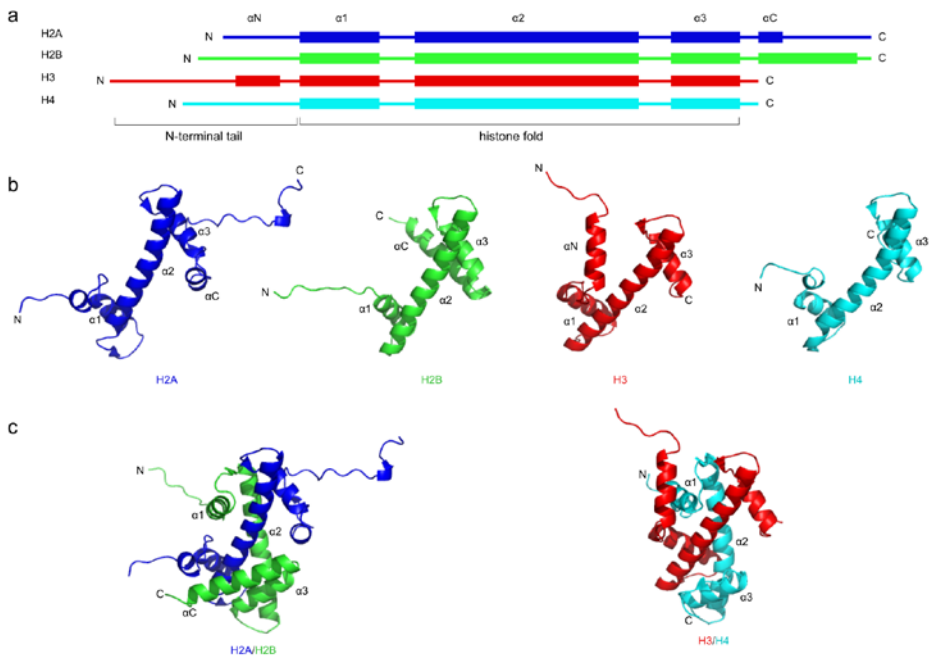

Figure 1 - The histone fold. (a) The location of alpha helical segments of the core histones. (b) Depiction of the histone fold of the core histones. (c) The structure of histone fold dimers orientated with respect to H2A and H3 from panel b with helices of H2B and H4 labelled for clarity. Figure was adapted (Alberts, Johnson et al. 2002) using the structures of histones from the crystal structure of the nucleosome (Luger, Mäder et al. 1997).

As can be seen from the structure of the octamer and nucleosome (Arents, Burlingame et al. 1991; Luger, Mäder et al. 1997) these initial observations hold true. The histone fold is a common feature of all of the core histones and their variants. It has also been observed in a number of non-histone proteins (Baxevanis, Arents et al. 1995; Xie, Kokubo et al. 1996). The fold consists of three helices, α1, α2 and α3, connected by loops (Figure 1A and B) and functions as a dimerisation interface allowing histones to combine pairwise, H2A with H2B and H3 with H4, in a handshake type interaction with extensive hydrophobic interactions between the long α2 helices (Figure 1C). Histones H3 and H2B have an additional α-helix at the N-terminus (αN) and C-terminus (αC) respectively and histone H2A has a long C-terminal tail. In addition to the histone fold the core histones have long unstructured N-terminal tails which protrude from the core of the nucleosome. Dimers of histones H3/H4 further combine to form a tetramer, the interface of which consists of a four helix bundle between the α2 and α3 helices of the two copies of histone H3 of the opposing dimers (Figure 2A). The tetramer of H3/H4 forms the core of the nucleosome interacting with ~70 bp of DNA, the centre of which is termed the dyad (Figure 2B). This sub-nucleosomal particle is termed the tetrasome and is capped on one

lateral surface by a H2A/H2B dimer which chelates a further ~40 bp of DNA forming a hexasome (Figure 2C). The addition of another H2A/H2B dimer on the opposite side of H3/H4 completes the nucleosome (Figure 2D).

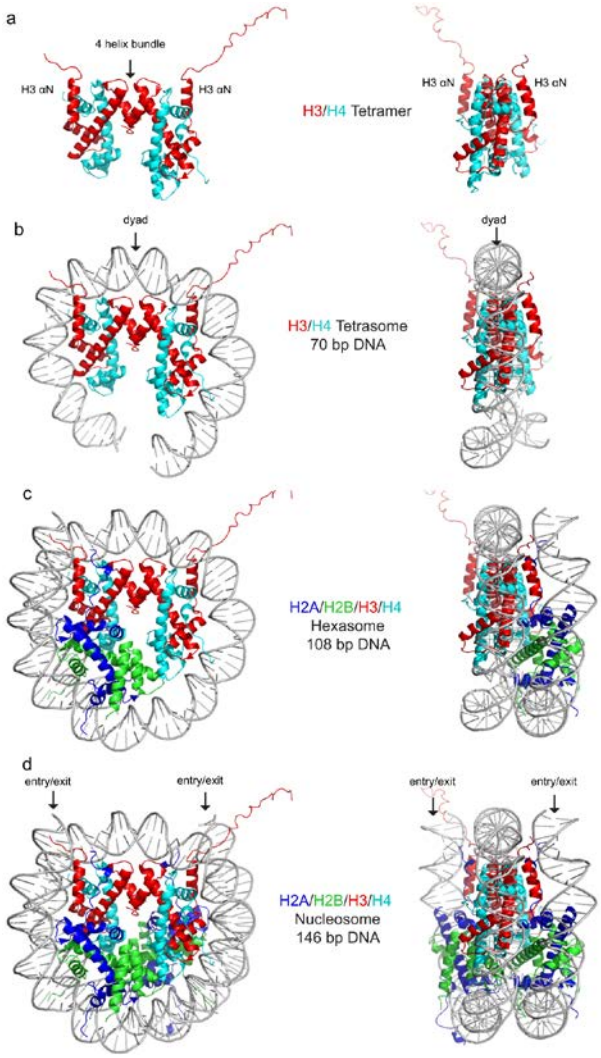

Figure 2 – Intermediates in nucleosome formation. (a) The H3/H4 tetramer is assembly by the formation of a four helix bundle between α2 and α3 helices of histone H3. (b) The H3/H4 tetramer is loaded onto ~ 70 base pairs of DNA to form the tetrasome. The centre of the DNA sequence is termed the dyad. (c) A H2A/H2B dimer associates with the tetrasome chelating another ~ 40 base pairs of DNA to form the hexasome. (d) The nucleosome is complete by the association of another H2A/H2B dimer with the hexasome wrapping the full ~146 base pairs of the canonical nucleosomal DNA with the entry/exit points of DNA highlighted. Figure was created from the crystal structure of the nucleosome (Luger, Mäder et al. 1997).

The nucleosome is a highly diverse species within the cell, not only are nucleosomes associated with an almost infinite array of DNA sequences they are also subject to modification by: DNA methylation; association of nucleosome binding proteins (including linker histones, high mobility group proteins and heterochromatin associated factors); ATP-dependent remodelling enzymes; the incorporation of histone variants (see Section 1.2); and a plethora of histone post translational modifications (see Section 1.3).

1.2 Histone Variants

In humans there are two main histone H3 variants histone H3.1 and H3.3. The major isoform is H3.1 and only differs from H3.3 by four to five residues. Histone H3.1 is expressed during S-phase of the cell cycle, whereas histone H3.3 is expressed throughout the cell cycle and has a role in transcriptional activation. These histone H3 variants are deposited into chromatin along with histone H4 by distinct pathways, with H3.1 deposition being coupled to DNA synthesis by the histone chaperone complex Chromatin Assembly Factor 1 (CAF-1) whilst H3.3 is deposited in a replication independent manner by the Histone Regulator A complex (HIRA) – to be discussed in Section 1.4. In *Saccharomyces cerevisiae* there are two identical copies of histone H3 encoded by the genes HHT1 and HHT2, transcripts of both peak during S-phase analogous to human histone H3.1 (Hereford, Osley et al. 1981; Spellman, Sherlock et al. 1998). Nethertheless, the presence of CAF-1 and HIRA in the budding yeast genome suggests that multiple pathways for H3/H4 deposition are present despite the lack of a histone H3.3 variant. Therefore it is possible that in yeast the pathway for deposition of H3/H4 may be specified by particular post-translational modifications on histones. For example, K56 acetylation on histone H3 (Section 3.1) has been shown enhance association of CAF-1 with histones H3/H4 (Li, Zhou et al. 2008). Alternatively the controlled expression of different chaperone complexes at different times during the cell cycle could direct nucleosome assembly via specific pathways.

Another histone variant related to histone H3 is the centromeric histone CENP-A (Centromere Protein A), known as Cse4 in budding yeast. CENP-A contains ~60 % sequence homology with H3 but not the more divergent N-terminus (Sullivan, Hechenberger et al. 1994). CENP-A is an essential component of the kinetochore and like H3, CENP-A forms a heterotetramer with histone H4 (Sekulic, Bassett et al. 2010) and can be incorporated into nucleosomes at the centromere (Tachiwana, Kagawa et al. 2011). The crystal structure of a CENP-A containing nucleosome indicates that the αN helix of CENP-A is shorter than the canonical nucleosome, only extending 7-8 residues compared to ~15 residues in the canonical nucleosome αN helix L48-Q55, and as a consequence the CENP-A nucleosome only wraps ~120 bp of DNA (Tachiwana, Kagawa et al. 2011). As well as highlighting differences in the structures of the canonical and centromeric

nucleosomes, which may facilitate the recognition of the centromere by kinetochore associated proteins, this also highlights pivotal role of the αN helix in nucleosome dynamics.

Variability in nucleosome composition can also be directed by the incorporation of histone H2A variants. The three main variants of H2A are H2AX, H2AZ and macroH2A, the latter only present in higher eukaryotes. These H2A variants have specific functions *in vivo*. Histone H2AZ has a role in transcriptional activation being associated with active genes and can prevent the spreading of heterochromatic silencing by the Sir silencing complex (Meneghini, Wu et al. 2003). The mechanism of silencing by the Sir complex is thought to be a two-step process in which initially histone H4 K16 is deacetylated by the Sir2 component of the complex which allows the Sir3 and Sir4 components to bind the tails of histones H3 and H4 nucleating the spread of heterochromatic silencing (Hoppe, Tanny et al. 2002). H2AZ can also prevent the spread of HP1α mediated silencing in mammals (Rangasamy, Greaves et al. 2004) and as such may act as a general boundary element to the spread of heterochromatic loci. The incorporation of H2AZ into nucleosomes is mediated by the ATP-dependent chromatin remodelling complex Swr1 which exchanges H2A/H2B dimers for H2AZ/H2B dimers (Mizuguchi, Shen et al. 2004) and the reverse reaction is catalysed by the INO80 remodelling complex (Papamichos-Chronakis, Watanabe et al. 2011). Interestingly the specificity of the exchange reaction with Swr1 is lost in nucleosomes that contain H3 acetylated at K56 which allow the exchange reaction to occur in either direction (Watanabe, Radman-Livaja et al. 2013).

The histone variant H2AX is best known for its role in the DNA damage response. In higher eukaryotes the phosphorylation of H2AX at Ser139 (known as γH2AX) is an early response signal to a DNA double strand break (DSB). In yeast the core histone H2A is phosphorylated in a similar manner in response to a DSB event. Upon formation of a double strand break the Ataxia Teleangiectasia Mutated (ATM) kinase is recruited to the DNA damage site causing γH2AX to spread from the damaged site which likely leads to the recruitment of DNA damage repair factors (Burma, Chen et al. 2001). In the event where a DSB is not repaired by non-homologous end joining, the DNA ends are converted into single stranded DNA by resection in a 5'-3' direction for repair via homologous recombination (Dudas and Chovanec 2004). During this resection process the exonuclease has to contend with chromatin and as such it comes as no surprise that chromatin remodelling enzymes are thought to play a role in this process (Chen and Symington 2013). Of specific interest is the

ATP-dependent remodelling enzyme Fun30 which is known to function in H2A/H2B dimer exchange (Awad, Ryan et al. 2010) and has recently been shown to facilitate the rate of double strand resection (Chen, Cui et al. 2012; Costelloe, Louge et al. 2012). Whether Fun30 is capable of utilising γH2AX/H2B dimers in an exchange reaction is a topic that is likely to be addressed in the future.

In mammals macroH2A is a H2A variant that is involved in X chromosome inactivation in female somatic cells (Costanzi and Pehrson 1998). The pathway for incorporation of macroH2A into chromatin is currently unknown but is dependent on the long non-coding RNA Xist (X-inactive specific transcript) which is required for X-chromosome inactivation. How macroH2A contributes to the silencing process of X-chromosome inactivation is also unknown. One possibility is that the extended C-terminal tail of macroH2A which contains a leucine zipper motif which have been shown to form dimers could be involved in the silencing process (Pehrson and Fried 1992).

1.3 Histone Modifications

The modification of lysine residues in histones was first described in 1964. Initially lysine methylation was discovered by amino acid analysis of histones isolated from the tissue of rabbits injected with ^{14}C-(methyl) labelled methionine[1] (Murray 1964). In the same year acetylation of the ε-amine group of lysine side chains in histones was described (Allfrey, Faulkner et al. 1964). This study demonstrated that ^{14}C labelled acetate, as well as the ^{14}C labelled methyl groups of methionine, was incorporated into histones quicker than ^{14}C labelled amino acids. Additionally the inhibition of protein synthesis by Puromycin did not affect the incorporation of the ^{14}C labelled methyl and acetyl groups into histones. Thus Murray and Allfrey et al. made the first discoveries of histone post translational modifications (PTMs) which have led to intense study in the field of chromatin. Many histone modifications are now known to exist including phosphorylation, ubiquitination,

[1] Methionine is converted to S-adenosyl methionine by methionine adenosyltransferase which acts as the methyl group donor for lysine methylation

sumolation, ribosylation, citrullination and crotonylation (Tan, Luo et al. 2011) but lysine methylation and acetylation remain the most widely studied.

Acetylation of lysine residues can directly affect histone DNA contacts through the neutralisation of the positive charge on the lysine side chain. In general, acetylation of lysine residues in histones is associated with transcriptionally active genes (Hebbes, Thorne et al. 1988), acetylation can lead to the decondensation of nucleosome arrays *in vitro* (Garcia-Ramirez, Rocchini et al. 1995) and increase sensitivity to DNase1 *in vivo* (Hebbes, Clayton et al. 1994). Most acetylation marks have been found in the N-terminal tails of histones. For example: H3 is acetylated in the tail at K4, K9, K14, K18, K23 and K27; H4 at K5, K8, K12 and K16; H2B at K12 and K15; and H2A at K5. The periodic spacing of acetylation sites in histone tails has drawn comparisons to the spacing of residues within an alpha helix and may be important in the combinatorial readout of such modifications as proposed by the histone code hypothesis (Strahl and Allis 2000). In addition to modifications within the histone tails, acetylation sites have been identified in the core of the histone octamer of which H3 K56 acetylation is perhaps the most widely studied (see section 3.1).

Histone acetylation marks are dynamic modifications which can be introduced by histone acetyl transferases (HATs) and removed by histone deacetylases (HDACs). Histone acetyl transferases have been classified as belonging to one of three main HAT families (Berndsen and Denu 2008): the Gcn5 related N-acetyltransferase (GNAT) family; the MYST family; and p300/CBP family (in which Rtt109 resides). All of which utilise the cofactor acetyl-coenzyme A (acetyl-CoA) as the acetyl group donor during a catalytic cycle which involves the nucleophilic attack of the acetyl group of acetyl-CoA or an autoacetylated active site residue by the primary amine of a lysine side which is deprotonated by an active site aspartate or glutamate residue (Berndsen and Denu 2008).

Gcn5 is the catalytic core of several HAT complexes including the SAGA, Gcn5/Ada2/Ada3, ATAC and TFTC. Although Gcn5 is catalytically active towards free histones (Brownell, Zhou et al. 1996) the additional Ada2 and Ada3 subunits of the 1.8 MDa SAGA complex are required for the acetylation of nucleosomal H3 at K9 and K14 (Balasubramanian, Pray-Grant et al. 2002). The catalytic core of the MYST family HAT complex NuA4 is Esa1 (Tip60 in humans). Esa1 is essential for cell cycle progression in yeast and promotes the acetylation of histone H4 at K5, K8, K12 and K16 (Allard, Utley et al. 1999). Other notable components

of the 1.2 MDa NuA4 HAT complex are the essential ATM kinase related protein Tra1p (Allard, Utley et al. 1999) and the Yaf9 subunit, the latter adopts a fold similar to the histone chaperone Asf1 and is common to the Swr1 remodelling complex (Schulze, Wang et al. 2009). In addition to HAT activity the p300/CBP enzymes contain bromodomains, which are known to specifically recognise acetyl-lysine and as such may promote the sequential addition of acetyl groups to histone tail residues (Moriniere, Rousseaux et al. 2009). In yeast Rtt109, also a member of the p300 class of HATs, does not encode an annotated bromodomain but retains the ability to acetylate multiple residues within the tail of histone H3 (Abshiru, Ippersiel et al. 2013) perhaps as a result of the proteins association with the histone chaperones Asf1 and Vps75 (see section 3.1).

In contrast to lysine acetylation, lysine methylation does not simply describe a single modification in fact mono, di and tri methylation have been found to occur on histones. Methylation can also occur on arginine side chains. Histone H3 is methylated at K4, K9, K27, K36 and K79 and histone H4 is methylated at K20. In organic synthesis the alkylation of a primary amine is a difficult reaction to control as the nitrogen lone pair of amine becomes more nucleophilic following each addition of an alkyl group due to the positive inductive effect of the alkyl groups. This tends to lead to the saturation of the amine nitrogen with alkyl groups forming a quaternary ammonium cation analogous to trimethyl-lysine. However *in vivo* the source of methyl groups (S-adenosyl methionine) is regulated and methylation events are catalysed by enzymes termed histone lysine methyl transferases (HKMTs). The complex nature of enzyme active sites allows for the selective control of lysine methylation on histone tails, for example the DIM-5 of *Neurospora crassa* and human SET7/9 HKMTs catalyse the trimethylation H3 K9 and monomethylation of H3 K4 respectively. Analysis of the active sites of these zinc dependent HKMTs revealed the replacement of a phenyl alanine residue in DIM-5 with a tyrosine residue in the SET7/9 active site (Xing, Zhe et al. 2003). This study found that upon mutating the phenyl alanine residue in the DIM-5 active site to tyrosine (F281Y) the methylation reaction did not proceed beyond the mono and di-methylated intermediates at H3 K9 presumably due to additional steric hindrance in the phenolic side chain.

Unlike acetylation which is mainly linked to transcriptional activation methylation marks can be either repressive or permissive towards transcription. Repressive methylation marks including H3 K9, K27 and H4 K20 lead to heterochromatin formation at specific loci *in vivo*. Methylated H3 K9 promotes silencing through

the interaction with heterochromatin protein 1 (HP1) and in a similar manner H3 K27 methylation recruits the Polycomb group silencing proteins. In both cases the methylated lysine residue is recognised by chromo-domains encoded in the proteins.

Active genes are enriched with H3 K4, K36 and K79 methylation marks. Additionally the position of these marks has been found to vary along the open reading frames of genes with H3 K4 trimethylation enriched at the 5' end, K36 trimethylation enriched at the 3' end and K79 trimethylation found throughout the open reading frame of active genes (Owen-Hughes and Gkikopoulos 2012).

Cross talk between lysine methylation and acetylation/ubiquitination pathways also occurs *in vivo*. For example, K36 trimethylation by Set2 is recognised by the chromo domain of Eaf3 which is a member of the NuA4 HAT complex as well as the Rpd3 HDAC complex (Joshi and Struhl 2005). The aforementioned SAGA complex not only has the ability to acetylate histones, but also specifically recognises trimethylated H3 K4 (Bian, Xu et al. 2011) and can direct de-ubiquitination of H2B K123 (Lee, Florens et al. 2005). It is notable that methylation of H3 K4 and K79 by Set1 and Dot1 respectively is a requirement for H2B K123 ubiquitination by Rad6 and Bre1 (Dover, Schneider et al. 2002; Sun and Allis 2002; Wood, Krogan et al. 2003). Thus the reversible nature of histone modifications and the cross-talk between the different modification pathways is of fundamental importance *in vivo*. One could imagine that the order of histone modifications appearing and disappearing is linked to the disassembly and reassembly of nucleosomes during the passage of a polymerase which requires access to the DNA template.

1.4 Histone Chaperones

In vitro nucleosome assembly can be achieved by mixing the histone octamer with DNA in the presence of high concentrations of monovalent ions followed by the reduction of the salt concentration by dialysis. This allows electrostatic histone – DNA interactions to be buffered, facilitating constructive nucleosome assembly and avoiding precipitation that occurs when histones and DNA are simply mixed at physiological salt concentrations. In living cells nucleosomes are assembled by the concerted efforts of a group of acidic

proteins which bind histones outside of chromatin, termed histone chaperones. These proteins direct the proper assembly of nucleosomes under physiological conditions.

Nucleoplasmin was the first protein to be classified as a histone chaperone due to its ability to promote the assembly of nucleosomes during DNA replication (Laskey, Honda et al. 1978). Subsequently histone chaperones have been implicated in a wide variety of processes including nucleosome assembly/disassembly coupled to DNA transcription, replication and repair, nucleosome remodelling, nuclear import/export and histone post translational modifications to name but a few. A general feature of histone chaperones is the presence of a long, thought to be unstructured, stretch of acidic residues at the C-terminus of the proteins. The exact role of the acidic C-terminal tails, many of which are dispensable for histone binding, is still unknown. Apart from the acidic C-terminal tails, histone chaperones are a structurally diverse set of proteins and increasing evidence suggests that this diversity is mirrored in their mode of interaction with histones (Figure 3).

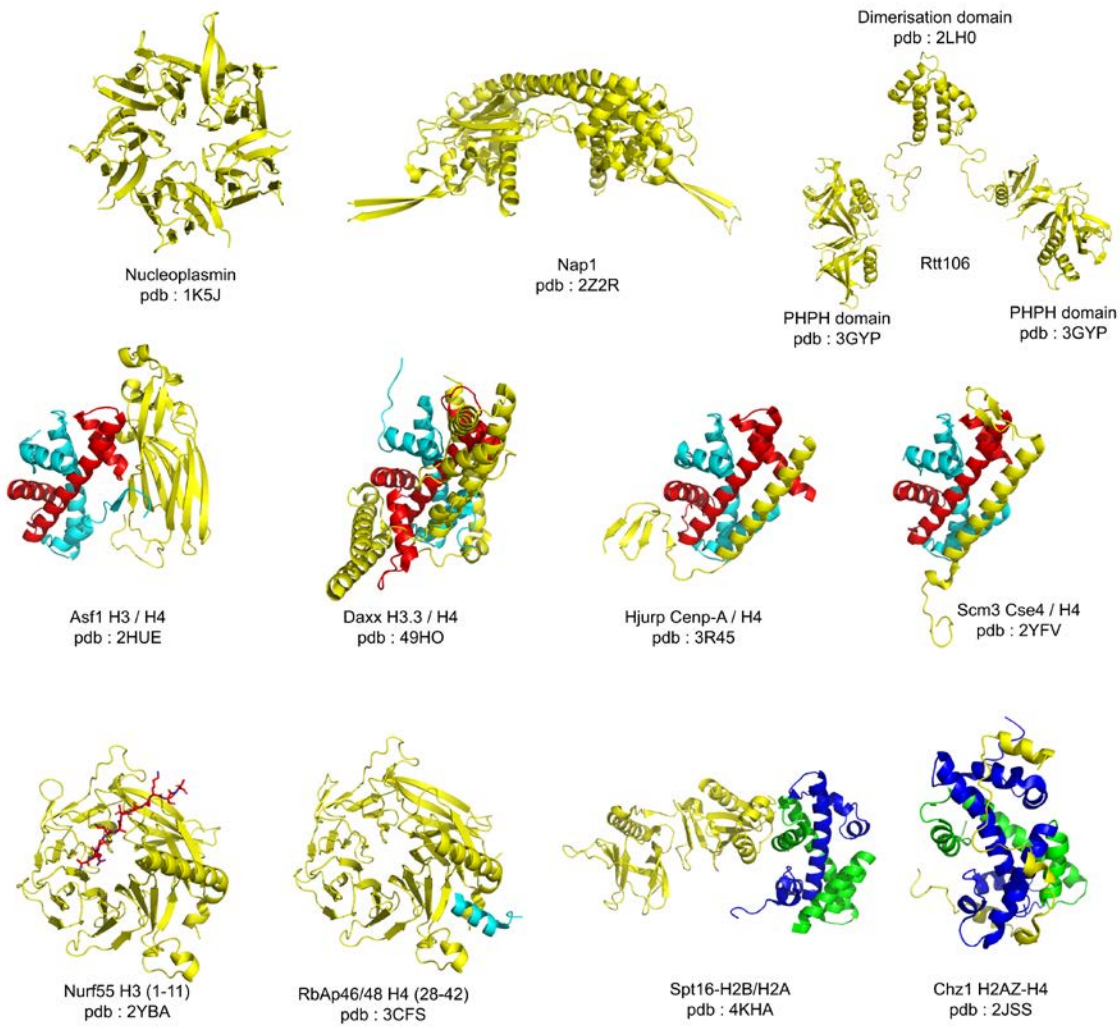

Figure 3 – Diversity in the folds of histone chaperones and their mode of interaction with histones. Chaperones are coloured in yellow with histones coloured according to type: H3 and related variants coloured red; H4 coloured cyan; H2A and related variants coloured blue and H2B coloured green.

Anti-silencing factor 1 (Asf1) was the first chaperone to be co-crystallised with histones and was shown to specifically interact with H3/H4 dimers (English, Adkins et al. 2006). Asf1 binds to the region of histone H3 which is also required for the tetramerisation of H3/H4 dimers. In addition Asf1 makes additional contacts with the C-terminus of histone H4 in a 'strand capture' mechanism that has been postulated to function during nucleosome disassembly (English, Adkins et al. 2006). More recent studies implicate Asf1 in nucleosome assembly pathways as Asf1 was found to promote tetrasome formation via a 'disome' intermediate (a H3/H4 dimer bound to DNA) but failed to disengage H3/H4 tetramers from DNA (Donham, Scorgie et al. 2011). This is supported by structural studies which have found that a region of Asf1 can bind the histone chaperone

complexes CAF-1 (Malay, Umehara et al. 2008) or HIRA (Tang, Poustovoitov et al. 2006) at which replication dependent and independent pathways of H3/H4 assembly are thought to converge. Asf1 is also required for the acetylation of histone H3 at lysine 56 (Driscoll, Hudson et al. 2007), a modification which enhances the association of H3/H4 with CAF-1 and another histone chaperone Rtt106 (Li, Zhou et al. 2008).

As mentioned, CAF-1 is thought to be the histone chaperone directly responsible for the deposition of H3/H4 onto DNA in a replication dependent manner (Stillman and Gluzman 1985; Stillman 1986). Although the fact that CAF-1 subunits are not essential in yeast suggests that redundant pathways for replication coupled nucleosome assembly exist. Consistent with its role in DNA synthesis coupled chromatin assembly CAF-1 has been found to directly bind the proliferating cell nuclear antigen (PCNA) responsible for clamping DNA polymerase delta (Pol δ) to its substrate (Shibahara and Stillman 1999). The interaction of CAF-1 with PCNA also directs nucleosomal transactions during DNA damage repair (Moggs, Grandi et al. 2000).

CAF-1 contains three subunits, Cac1, Cac2 and Cac3 in yeast which are also commonly referred to as p150, p60 and p48 (RbAp46/48) (Ridgway and Almouzni 2000). The p150 subunit is required to anchor CAF-1 to PCNA during DNA synthesis dependent chromatin assembly pathways, the middle domain possesses a region of acidic residues and the C-terminus of the protein interacts with the p60 subunit (Kaufman, Kobayashi et al. 1995). The p60 subunit, which interestingly bears homology to Hir1 – a component of the HIRA complex, contains seven WD40 repeats arranged in a beta-propeller fold. The somewhat promiscuous p48 subunit of CAF-1, which moonlights in several chromatin regulation associated complexes including the NURF, NURD and PRC-2 complexes, also adopts a WD40 repeat beta-propeller type fold. Structural insights into the mode of interaction of p48 (Murzina, Pei et al. 2008), which is also known as retinoblastoma associated protein 48 or RbAp48, and the Drosophila homologue Nurf55 (Schmitges, Prusty et al. 2011) with histones show stable interactions are formed with the H4 α1 helix and the H3 N-terminus (Figure 3). A recent study found that p48 can bind H3/H4 in the presence of Asf1 and that structural changes in H3/H4 upon p48 binding reduce the affinity of Asf1 for H3/H4 (Zhang, Tyl et al. 2013). This provides the potential basis for the handover of histones from Asf1 to CAF-1 during the DNA synthesis dependent nucleosome assembly. Consistent with this theme CAF-1 was also recently reported to be capable of loading newly synthesised H3/H4 tetramers

onto DNA (Winkler, Zhou et al. 2012) but in contrast to p48 the interaction of the full CAF-1 complex with H3/H4 was found to be mutually exclusive to Asf1 binding (Liu, Roemer et al. 2012).

The HIRA complex of higher eukaryotes is required for the replication independent deposition of H3.3/H4 into chromatin (Ray-Gallet, Quivy et al. 2002; Tagami, Ray-Gallet et al. 2004). In yeast the HIRA complex is comprised of four subunits Hir1, Hir2, Hir3 and Hpc2 which co-purify with Asf1 (Green, Antczak et al. 2005). Thus Asf1 seems provide the source of histones for both replication coupled and replication independent H3/H4 deposition. The Hir1 subunit bears homology to the WD40 repeats of the p60 subunit of CAF-1 but lacks the C-terminal HIRA domain present in human HIRA. As a result Hir1 likely combines with Hir2 which contains the HIRA domain but not the WD40 repeats to reconstitute human HIRA function (Gunjan, Paik et al. 2005). The histone variant H3.3 is enriched in post translational modification associated with gene activation and as such HIRA may play a role in the replacement of histones containing transcriptionally repressive histone marks during this process (McKittrick, Gafken et al. 2004). Although mainly implicated in replication independent nucleosome assembly, redundancy has been observed between CAF-1 and HIRA assembly pathways in, for example, heterochromatic silencing at telomeres (Sharp, Fouts et al. 2001). This suggests that silencing requires general assembly of chromatin which can be directed by either CAF-1 or HIRA in yeast.

Rtt106 was originally identified as a repressor of the incorporation of the transposable element Ty1 of virus like particles into the genome (Scholes, Banerjee et al. 2001). More recently Rtt106 was classified as a histone chaperone capable of specifically binding H3/H4 *in vivo* and *in vitro* (Huang, Zhou et al. 2005). The same study demonstrated a direct interaction of Rtt106 with CAF-1 through the large Cac1/p150 subunit. Supercoiling assays of Rtt106 with H3/H4 demonstrated increased supercoiling dependent on Rtt106, however the large excess of Rtt106 required to markedly increase supercoiling suggests that the protein is not solely responsible for deposition of histones H3/H4 onto DNA. Structural analysis of Rtt106 reveals the protein forms dimers through its N-terminal domain (Figure 3, pdb code : 2LH0) which is connected via a structurally heterogeneous region to the middle double pleckstrin homology (PHPH) domain (Figure 3, pdb code : 3GYP) with a presumably disordered C-terminal acidic domain (Liu, Huang et al. 2010; Su, Hu et al. 2012). There is evidence to suggest that H3 K56 acetylation is recognised by the PHPH domain of Rtt106 (Li,

Zhou et al. 2008; Su, Hu et al. 2012). However, whether this is a result of specific recognition of the acetyl-lysine moiety or due to recognition of a change in the overall structure of H3 dependent on K56 acetylation has yet to be determined.

Another histone chaperone complex that contains PHPH domain proteins is the FACT complex which facilitates chromatin transcription (Orphanides, LeRoy et al. 1998). The FACT complex is a heterodimer of Spt16 and Pob3 both of which contain tandem pleckstrin homology domains which have been structurally characterised (VanDemark, Blanksma et al. 2006; Hondele, Stuwe et al. 2013). Interestingly the latter publication also determined the structure of a chimera of Spt16 fused to the N-terminus of H2B in complex with H2A and found the mode of interaction between H2A/H2B and Spt16 to mediated by a four helix bundle between the α1 and α2 helices of H2B and the α3 and α4 helices of middle domain of Spt16 (Figure 3, pdb: 4KHA). If the Rtt106 PHPH domain were to recognise H3/H4 in a similar manner via the α1 and α2 helices of H4, the mode of interaction would be incompatible with the αN helix occupying a conformation observed in the histone octamer.

The structures of other histone chaperones in complex with histones reveal the structure of the histone fold domain is fairly stable (Figure 3). Many of these chaperones stably bind histone dimers however the mode of recognition of the various histone subtypes by these chaperones is diverse. For example, the homologous histone variant chaperones Hjurp and Scm3 recognise human Cenp-A/H4 and yeast Cse4/H4 dimers respectively (Figure 3, pdb 3R45 and 2YFV) via the long α2 helix of the respective centromeric H3 variant (Cho and Harrison 2011; Hu, Liu et al. 2011). Recently Hjurp has been found to dimerise via its C-terminus and hence Hjurp may direct the pre-assembly of Cenp-A/H4 tetramers during centromeric nucleosome assembly (Zasadzinska, Barnhart-Dailey et al. 2013). In contrast the H2AZ/H2B specific chaperone Chz1 makes contacts with H2AZ throughout the histone fold (Zhou, Feng et al. 2008). The H3.3 chaperone Daxx adds to the diversity of histone recognition by encapsulating ~40% of the solvent accessible surface of a H3.3/H4 dimer (Elsässer, Huang et al. 2012). Interestingly although the major features of the histone fold remain intact in this complex, the trajectory of the H3.3 αN helix is markedly different to that observed in the histone octamer and nucleosome (Figure 3, pdb 49HO) – as discussed in section 3.

The multifaceted family of proteins related to the yeast nucleosome assembly protein 1 (Nap1) protein function in a diverse range of processes (as discussed in sections 4 and 5). As the name suggests NAP-1 fold proteins from multiple species are best characterised for their ability to direct nucleosome assembly (Ishimi, Yasuda et al. 1983; Ishimi and Kikuchi 1991; Muto, Senda et al. 2007; Gill, Kumar et al. 2010). The mechanism by which Nap1 assembles nucleosomes is still under debate as the histone chaperone is not too discerning with respect to the cargo it associates with. Nap1 has been found to bind H2A/H2B, H2AZ/H2B and H3/H4 with comparable affinities and as such may recognise the histone fold in a non-specific manner (Andrews, Downing et al. 2008). Structural analysis of NAP-1 fold proteins from a variety of species has consistently shown the proteins to adopt a homo-dimeric fold (Park and Luger 2006; Muto, Senda et al. 2007; Gill, Kumar et al. 2010) in the confines of a crystal lattice (Figure 3, pdb 2Z2R).

Another yeast Nap1 related protein - Vps75, is involved in the acetylation of newly synthesised histones by its cognate binding partner Rtt109. Recent findings have linked Nap1 and Vps75 to transcription dependent chromatin assembly (Selth, Lorch et al. 2009; Xue, Kowalska et al. 2013). Although the CAF-1 and HIRA pathways are thought to be the major pathways for replication dependent and independent H3/H4 deposition into chromatin, a role for Nap1 related proteins in the final stages of chromatin assembly cannot be ruled out. For example, Nap1 may be involved in recycling chromatin bound ‘old’ histones following the passage of various polymerases. Consistent with this theme, Nap1 and Vps75 have been shown to specifically recognise H3/H4 tetramers (Bowman, Ward et al. 2011) and as such may provide a means of maintaining epigenetic histone marks in the genome during processes such as DNA transcription, replication and repair.

The aims of this study are to characterise the interactions of Vps75 and Nap1 with histones H3/H4 and to study the potential structural effects of histone H3 K56 acetylation using various biophysical experimental approaches. Intrinsic to these studies is the application of an electron paramagnetic resonance (EPR) based experiment called PELDOR which is not a widely adopted technique and as such requires further introduction.

1.5 Pulsed Electron Double Resonance

From a biochemistry perspective the PELDOR technique is a powerful tool for the structural analysis of macro molecular protein complexes and other biomolecules. The technique relies on the incorporation of two spin labels, which contain a single unpaired radical electron, in a site specific manner as to allow distances between the labelling sites to be measured. Spin labels are generally incorporated into protein by the conjugation of thiol reactive spin label with a cysteine residue (Figure 4), which can be strategically placed within a protein via mutagenesis in a site specific manner.

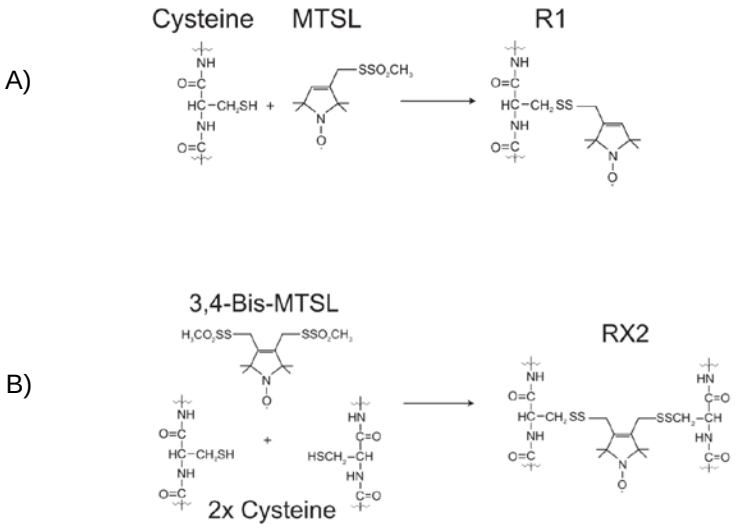

Figure 4 – Introducing spin labels into proteins by conjugation to cysteine residues. (A) The popular nitroxide radical spin label MTSL can be used to label a single cysteine residue. (B) The bivalent nitroxide radical spin label 3,4-Bis-MTSL can be used to cross-link label two adjacent cysteine residues.

PELDOR is an EPR experiment which allows the measurement of distances between two unpaired radical electrons due to the dipolar coupling interactions between the spins of the unpaired electrons. The spin of an unpaired electron acquires a magnetic moment when an external magnetic field is applied. When the magnetic moment of a spin is aligned in parallel or antiparallel with respect to the external magnetic field the spin occupies low energy (ground) or high energy (excited) states respectively. The splitting of the energy levels of electrons by an external magnetic field is termed Zeeman splitting and increases with the strength of the external magnetic field (Figure 5A). The hyperfine coupling of the electron spins with surrounding nuclear

spins, which also undergo Zeeman splitting (Figure 5B), leads to a population of electrons occupying different energy states. Transitions of electrons within this population between excited and ground states can occur when a photon with a quantum of energy equal to the energy difference between the two states is absorbed or emitted. In PELDOR experiments the strength of the external magnetic field allows these transitions to occur by the absorption and emission of microwave frequency radiation (Prisner, Rohrer et al. 2001).

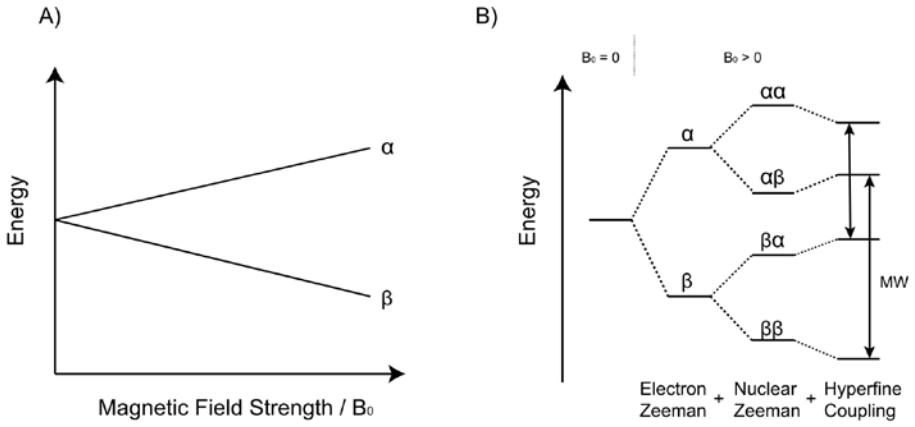

Figure 5 – The Zeeman splitting of unpaired electrons in a magnetic field. (A) As the strength of the external magnetic field is increased the difference in energy between spins aligned with (β) and against (α) the magnetic field increases. (B) The hyperfine coupling of the Zeeman effect on electrons and nuclear spins with microwave frequency transitions of electrons between energy levels indicated. Figure adapted from Prisner, Rohrer et al. 2001.

The different environments of the radical electrons in the population cause the electrons to populate multiple ground state energy levels. As a result sub-populations of electrons within the sample can be excited by pulses of microwave radiation at certain frequencies. In order to identify the frequency of microwave radiation required to excite sub-populations of electrons an external magnetic field sweep experiment is performed using a constant pulse of microwave frequency radiation (Figure 6A). This allows the identification of the frequencies of microwave radiation required to excite different sub-populations of spins at a constant external magnetic field strength (Jeschke, Chechik et al. 2006).

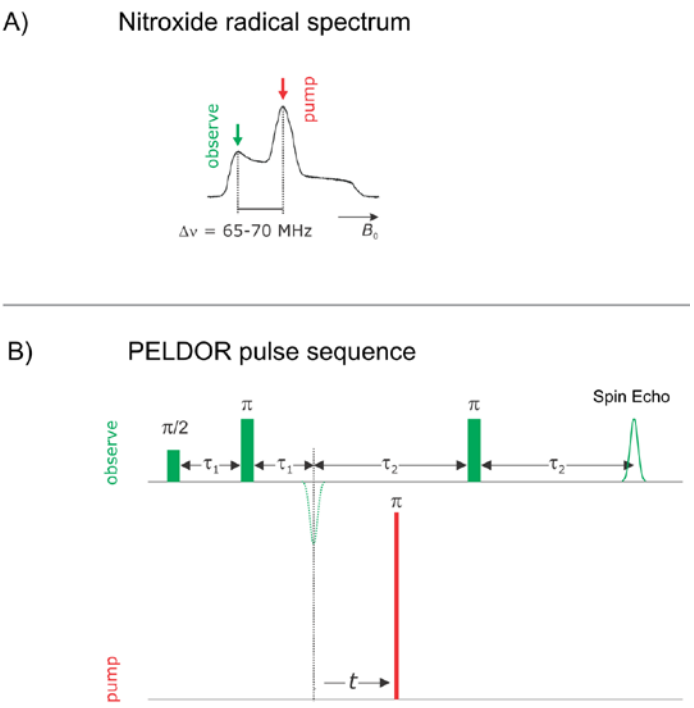

Figure 6 – The nitroxide radical electrons have different energies. (A) A magnetic field strength sweep spectrum of a nitroxide radical excited by a constant frequency of microwave radiation identifies sub-populations of spins which can be excited by various frequencies of microwave radiation when the external magnetic field (B_0) is kept constant. (B) The PELDOR pulse sequence required to create a spin echo in one sub-populations which is observed as the another sub-population of spins are excited by a "pump" pulse of microwave radiation at increasing time intervals. Figure taken from the DeerAnalysis 2006 manual – referred to by Jeschke, Chechik et al. 2006.

In a PELDOR experiment a sequence of microwave pulses at a given frequency, known as the observer pulse, are utilised to excite a sub-population of radical electrons in a manner that creates what is known as a "spin echo" (Jeschke, Chechik et al. 2006), which can be observed over time (Figure 6B). The spin echo is essentially refocused microwave frequency radiation which is released during the relaxation of excited unpaired electrons to their ground state. In a PELDOR experiment, in addition to the observer pulse, another sub-population of spins is excited by a pulse of microwave radiation at a different frequency, this is known as the "pump" pulse (Jeschke, Chechik et al. 2006). The dipolar coupling between a proportion of the electrons excited by the observer pulse sequence and those excited by the pump pulse reduces the intensity of the spin echo signal. The intensity of the spin echo modulates as a function of the timing difference between the observer and pump pulses when two spins are coupled in space and the timing of the modulation of the spin echo is related to the distance between the spins in the system.

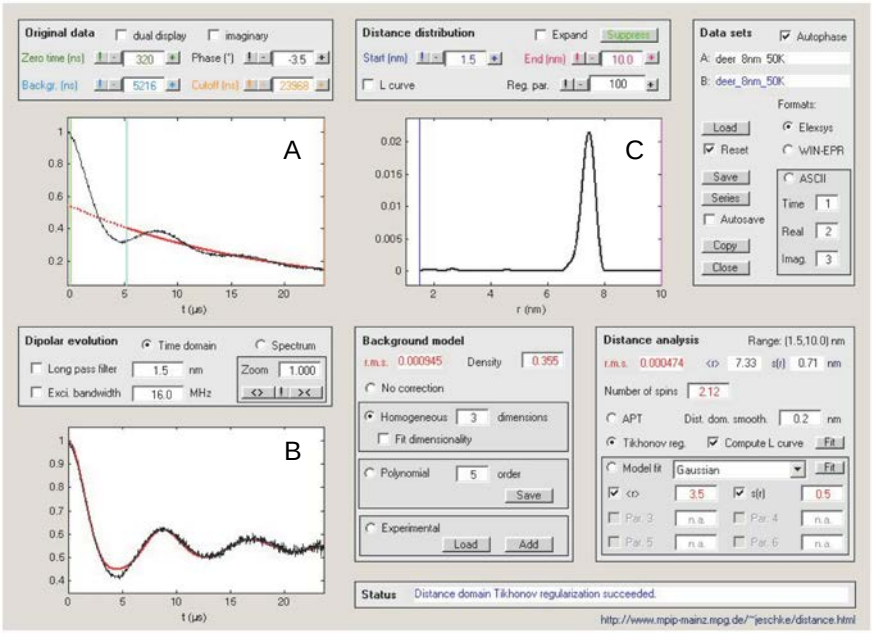

Figure 7 – A screen capture of the DeerAnalysis software. (A) The raw dipolar evolution function overlayed with the background correction function. (B) The background corrected dipolar evolution function. (C) The distance distribution as a result of Tikonov transformation of the background corrected dipolar evolution function. Figure taken from the DeerAnalysis 2006 manual – referred to by Jeschke, Chechik et al. 2006.

The raw data from a PELDOR experiment (Figure 7A), known as the dipolar evolution function or echo modulation, is a measure of the echo intensity as a function of the time interval between the pump pulse and the observer pulse (Figure 6B). As mentioned the modulation of the echo contains information about the distances between coupled spins within the system. In order to remove intermolecular spin-spin contributions to the dipolar evolution function a background correction function is applied (Figure 7B). The final intra-molecular distance distribution (Figure 7C) is obtained upon Tikhonov transformation of the background corrected dipolar evolution function (Jeschke, Chechik et al. 2006).

The quality of the dipolar evolution function has a knock on affect for the quality of the distance distribution data. In general one full oscillation is required to accurately deduce distance distributions. The time required to measure one full spin echo oscillation increases with the distance between spin labels and is subject to several relaxation phenomena. One such relaxation phenomena is transverse relaxation, known as T_2 or T_m, which is essentially a loss of coherent signal due to the dephasing of the spin echo. A significant contribution to such dephasing is apportioned to the interaction of the electron spin with nuclear spins of surrounding

protons. As such it is regular practice to perform PELDOR experiments in deuterated solvents, which have reduced hyperfine coupling, as to prolong the lifetime of the spin echo oscillation by lengthening the T_m. In addition the deuteration of the protein further extends the lifetime of the spin echo (Ward, Bowman et al. 2009).

In a structurally homogeneous protein complex an oscillation is observed in the dipolar evolution function. When additional distances are present in a structurally heterogeneous sample the oscillations combine which depending on the level of heterogeneity can lead to a complex oscillation or dampening of the oscillation all together. This can also be observed in systems where more than two spins are interacting. In the absence of oscillating features in the dipolar evolution function the gradient of the initial drop in the dipolar evolution function can still report on the average position of the distance distribution, however specific features of the distribution become less reliable.

2 Materials and Methods

2.1 Mutagenesis

Mutagenesis was performed via an adaptation of the QuickChange® Site-Directed Mutagenesis (Stratagene) protocol. Complementary primers were designed with 15 bases of homology to the plasmid either side of the mutated codon. The plasmid was PCR amplified using the following recipe:

	Concentration	Volume / µl
Plasmid	60 ng/µl	1
Forward Primer	100 ng/µl	1.25
Reverse Primer	100 ng/µl	1.25
dNTPs	2.5 mM each	2
Pfu Ultra buffer	10x	5
Water		40.5
Pfu Ultra II (Stratagene)		0.25
Total		51.25

Temperature / ^{o}C	Time	
95	Hold	
95	2 mins	
95	30 s	Repeat 15-25 times
55*	30 s	
68	6 mins*	
68	10 mins	

* Temperature varied according to primer T_m

**Time used was equivaelnt to 1 min per kb of plasmid

Table 1 – Typical conditions used for QuickChange mutagenesis.

Following the QuickChange mutagenesis amplification of the plasmid Dpn1 (1 µl) was added to each reaction and the mixture was incubated at 37^{o}C for 1 hour. To check the PCR worked 10 µl of the reaction following DpnI digestion was run on a 0.8 % agarose TBE gel. The presence of a band at the molecular weight of the plasmid indicated the likely success of the mutagenesis protocol. Clones were then isolated using the QIAprep Spin MiniPrep Kit (Qiagen) of XL10-Gold Ultracompetent cells (Stratagene) transformed with 2-5 µl of the PCR purified (Qiagen) DNA. The isolated clones were sequenced to confirm the integrity of the open reading frame and the presence of the mutated codon.

2.2 Histone Expression and Purification

Xenopus laevis histones were purified from BL21 DE3 *E. coli* (Invitrogen) inclusion bodies as per standard procedures (Luger, Rechsteiner et al. 1999). Following purification by cation exchange, histones were extensively dialysed into water containing β-mercaptoethanol (5 mM) prior to lyophilisation and final storage at room temperature.

2.3 Reconsitution of Histone Octamers, Tetramers and Dimers

Histone octamers and tetramers were reconstituted as reported previously (Luger, Rechsteiner et al. 1999) with the following adaptions to the method. Aliquots of lyophilised histones (1-2 mg) were dissolved in 1 ml of unfolding buffer (6M guarnidine hydrochloride, 20 mM HEPES-KOH pH 7.5) and concentrations determined spectophotometrically. For octamers H3, H4, H2A and H2B, for tetramers H3 and H4 and for dimers H2A and H2B were mixed together in stoichiometric amounts. The total volume of the combined histones was made up to 12 ml with unfolding buffer and filtered with a 0.45 μm syringe filter. The mixture was dialysed against 4 litres of 2 M sodium chloride, 20 mM HEPES-KOH, 1 mM EDTA and 5 mM 2-mercaptoethanol until striation lines had disappeared indicating equilibration with the dialysis buffer which usually took ~ 6 hours. The mixture was further filtered using a 0.45 μm syringe filter and concentrated to ~ 1 ml using an a 10 kDa MWCO Amicon Ultra centrifugal filter (Millipore) and purified via size exclusion chromatography on a Superdex S200 GL 10/300 (GE Healthcare) pre-equilibrated with 1 M sodium chloride, 20 mM HEPES-KOH pH 7.5.

2.4 Histone Chaperone Expression and Purification

Asf1, Nap1 and Vps75 were expressed recombinantly in *E. coli* Rosetta 2 cells (Millipore) and purified as reported previously (Bowman, Ward et al. 2011). Nap1 and Vps75 for PELDOR experiments were expressed in Spectra9 deuterated media (Cambridge Isotope Laboratories).

Briefly, following sonication and DNAse I treatment the protein lysate was clarified by centrifugation and filtration using 0.45 μm syringe filters. The clarified lysates of 6x histidine tagged chaperone proteins were affinity purified by applying to HisPur™ Cobalt resin (Thermo Scientific) (2 ml of slurry per litre of expression culture) which had been pre-equilibrated with 4 column volumes of 500 mM sodium chloride, 20 mM HEPES-KOH pH 7.5. The immobilised protein was washed with 3 column volumes of 500 mM sodium chloride, 20 mM HEPES-KOH pH 7.5 and 10 mM imidazole. Finally the protein was eluted with 3 column volumes of 500 mM sodium chloride, 20 mM HEPES-KOH pH 7.5 and 250 mM imidazole.

The elution buffer was supplemented with 50 mM DTT (from 1 M stock made up in 500 mM sodium chloride 20 mM HEPES pH 7.5), 5 mM EDTA and 5 mM EGTA and tags were cleaved (when stated in text) using PreScission protease (for Nap1 and Asf1) and TEV protease (for Vps75). The eluted protein was concentrated using a 10 kDa MWCO Amicon Ultra centrifugal filter (Millipore) and purified from remaining contaminants and aggregates via size exclusion chromatography using a Superdex S200 GL 10/300 (GE Healthcare) column pre-equilibrated with degassed buffer, 500 mM sodium chloride and 20 mM HEPES pH 7.5. The size exclusion chromatography step also served as a means of removing EDTA, EGTA and reducing agents from the protein for subsequent cysteine directed labelling approaches.

2.5 Site directed spin labelling

Following size exclusion chromatography, fractions spanning the eluted peak were pooled and concentrated to ~ 1 ml using a 10 kDa MWCO Amicon Ultra centrifugal filter (Millipore). Following spectrophotometric determination of the protein concentration - using protein extinction coefficients calculated based on their amino acid sequence using the online ExPASy ProtParam tool (http://web.expasy.org/protparam/) - a tenfold molar excess (per cysteine) of 50 mM MTSL (Toronto Research Chemicals Inc.) in DMSO was added and the reaction was allowed to proceed for 1 hour at room temperature. For Vps75 Y35RX2 labelling, the protein was added to 0.2 equivalents of 3,4-Bis-MTSL (Toronto Research Chemicals Inc.) per Vps75 dimer and allowed to react for 5 minutes at room temperature and the process was repeated until 2 equivalents of 3,4-Bis-MTSL label was reached. Excess label was removed by dialysis overnight at 4^{o}C against a buffer

containing twice the final concentration of sodium chloride in the PELDOR sample (see section 2.6) and 20 mM HEPES-KOH pH 7.5.

2.6 PELDOR Sample Preparation

Following overnight dialysis several rounds of concentration and dilution with the equivalent buffer made with D_2O were performed in a 10 kDa MWCO Amicon Ultra centrifugal filter (Millipore). Each round of concentration and dilution diluted the non-detuerated buffer with approximately 5 equivalents of deuterated buffer and the process was repeated 5 times. During the final round of concentration the protein was concentrated to > 100 μM and either mixed with other components of the sample (buffer exchanged in the same way) or diluted with deuterated buffer in a manner to obtain a 100 μM concentration of spin label pairs in 50 μl of buffer at twice the final sodium chloride concentration of the sample. The sample was then diluted 1:1 with D_8-glycerol to obtain the PELDOR sample at a concentration of 50 μM spin label pairs in 50 % D_8-glycerol, 10 mM HEPES-KOH pH 7.5 and the final sodium chloride concentration (as noted in sections 2.6.1 - 6).

2.6.1 Histone Tetramer PELDOR samples

Histone tetramers were reconstituted (as described in section 2.3) and labelled with MTSL as described in section 2.5 and then dialysed against 2 M sodium chloride, 20 mM HEPES-KOH pH 7.5 prior to buffer exchange for deuterated buffer (as described in section 2.6). The final conditions of the PELDOR samples was 50 μM spin label pairs in 1M sodium chloride, 50 % D_8-glycerol, 10 mM HEPES-KOH pH 7.5 in D_2O.

2.6.2 Histone Octamer PELDOR samples

Histone octamers were reconstituted (as described in section 2.3) and labelled with MTSL (as described in section 2.5) and then dialysed against 2 M sodium chloride, 20 mM HEPES-KOH pH 7.5 prior to buffer exchange for deuterated buffer (as described in section 2.6). An additional equivalent of unlabelled H2A/H2B dimers in the same buffer was added to the sample to prevent octamer dissociation. The final conditions of the PELDOR samples was 50 μM spin label pairs in 1 M sodium chloride, 50 % D_8-glycerol, 10 mM HEPES-KOH pH 7.5 in D_2O.

2.6.3 Asf1 H3/H4 PELDOR samples

Histone tetramers were reconstituted (as described in section 2.3), labelled with MTSL (as described in section 2.5) and then dialysed against 1 M sodium chloride, 20 mM HEPES-KOH pH 7.5 prior to buffer exchange for deuterated buffer (as described in section 2.6). The buffer exchanged histone tetramer was added to 2.5 equivalents of globular Asf1 (1-164) - to ensure full splitting of the H3/H4 tetramer by Asf1 - in the same deuterated buffer (1 M sodium chloride, 20 mM HEPES-KOH pH7.5, D_2O). The final conditions of the PELDOR samples was 50 μM spin label pairs in 500 mM sodium chloride, 50 % D_8-glycerol, 10 mM HEPES-KOH pH 7.5 in D_2O.

2.6.4 Vps75 and Nap1 R1 PELDOR samples

Deuterated Vps75 and Nap1 (purified as per section 2.4) were labelled with MTSL (as described in section 2.5) and dialysed against 1 M sodium chloride, 20 mM HEPES-KOH pH 7.5 prior to buffer exchange for deuterated buffer (as described in section 2.6). For analysis of the tetrameric forms of Vps75 and Nap1, the protein was additionally diluted with 20 mM HEPES-KOH pH 7.5 to 300 mM sodium chloride prior to the addition of D_8-glycerol to give a final concentration of 50 μM Vps75/Nap1 tetramer at 150 mM sodium chloride, 50% D_8 glycerol 10 mM HEPES-KOH in D_2O. The final conditions of the dimeric PELDOR

samples for Nap1 and Vps75 was 50-100 μM spin label pairs in 500 mM sodium chloride, 50 % D_8-glycerol, 10 mM HEPES-KOH pH 7.5 in D_2O.

2.6.5 Vps75 Y35RX2 PELDOR sample

Deuterated Vps75 Y35RX2 (purified as per section 2.4) was labelled with 3,4-Bis-MTSL (as described in section 2.5) and dialysed against 300 mM sodium chloride, 20 mM HEPES pH 7.5 prior to buffer exchanged for deuterated buffer (as described in section 2.6). The PELDOR sample was 50 μM spin label pairs in 150 mM sodium chloride, 50 % D_8-glycerol, 10 mM HEPES-KOH pH 7.5 in D_2O.

2.6.6 Vps75 – Asf1 – H3/H4 samples

Histone tetramers were reconstituted (as described in section 2.3) and labelled with MTSL (as described in section 2.5) and then dialysed against 800 mM sodium chloride, 20 mM HEPES pH 7.5 prior to buffer exchanged for deuterated buffer (as described in section 2.6). Similarly, deuterated Vps75 Y35RX2 (purified as per section 2.4) was labelled with 3,4-Bis-MTSL (as described in section 2.5) and dialysed against 800 mM sodium chloride, 20 mM HEPES pH 7.5 prior to buffer exchanged for deuterated buffer (as described in section 2.6). To prevent precipitation of histone chaperone complexes the spin labelled histone tetramer sample was added to 2 equivalents of Vps75 Y35RX2 dimers which were previously mixed with 2.5 equivalents of globular Asf1 (1-164) monomer in the same deuterated buffer (800 mM sodium chloride, 20 mM HEPES-KOH pH7.5, D_2O). If the chaperones were added to the histones precipitation was frequently observed, precipitation was also observed when the stoichiometry of one H3/H4 dimer to one Vps75 dimer was exceeded. The final conditions of the PELDOR samples was 50 μM spin label pairs in 400 mM sodium chloride, 50 % D_8-glycerol, 10 mM HEPES-KOH pH 7.5 in D_2O.

2.7 PELDOR Data Collection

PELDOR experiments were performed using a Bruker ELEXSYS E580 spectrometer at X-band frequency microwave radiation as described previously (Bowman, Ward et al. 2010) by Dr Hassane El Mkami, School of Physics and Astronomy, University of St Andrews, St Andrews FE2 4KM, UK. Data was analysed using DeerAnalysis2013 (Jeschke, Chechik et al. 2006).

2.8 Circular Dichroism

Peptides were ordered HPLC purified from GL Biochem (Shanghai) Ltd. amino capped at the c-terminus and concentrations were determined using the extinction coefficient of tyrosine (A_{280nm} = 1490 $M^{-1}cm^{-1}$). Stock concentrations of peptides were prepared at high concentration in deionised water which could be diluted with appropriate buffers to a final concentration of 150 μM peptide in order to test different conditions.

Circular dichroism experiments were performed on a J-810 JASCO Spectropolarimeter purged with N_2 gas in a 0.02 cm pathlength polarised cuvette. The following parameters were used:

Band width	10 nm
Response	0.5 sec
Sensitivity	Standard
Measurement range	260 - 180 nm
Data pitch	0.2nm
Scanning speed	50 nm/min
Accumulation	8
Concentration	150 μM

Table 2 – Parameters used during CD data aquisition

Spectra collected were background subtracted with buffer only spectra and smoothed using the binomial smoothing algorithm in the Spectra Analysis v 1.53.04 (Build 1) software (JASCO Corporation). The data was saved in ASCII format for analysis of secondary structure on the Dichroweb server - http://dichroweb.cryst.bbk.ac.uk/html/home.shtml (Whitmore and Wallace 2004) using the CDSSTR program with protein reference dataset 3 (Sreerama and Woody 2000). The normalised root mean squared deviation

between the experimental data and the reconstituted data was less than 0.01 for all samples. Dichroweb was also used to convert data points from the Spectropolarimeter's units of theta (mdeg) to molecular ellipticity / [θ] (deg.cm^2.dmol^{-1}) using the following values:

Mean Residue Weight = M_w of peptide/(Number of amino acids -1)
Protein concentration (mg/ml) = 150 x10^{-6} mol.l^{-1} * M_w
Cuvette path length (cm) = 0.02 cm

2.9 Size Exclusion Chromatography coupled to Multi Angle Light Scattering

SEC-MALS experiments were performed on a Dionex Ultimate 3000 HPLC system with an inline miniDAWN TREOS multi angle light scattering (MALS) detector (Wyatt) and Optilab T-rEX differential refractive index (dRI) detector (Wyatt). Prior to performing SEC-MALS experiments a Superdex S200 GL 10/300 (GE Healthcare) column was washed with 1.5 column volumes of 0.1 M HNO_3 and then equilibrated overnight at 300 µl/min with 0.2 µm filtered buffer containing sodium chloride (concentrations as stated in the text) and 20 mM HEPES-KOH pH 7.5 and the differential refractive index (dRI) detector's reference cell was purged with the running buffer. For accurate mass determination: typically 200-300 µg of protein in less than 200 µl volume was injected onto the column when flat baselines were observed for all light scattering (LS) angle detectors and the dRI index detector with background scattering in LS detector 2 not in excess of 0.0001 Volts. Molar masses across elution peaks were calculated using ASTRA v6.0.0.108 software (Wyatt).

2.10 Amine Reactive Cross Linking

BS_2G, BS3 and DTSSP cross-linkers (Thermo Scientific) were made as 50 mM stock solutions in DMSO and stored at -20 ^oC for up to 1 week. For cross-linking titrations the following components, in 400 mM sodium chloride, 20 mM HEPES-KOH, were mixed together:

	Volume / µl						
$(Vps75)_2$ (5 µM)	10	10	10	10	10	10	10
$(H3H4)_2$ (20 µM)	0	0.5	1	1.5	2	2.5	5
Buffer (400 mM NaCl)	10	9.5	9	8.5	8	7.5	5

Table 3 – Concentrations and volumes of Vps75 and H3/H4 mixed together at 400 mM sodium chloride and 20 mM HEPES-KOH pH 7.5

10 µl of the mixture (as per Table 3) was diluted with 10 µl of either 0 M sodium chloride or 400 mM sodium chloride with 20 mM HEPES-KOH pH 7.5 to make a final reaction volume of 20 µl at 200 mM or 400 mM sodium chloride. The final amounts of protein for each titration point are summarised in Table 6:

	1	2	3	4	5	6	7
$[(vps75)_2]$ /pmol	25	25	25	25	25	25	25
$[(H3H4)_2]$ /pmol	0	5	10	15	20	25	50

Table 4 – Final amounts of Vps75 and H3/H4 in cross-linking titration points

After incubating the mixtures at room temperature for 30 minutes the samples were cross-linked with 2 mM BS_2G for 1 hour and quenched with 50 mM Ammonium Carbonate prior to SDS-PAGE analysis.

For DTSSP cross-linking prior to SEC-MALS analysis (as described in section 2.9) 5 nmoles of Vps75 dimers was mixed with 5 nmoles of H3/H4 or H2A/H2B dimers at a final concentration of 10 µM in 200 mM sodium chloride, 20 mM HEPES-KOH. Following equilibration at room temperature for 30 minutes 2 µl of DTSSP (50 mM) was added and cross-linking was allowed to proceed for 30 minutes before quenching the reaction with 10 µl with ammonium carbonate (1 M). Any precipitate was removed via centrifugation and the supernatant was concentrated to > 100 µl prior to SEC-MALS analysis at 400 mM sodium chloride, 20 mM HEPES-KOH pH 7.5 (as described in section 2.9).

2.11 Molecular Modelling

MTSL side chains were added to crystal structures using the MTSSLWizard (Hagelueken, Ward et al. 2012) Pymol plugin. For modelling of the tetrameric assemblies of Vps75 and Nap1, the position of nitrogen atoms in the ensemble of spin labelled side chains for each labelling site (modelled with MTSSLWizard) were

incorporated into the pdb coordinates for Nap1 (pdb code: 2Z2R) and Vps75 (pdb code: 2ZD7). Distance measurements obtained from PELDOR experiments were used as restraints with additional non-crystallographic symmetry restraints to model the tetrameric assemblies using rigid body energy minimisations in XPLOR-NIH.

2.12 Pyrene Excimer Studies

Following size exclusion chromatography, fractions spanning the eluted peak of Vps75 K78C were pooled and concentrated to ~ 1 ml using a 10 kDa MWCO Amicon Ultra centrifugal filter (Millipore). To the concentrated protein 1-2 mg of N1-(pyrene)maleimide (Sigma Aldrich) was added as a powder, the reaction was allowed to proceed overnight with agitation at 4 ^{o}C. The following day precipitate was removed by centrifugation and size exclusion chromatography was performed to remove unreacted N1-(pyrene)maleimide and soluble aggregates. The eluted protein was concentrated and the concentration was calculated spectrophotometrically using the protein extinction coefficient of a Vps75 dimer 90760 M^{-1} cm^{-1} at 280 nm.

Pyrene fluorescence experiments were performed on a Cary Eclipse Fluorescence Spectrophotometer (Varian) with parameters for excitation and emission spectra as per Table 5.

Scan mode	Excitation	Emission
Start (nm)	260	325
Stop (nm)	360	550
Em. Wavelength (nm)	400	345
Ex. Slit (nm)	5	5
Em. Slit (nm)	5	5
Scan rate (nm/min)	120	120
Data interval (nm)	1	1
Averaging Time (s)	0.5	0.5
Excitation filter	Auto	Auto
Emission filter	Open	Open
PMT voltage (V)	Medium	Medium
Corrected spectra	OFF	OFF
Smoothing	ON	ON
Type	Savitzky-Golay	Savitzky-Golay
Filter size	5	5

Table 5 – Parameters used for pyrene fluorescence studies on the Cary Eclipse Fluorescence Spectrophotometer

2.13 Analytical Gel Filtration

Analytical gel filtration experiments were performed on a Dionex Ultimate 3000 HPLC system using a 2.4 ml Superdex 200 PC 3.2/30 (GE Healthcare) equilibrated with 400 mM sodium chloride, 20 mM HEPES-KOH pH 7.5 and 30% glycerol at 80 µl/min. A total of 24x 80 µl (1 min) fractions were collected spanning the void to bed volume of the column from 0.48 - 2.40 ml (6 - 30 mins). A maximum of 6 nmoles of total protein in less than 25 µl was injected per run. Fractions were analysed by SDS-PAGE.

3 The structural effects of acetylation of histone H3 lysine 56

3.1 Introduction

It is now thought that in *Saccharomyces cerevisiae* all newly synthesised copies of histone H3 are acetylated at K56 during S-phase and this modification promotes association of H3/H4 with deposition factors such as CAF-1 and Rtt106 which results in chromatin assembly (Li, Zhou et al. 2008). In Saccharomyces cerevisiae, K56 acetylation is catalysed by the histone acetyl transferase (HAT) Rtt109 (Regulator of Ty1 Transposition 109), the specificity of which towards K56 is stimulated by the histone chaperone Asf1 (Anti-Silencing Function 1). Additionally, when bound by Vps75 (Vacuolar Protein Sorting 75) the catalytic activity of Rtt109 towards H3 K9 and K23, and to a lesser extent K14, K18 and K27, acetylation is enhanced. Whilst H3 K56 acetylation is dependent on the presence of Asf1 and Rtt109, the H3 'tail' acetylation events catalysed by Rtt109 and Vps75 are partially redundant with Gcn5 (Fillingham, Recht et al. 2008; Burgess, Zhou et al. 2010; Abshiru, Ippersiel et al. 2013). From a structural perspective, Rtt109 stably associates with Vps75 and two alternate stoichiometries of the complex have been crystallised. Both of which contain a Vps75 dimer with one (Su, Hu et al. 2011) or two copies of Rtt109 (Tang, Holbert et al. 2011). To date, no structural information has been published on the interaction of Asf1 with Rtt109, although the fact that Asf1 can co-immunoprecipitate Rtt109 in the absence of Vps75 (Tsubota, Berndsen et al. 2007) suggests Asf1 may occupy a similar binding surface as Vps75.

The absence of a clear mammalian homologue of Rtt109 has led to speculation as to whether K56 acetylation is a fungal specific modification, however the discovery that Gcn5 and CBP/p300 can also acetylate K56 in humans and flies has laid rest to these doubts (Das, Lucia et al. 2009; Tjeertes, Miller et al. 2009). Additionally, the *S. cerevisiae* NAD-dependent histone deacetylases Hst3 and Hst4 which remove K56 acetylation have human orthologues: the NAD-dependent deacetylases SIRT1 and SIRT2. However not all aspects of K56 acetylation are conserved, the S-phase peak of K56 acetylation for example has not been observed in humans. As the misregulation of K56 acetylation is associated with many cancer types (Das,

Lucia et al. 2009) it is possible that the modification is more tightly regulated in humans than yeast as to prevent DNA damage events.

Lysine 56 acetylation also appears to have a role in transcription and has been found to be enriched in active genes (Xu, Zhang et al. 2005), required for transcription through heterochromatic loci (Värv, Kristjuhan et al. 2010) and be present on newly incorporated H3 deposited in a replication independent manner (Rufiange, Jacques et al. 2007). The fact that H3 K56 acetylation promotes both the assembly of nucleosomes and transcriptional output seems counter-intuitive. This could be explained if H3 K56 acetylation was to promote the formation of an intermediate in nucleosome assembly which was also common to the disassembly process. This may be explained by the fact that studies of histone exchange suggest that during the first round of transcription only a H2AH2B dimer is lost from a nucleosome forming a 'hexasome' (Kulaeva, Hsieh et al. 2013), as H3 K56 lies at the H2AH2B and H3/H4 interface acetylation may reduce the affinity of H2AH2B for H3/H4 and hence reduce the nucleosomal barrier for multiple rounds of transcription. There is a possibility that the positive superhelical tension in front of a processing RNA polymerase is released during the disassembly nucleosomes (Durand-Dubief, Svensson et al. 2011), which wrap DNA in a negative superhelical fashion, and thus the reassembly of chromatin in the wake of a polymerase may be a requirement for multiple rounds of transcription.

Histone H3 K56 acetylation seems to be implicated in most processes that necessitate the disassembly and reassembly of nucleosomes in the wake of a DNA processing enzyme. Indeed the interplay of K56 acetylation in the DNA damage response is a hot topic in the DNA repair field (Downs 2008). Strains lacking the ability to acetylate K56 are hypersensitive to DNA damaging agents (Masumoto, Hawke et al. 2005). Following a double strand break double stranded DNA is resected leading to a loss of nucleosomes around the damaged site, after the subsequent DNA repair by non-homologous end joining these nucleosomes have to be reassembled. During this process K56 acetylation is induced and is thought to be required to turn off the DNA damage checkpoint (Chen, Carson et al. 2008). Interestingly replacing K56 with the acetyl-lysine mimic glutamine (K56Q) bypasses the need for Asf1 for chromatin reassembly and subsequent DNA damage checkpoint recovery (Chen, Carson et al. 2008).

The αN helix of histone H3 is located between the two gyres of DNA within the nucleosome forming direct and water mediated hydrogen bonds with the phosphate backbone of the central gyre of DNA and the entry/exit gyre of DNA (Figure 8). The H3 αN helix stacks in a perpendicular fashion onto the α1 helix of histone H4 and is wedged against the DNA by the C-terminal extension of histone H2A. Due to the close proximity of the H3 αN helix to both gyres of DNA and the so called docking domain of H2A, perturbation in this region can have marked effects on nucleosome dynamics.

Lysine 56 acetylation is perhaps the best characterised modification in the H3 αN helix. Located at the C-terminus of the αN helix, lysine 56 forms a water mediated hydrogen bond with the phosphate backbone of the entry/exit gyre of DNA within the nucleosome. As a result, the charge neutralisation of lysine 56 upon acetylation is thought to have a direct effect on nucleosome dynamics. As such nucleosomes containing the acetylation mimic glutamine at lysine 56 (K56Q) were seen to have a 1.8 fold increase in nucleosome sliding assays and an 18% decrease in FRET efficiency of end-to-end labelled nucleosomal DNA (Ferreira, Somers et al. 2007). Consistent with this effect genetically incorporated K56 acetylation was found to increase DNA breathing at the entry-exit regions of mononucleosomes two fold *in vitro* compared to wild type (Neumann, Hancock et al. 2009).

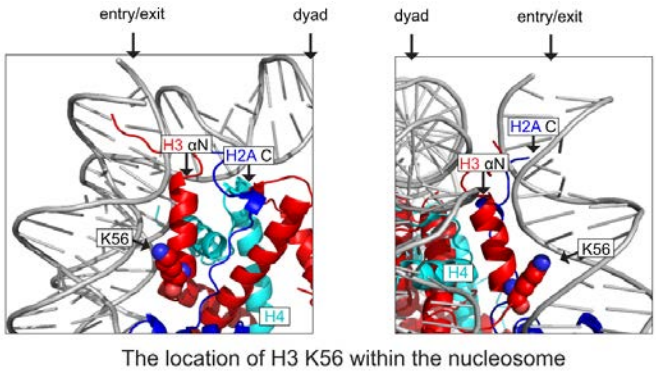

Figure 8 – The location of H3 K56 within the nucleosome. Figure was created from the crystal structure of the nucleosome (Luger, Mäder et al. 1997).

Despite K56 acetylation and the acetyl lysine mimic K56Q affecting nucleosome dynamics this does not address the fact that the substrate for the modification is thought to be newly synthesised non-nucleosomal histone H3 (Han, Zhou et al. 2007; Li, Zhou et al. 2008) and hence K56 acetylation may be important outside of chromatin. Effects of K56 acetylation outside of the nucleosome have been studied with respect to the modifications ability to promote association with the histone chaperones CAF-1 and Rtt106 (Li, Zhou et al.

2008; Su, Hu et al. 2012). Although a crystal structure of the middle PHPH domain of Rtt106 in complex with acetyl-histidine has been solved (Su, Hu et al. 2012) this does not exclude the possibility that Rtt106 is recognising the overall fold of histone H3 which may be modified in a K56 dependent manner. The PHPH domain of Rtt106 is closely related to the middle domain of Spt16 of the FACT complex which makes a four helix bundle with H2A/H2B via the α1 and α2 helices of H2B (Hondele, Stuwe et al. 2013) (Figure 3, pdb : 4KHA). The structurally equivalent region of H3/H4, to which Rtt106 could bind, would be the α1 and α2 helices of H4 which are obscured by the H3 αN helix in the histone octamer.

In this study the hypothesis that K56 acetylation is having a structural effect on the H3 αN helix outside of the nucleosome has been pursued. The fact that the H3 αN helix appears to be somewhat disordered in the H3/H4 tetramer (Bowman, Ward et al. 2010) and additionally that acetylation increases the alpha helical content of histone H4 tail peptides (Wang, Moore et al. 2000) lends strength to this hypothesis. The effect of acetylation may depend on the local environment of the modification and may not merely be a general effect. In this instance, the fact that the positively charged lysine 56 side chain is on the same side of the helix as arginines 52 and 53 may, in the absence of charge neutralisation by DNA and additional structural stabilisation by H2A C-terminus, cause destabilisation of the helix. Thus the acetylation of K56 would be hypothesised to stabilise the H3 αN helix, outside of the nucleosome and histone octamer, by neutralising the electrostatic repulsion with other positively charged residues.

3.2 Results

3.2.1 Acetylation of histone H3 lysine 56 affects the secondary structure of H3 peptides

In order to investigate the effect of acetylation at K56 (K56Ac) on the helical content of the αN helix a series of circular dichroism (CD) experiments were performed on H3 αN peptides from *Xenopus laevis* (P43-S57) amino capped at the C-terminus (H-PGTVALREIRRYQKS-NH_2). The *X. laevis* sequence was chosen for initial studies as the presence of a tyrosine residue at position 54 (A_{280nm} = 1490 $M^{-1}cm^{-1}$) enabled more accurate concentration determination of the peptides than the comparative *Saccharomyces cerevisiae* peptide which contains a single conservative phenylalanine mutation at position 44 (A_{257nm} = 220 $M^{-1}cm^{-1}$).

In water the wild type, K56Q and K56Ac peptides all displayed characteristic CD spectra of random coils in solution with a trough at 200 nm (see 0% TFE curve Figure 9A-C). The random coil spectrum was observed under a range of conditions which were designed to assess the effect of pH, ionic strength and anion types. This suggested that in isolation, over a variety of conditions the αN is essentially a random coil with no helical content induced by acetylation. In such instances, a fluorinated alcohol 2,2,2-trifluoroethanol (TFE) is commonly used in CD studies on isolated peptides as it can induce secondary structure in isolated peptides which have a certain propensity to form secondary structures (Wang, Moore et al. 2000), which may support structure in the absence of stabilising interactions with tertiary structural elements. The mechanism by which TFE stabilises secondary structure is subject to debate in the literature. It is thought the main effect of TFE is to strengthen the backbone hydrogen bonds required to form secondary structure by the excluding water from the local environment of the peptide. Additionally the amphipathic nature of TFE with its hydrophobic trifluoromethyl group and hydrophilic alcohol group enables it to support the clustering of hydrophobic and hydrophilic residues down opposing faces of the alpha helix (Roccatano, Colombo et al. 2002) as is the case of the H3 αN helix.

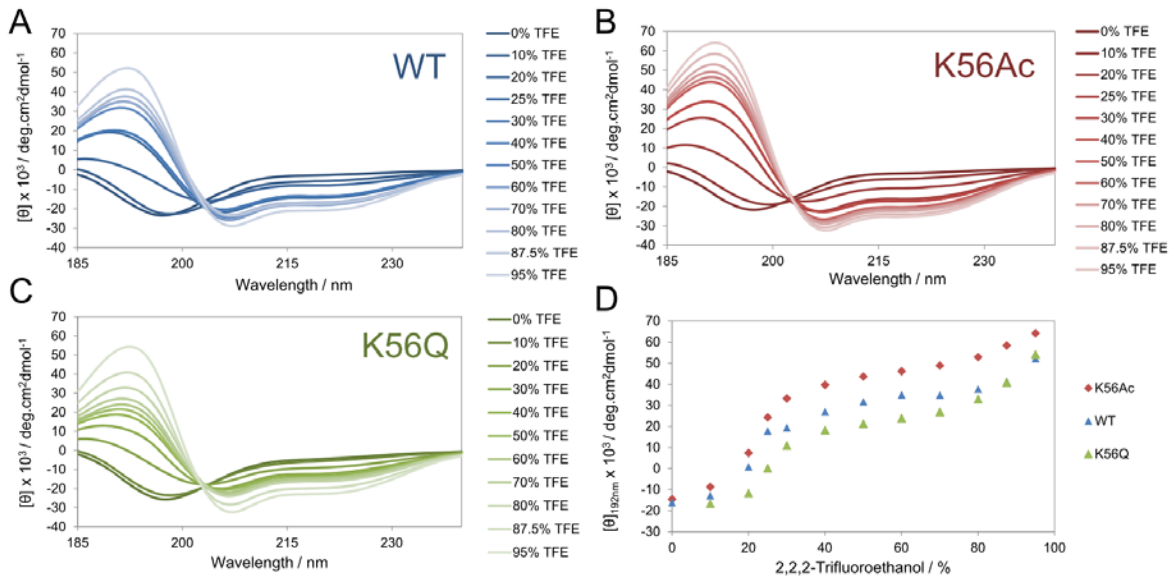

Figure 9 – Circular dichroism spectra of P43-S57 peptides across a titration of 2,2,2-trifluoroethanol for X. laevis (A) wild type, (B) K56 acetylated and (C) K56Q mutant peptide. (D) The molecular ellipticity [θ] at 192 nm of peptides across the titration series.

The characteristic CD spectra of an alpha helix has a maximum molecular ellipticity ([θ]) at 192 nm and two minima at 208 nm and 220 nm the magnitude of these peaks and troughs is proportional to the amount of alpha helical content. As can be seen in above 20% TFE the αN helix begins to adopt a helical conformation in the wild type, K56Q and K56Ac peptides (Figure 9 A-C). At 30% TFE and above the acetylated αN helix is significantly more helical than the wild type peptide; however the acetyl lysine mimic K56Q appears to be less helical than the wild type peptide. As circular dichroism is an ensemble approach these spectra represent the average secondary structure content of peptides within the population of peptides in the sample. Therefore one cannot differentiate whether the differences in alpha helicity observed are attributed to the position of the equilibrium between random coil and α-helical structures for a given condition or differing degrees of helicity of peptides within the population.

Due to the proximity of K56 to the C-terminus of the initial peptides tested it was possible that the full effect of acetylation, albeit at a peptide level, was masked because the effect of K56 acetylation could only propagate one residue in a C-terminal direction. Additionally it was possible that a similar effect at the N-terminus was restricting the nucleation of secondary structure elements within the peptide. This could

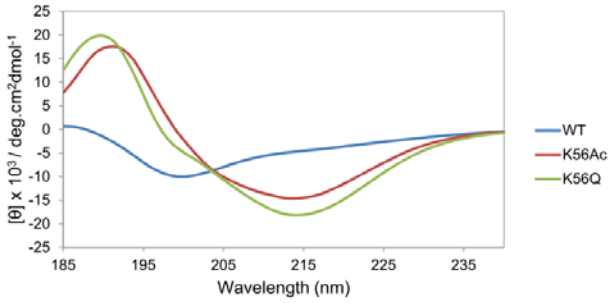

Secondary structure / %

Peptide	αR	αD	βR	βD	T	U	Total
WT P38-I62	1	4	23	12	23	37	100
K56Ac P38-I62	12	7	21	14	16	30	100
K56Q P38-I62	12	7	23	14	14	30	100

Figure 10 – *Top:* Circular dichroism spectra of P38-I62 wild type, K56Ac and K56Q peptides in 150 mM NaF, 5 mM Tris HCl pH 7.5. *Bottom:* Secondary structure content as assessed using the CDSSTR method of the Dichroweb suite against the protein reference set 3. Where α = alpha helix, β = beta sheet, R = regular form and D = distorted form of secondary structural element, T = turn, U = unordered.

potentially explain why the initial peptide series did not form stable secondary structures in the absence of TFE.

Initially the peptide sequence was extended five amino acids in the N-terminal direction to (P38-S57) amino capped at the C-terminus (H-PHRYKPGTVALREIRRFQKS-NH_2), the incorporation of another tyrosine residue (Y41) for spectrophotometric concentration determination allowed the *S. cerevisiae* H3 sequence to be probed for structural effects of acetylation. Again the CD spectra of both wild type and K56Ac peptides were indicative of random coils in solution in a range of aqueous conditions. Similarly, both peptides became alpha helical upon titration with TFE with the acetylated from displaying increased alpha helical propensity across the titration series (data not shown). This suggested that extending the peptide at the N-terminus had little effect of the structure. The comparative K56Q peptides were not assayed as no significant differences were observed in the secondary structural content of the P43-S57 and P38-S57 peptides for both wild type and K56Ac peptides and the cost of the additional peptide was deemed unnecessary.

The hypothesis that the effect of K56 acetylation could propagate beyond the C-terminus of the H3 αN helix was tested by extending the *S. cerevisiae* H3 sequence five residues at the C-terminus to isoleucine 62 (H-PHRYKPGTVALREIRRFQKSTELLI-NH_2). Once again the CD spectrum of the wild type peptide was indicative of a random coil structure in solution in the absence of TFE (Figure 10). Note: although the secondary structure analysis suggests the presence of β-sheet and turn content the spectral form is still consistent with a random coil in solution. However, in this instance marked differences in the CD spectra of K56Ac and K56Q peptides were observed. Under the conditions of 150 mM sodium fluoride (a common substitute for sodium chloride which is incompatible in CD studies due to high absorbance at far-UV

wavelengths) and 5 mM Tris HCl pH 7.5, both P38-I62 K56Ac and K56Q peptides produced CD spectra consistent with a mixture of both α-helical and β-sheet structures in solution (Figure 10). Secondary structure analysis of the two peptides suggests they may be forming very similar structures in solution; both K56Ac and K56Q contain 19 % total helicity and 35-37% β-strand structure respectively, compared to the 5% total helicity and 35 % β-strand structure in the wild type peptide. The differences in secondary structure compared to the wild type peptide suggests that K56 acetylation nucleates α-helical structure at the C-terminus of the H3 αN region and that glutamine sufficiently mimics the post translational modification at a structural level.

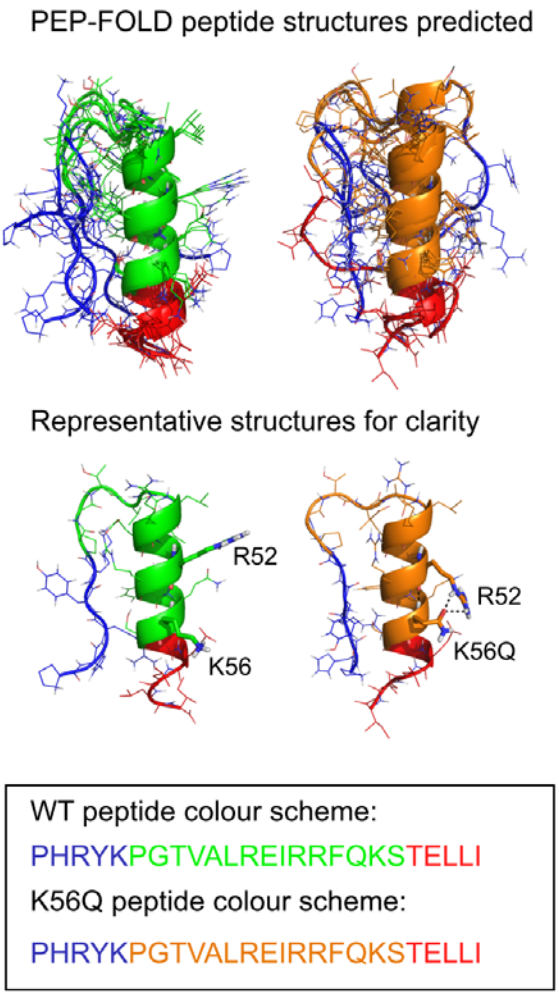

Figure 11 – PEP-FOLD structure prediction for P38-I62 peptides. *Top:* Top five minimum energy structures for P38-I62 peptides aligned by peptide backbone atoms of residues 49-56. Residues in the present in the canonical histone octamer αN helix are coloured green for wild type and orange for K56Q mutant peptides with the additional N-terminal and C-terminal residues coloured in blue and red respectively. *Middle:* Representative structures from each peptide cluster depicting key residues which differentiate the wild type and K56Q peptide structures. *Bottom:* Residue colour scheme.

In order to gain an insight of how acetylation could be acting to nucleate alpha helical structure, the structure of the wild type and K56Q P38-I62 peptides were predicted with PEP-FOLD (Maupetit, Derreumaux et al. 2009). PEP-FOLD predicts the structural alphabet of a peptide using a hidden Markov model and then using the structural alphabet codes of the peptide, which represent different ways of folding four residue peptides, performs several force field energy minimisations to predict the structure of the peptide sequence provided. PEP-FOLD predictions for test set of 37 linear peptides

whose structures have been solved by NMR are accurately predicted to within a 3 Å RMSD for the rigid peptide core. The top five PEP-FOLD predicted minimum energy structures for the P38-I62 wild type and K56Q mutant peptides adopt a broadly similar structure (Figure 11).

With the exception of one instance in the K56Q cluster of structures, both wild type and K56Q predicted structures are alpha helical from L48 to K56/K56Q, with the majority of structures incorporating an extra turn of alpha helix beyond C-terminus of the canonical αN helix to L60. Interestingly the N-terminus of the canonical αN helix has a tendency to fold down alongside the helical segment in both structures. One observable difference between the wild type and K56Q mutant peptide structures is the position of side chains R52 and K56/K56Q. In the case of the K56Q mutant peptide, for all structures, the carbonyl oxygen of the glutamine 56 side chain accepts a hydrogen bond form the arginine 52 side chain; this contrasts with the wild type peptide where electrostatic repulsion between lysine 56 and arginine 52 causes the side chains to occupy more distal locations relative to one another (Figure 11). PEP-FOLD structure predictions could not be performed in the current version of the software for the acetylated form of the peptide. However, one could imagine the carbonyl oxygen of the acetyl group of K56Ac could act as a hydrogen bond acceptor from arginine 52 to stabilise secondary structure in an analogous manner to K56Q. This type of interaction could explain why both P38-I62 K56Ac and K56Q peptides have higher total helical content than the wild type peptide. Mutations in R52 to are lethal in S. cerevisiae which may highlight the importance of the interplay of this residue with K56 (Hyland, Cosgrove et al. 2005).

3.2.2 The acetyl mimicking mutation K56Q has no significant observable effect on the H3 αN helix when probed by PELDOR in the context of the histone tetramer or octamer

The CD studies of peptides incorporating the H3 αN helix suggest that the structure of this region is modulated in an acetylation dependent manner and that glutamine sufficiently mimics the modification when the peptide is extended beyond the canonical αN helix C-terminus. In order to gain a fuller understanding of how the modification is affecting structure a series of PELDOR EPR experiments were performed on full length proteins with lysine 56 mutated to glutamine.

Previously (Bowman, Ward et al. 2010) performed PELDOR EPR distance measurements on a number of labelling sites within the histone octamer and compared the distance distributions obtained with those in the histone H3/H4 tetramer. One key finding was that when residues in the H3 αN helix (V46 and R49) were probed they were seen to form stable distance distributions in the histone octamer but the distance distributions became somewhat heterogeneous in the H3/H4 tetramer. As a result of the structure of the H3 αN being modulated in an acetylation dependent manner analogous EPR experiments were performed in the presence of K56Q to observe any structural changes within the histone octamer and tetramer as a result of acetylation. Of the H3 αN labelling sites, probed previously by EPR, V46 was chosen over R49 as to avoid disrupting any electrostatic interactions of R49 which may be structurally important.

Refolded *X. laevis* histone octamers containing H3 V46C (C110A) were labelled with the S-(2,2,5,5-tetramethyl-2,5-dihydro-1H-pyrrol-3-yl)methyl Methanethiosulfonate (MTSL) to produce the spin labelled side chain V46R1 in the presence or absence of the additional mutation K56Q. PELDOR measurements produced stable distance distributions both in the presence and absence of K56Q for octameric H3 V46R1. The modal distance between spin labels increased slightly from 6.03 nm to 6.24 nm in the presence of the acetyl mimic K56Q (Figure 12). This relatively small increase in the distance distribution may be more significant in the H3/H4 tetramer as the loss of the H2A C-terminal extension may lead to the destabilisation of the H3 αN helix which could be somewhat compensated for by the K56Q mutation.

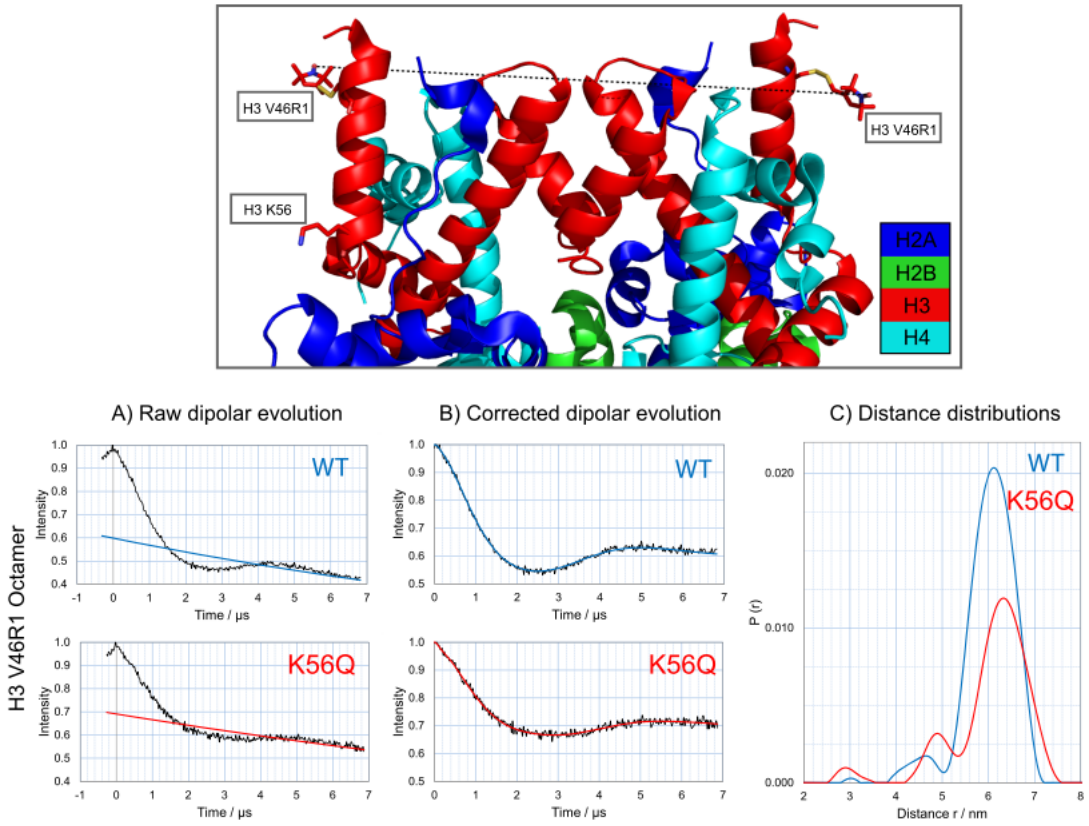

Figure 12 – H3 V46R1 Octamer PELDOR EPR data. *Top:* Crystal structure of histone octamer (pdb: 1TZY) with histones H2A, H2B, H3 and H4 coloured as per key. *Bottom:* H3 V46R1 octamer PELDOR EPR data in a wild type (blue) and K56Q mutant (red) background. (A) Raw dipolar evolution functions (B) Background corrected dipolar evolution functions (C) Tikhonov distance distributions. * Data for wild type EPR samples for the histone octamer and tetramer is re-plotted from Bowman, Ward et al. 2010.

No significant stabilisation was observed in the PELDOR distance distributions for *X. laevis* H3 V46R1/H4 tetramers when the K56Q mutation was introduced (Figure 13C). The heterogeneity in the distance distributions for H3 V46R1 tetramers in a wild type and K56Q background is evident not only in the broad distance distribution but also in the raw data which does not show the decaying oscillation which is observed in more structurally homogeneous samples. The source of this heterogeneity could be attributed directly to the αN helix sampling distinct conformations in solution and this would therefore be amplified in the histone tetramer which contains two copies of histone H3. Additionally there are other possible sources of heterogeneity, for instance movements across the tetramerisation interface would confer some degree of heterogeneity to the positioning of the αN helix. Movements in the tetramerisation interface can be reported on by labelling positions in the H4 α2 and α3 helices. Previously residues in this region of H4, E63 of the α2

and T82 of the α3 helix, produced significantly different distance measurements in the histone tetramer compared to the octamer when probed by PELDOR experiments (Bowman, Ward et al. 2010). This suggests that movements in the tetramerisation interface may contribute to the heterogeneity observed in the sample. As such an alternative labelling strategy to probe the αN from sites on histone H4 was explored.

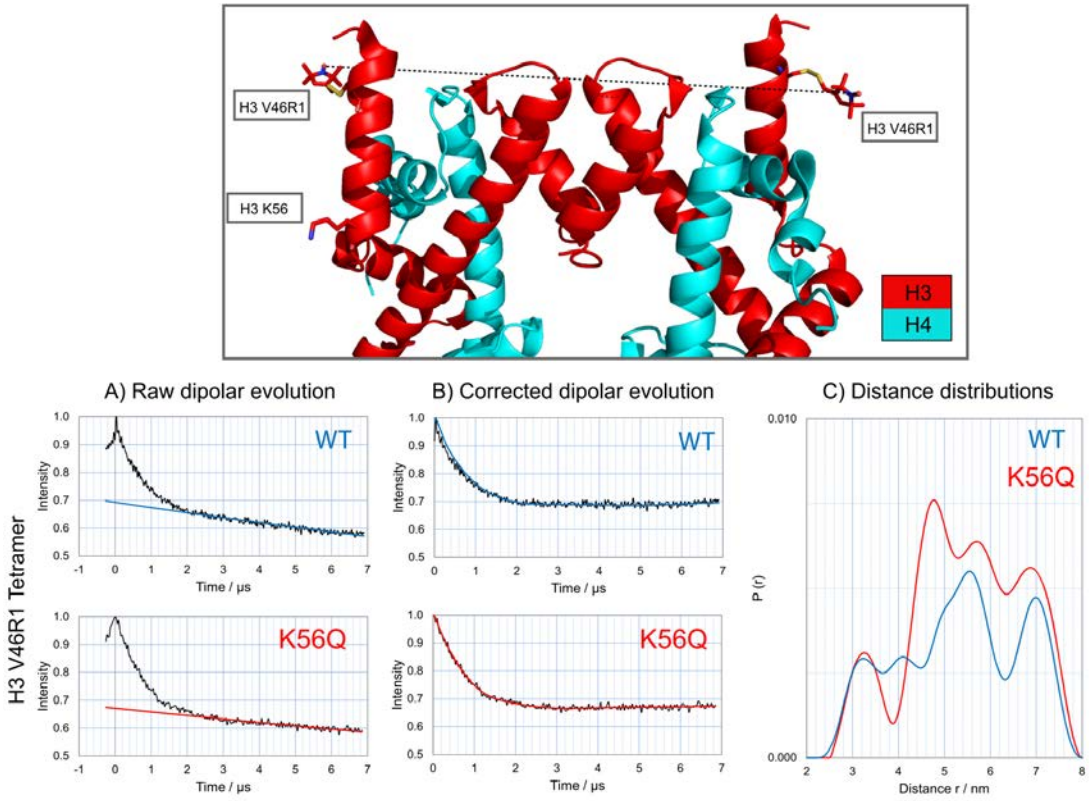

Figure 13 – H3 V46R1 tetramer PELDOR EPR data. *Top:* Model of H3/H4 tetramer extracted from the crystal structure of histone octamer (pdb: 1TZY) with histones H3 and H4 coloured as per key. *Bottom:* H3 V46R1 tetramer PELDOR EPR data in a wild type (blue) and K56Q mutant (red) background. (A) Raw dipolar evolution functions (B) Background corrected dipolar evolution functions (C) Tikhonov distance distributions. * Data for wild type EPR samples for the histone octamer and tetramer is re-plotted from Bowman, Ward et al. 2010.

3.2.3 The stabilising effect of the acetyl lysine mimic K56Q on the αN region of H3 is observed when probed at high resolution from H4 in the presence of Asf1.

In order to probe the αN in more detail the H3/H4 tetramer was split by Asf1 enabling spin labelling positions in H4 to be utilised to probe the H3 αN V46R1 position whilst maintaining a two spin system. For this purpose residues N25 and T30 of H4 where chosen on the basis that they provide homogeneous distance distributions in the context of the histone tetramer and octamer (Bowman, Ward et al. 2010).

No oscillation was observed in the raw PELDOR data for wild type H3 V46R1 to H4 N25R1 in the presence of Asf1 (Figure 14A) and following background correction (Figure 14B) and Tikhonov transformation, a broad distance distribution was observed (Figure 14C). However, in the presence of K56Q an oscillation was observed in the raw dipolar evolution function (Figure 14A), with a periodicity of ~0.5 μs from peak to peak, which upon background correction (Figure 14B) and Tikhonov transformation gave a significantly more homogeneous distance distribution than wild type with a modal distance of 2.90 nm and an additional minor distance of 3.55 nm (Figure 14C).

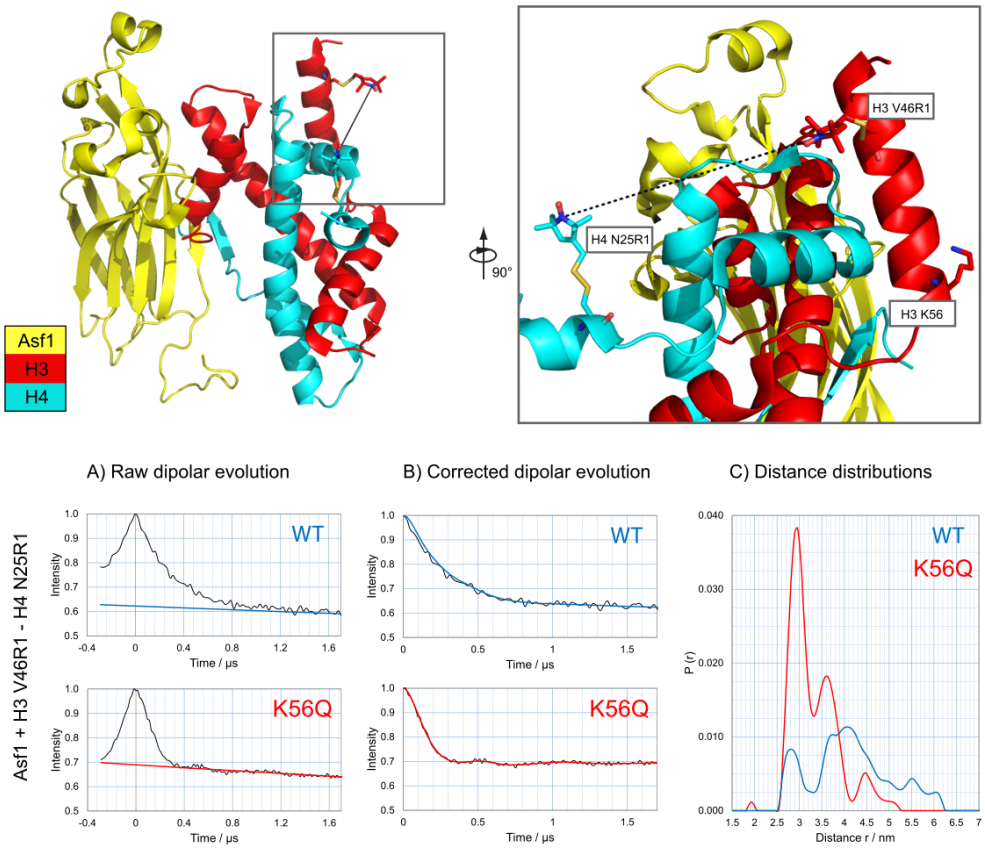

Figure 14 - Asf1 + H3 V46R1 – H4 N25R1 PELDOR EPR data. *Top left:* Crystal structure of Asf1 (yellow) in complex with the H3/H4 dimer (in red and cyan respectively) – pdb code 2HUE. Note: the αN helix is modelled in by aligning to H3/H4 dimer in the histone octamer – pdb code 1TZY. *Top right:* Location of labelling sites used in PELDOR experiments. *Bottom:* Asf1 + H3 V46R1 – H4 N25R1 PELDOR EPR data in a wild type (blue) and K56Q mutant (red) background. (A) Raw dipolar evolution functions (B) Background corrected dipolar evolution functions (C) Tikhonov distance distributions.

Again in the case of wild type H3 V46R1 to H4 T30R1 in the presence of Asf1 the PELDOR data showed no oscillation in the dipolar evolution function (Figure 15A) and following background correction (Figure 15B) and Tikhonov transformation, a broad distance distribution was observed (Figure 15C). Once again, the presence of K56Q had a stabilising effect on the distance distribution of the sample producing an oscillation in the raw dipolar evolution function (Figure 15A), with a periodicity of ~0.5 µs from peak to peak, which upon background correction (Figure 15B) and Tikhonov transformation lead to significantly more homogeneous distance distribution than wild type with a modal distance of 2.85 nm and an additional minor distance of 3.60 nm (Figure 15C).

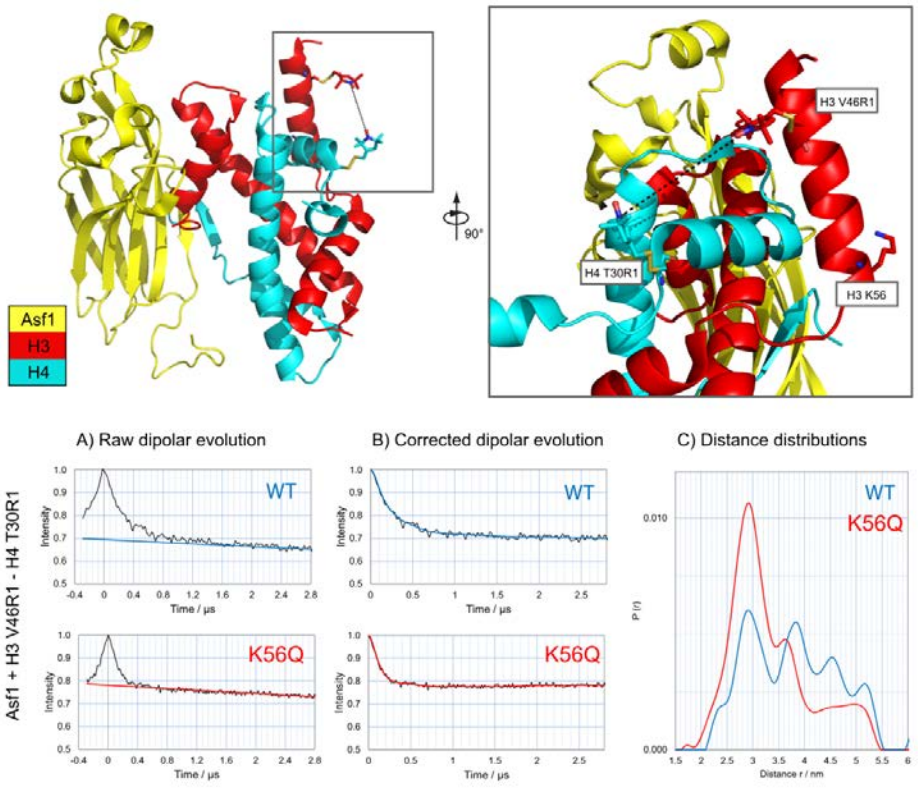

Figure 15 - Asf1 + H3 V46R1 – H4 T30R1 PELDOR EPR data. Top left: Crystal structure of Asf1 (yellow) in complex with the H3/H4 dimer (in red and cyan respectively) – pdb code 2HUE. Note: the αN helix is modelled in by aligning to H3/H4 dimer in the histone octamer – pdb code 1TZY. Top right: Location of labelling sites used in PELDOR experiments. Bottom: Asf1 + H3 V46R1 – H4 T30R1 PELDOR EPR data in a wild type (blue) and K56Q mutant (red) background. (A) Raw dipolar evolution functions (B) Background corrected dipolar evolution functions (C) Tikhonov distance distributions.

Initial measurements indicated that the αN helix may be adopting an alternative conformation to the canonical αN helix from this histone octamer. Therefore in order to get an indication as to the direction in which the H3 αN helix had relocated the H3 αN labelling site V46R1 was further probed from H4 R45R1. As in the previous cases no oscillation was observed in the dipolar evolution function for the wild type H3 V46R1 to H4 R45R1 in the presence of Asf1 (Figure 16A) and following background correction (Figure 16B) and Tikhonov transformation, a broad distance distribution was observed (Figure 16C). The consistent stabilising effect of K56Q was again observed with a complex oscillation in the raw dipolar evolution function (Figure 16A), which upon background correction (Figure 16B) and Tikhonov transformation lead to a significantly

more homogeneous distance distribution than the wild type distribution with a modal distance of 2.05 nm and an additional minor distance of 3.90 nm (Figure 16C).

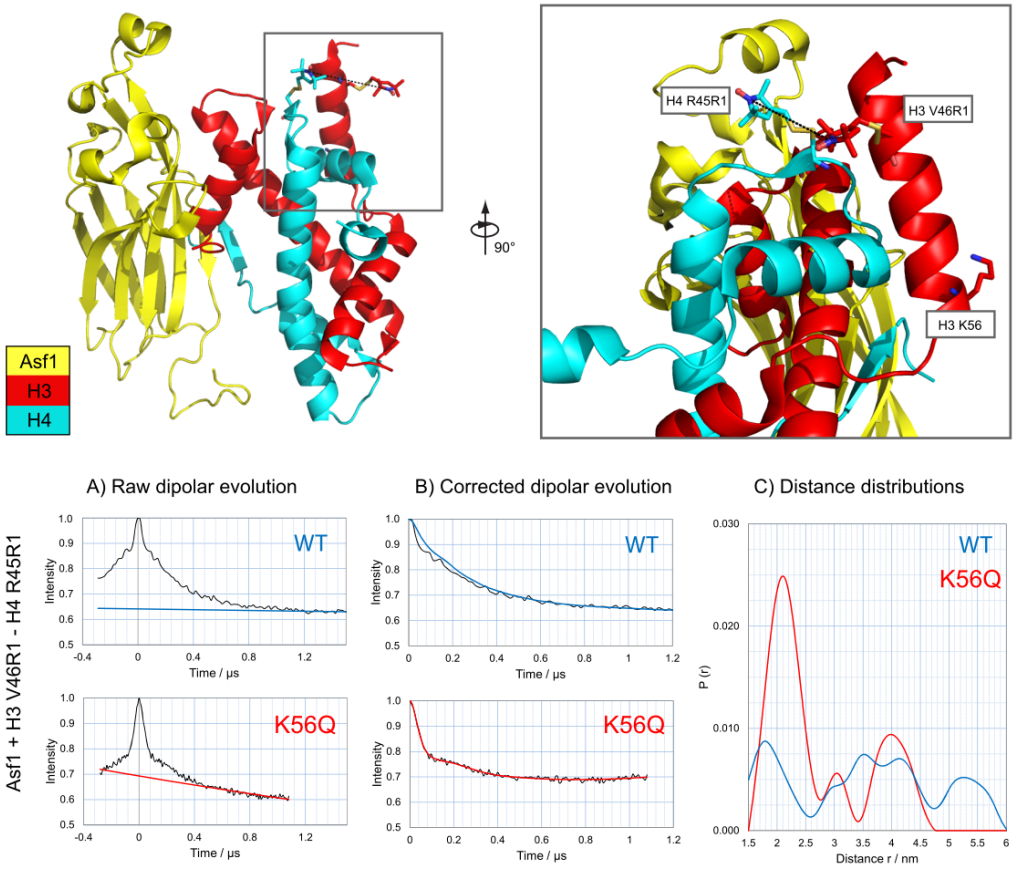

Figure 16 - Asf1 + H3 V46R1 – H4 R45R1 PELDOR EPR data. *Top left:* Crystal structure of Asf1 (yellow) in complex with the H3/H4 dimer (in red and cyan respectively) – pdb code 2HUE. Note: the αN helix is modelled in by aligning to H3/H4 dimer in the histone octamer – pdb code 1TZY. *Top right:* Location of labelling sites used in PELDOR experiments. *Bottom:* Asf1 + H3 V46R1 – H4 R45R1 PELDOR EPR data in a wild type (blue) and K56Q mutant (red) background. (A) Raw dipolar evolution functions (B) Background corrected dipolar evolution functions (C) Tikhonov distance distributions.

3.2.4 Locating the αN helix of H3 in the Asf1-H3/H4 complex using PELDOR distance measurements

As mentioned previously initial measurements indicated the possibility that the αN helix adopts an alternative conformation to the canonical αN helix. The distance distributions for H3 V46R1-H4 N25R1 and H3 V46R1-

H4 T30R1 in the presence of K56Q are similar (Figure 14C and Figure 15C), with modal distance distributions centred at 2.90 and 2.85 nm respectively and both with minor distributions centred around 3.55 nm. However, when these distances were modelled with MtsslWizard (Hagelueken, Ward et al. 2012) using the crystal structure of Asf1 bound to H3/H4 (with the αN region modelled in an octameric conformation large deviations from the experimental data were observed. The MtsslWizard simulated distance distribution for H3 V46R1 – H4 N25R1 gave an average distance of 2.53 nm (*cf.* 2.90 nm from EPR data) and V46R1 – H4 T30R1 gave an average distance of 1.62 nm (*cf.* 2.85 nm from EPR data). The distance distribution for H3 V46R1 – H4 R45R1, simulated by MtsslWizard, gave a distance of 1.41 nm (cf. 2.10 nm from EPR data) with a minor distribution centred at 3.90 nm (Table 6). The average deviation of each distance measured to that simulated with the αN helix in a octameric configuration was 0.84 nm or 8.4 Å (RMSD). The significant deviation between the experimental data and the simulated data lead to the conclusion that the αN was adopting an alternative conformation to that in the histone octamer.

The H3.3 αN helix is known undergo a large conformational change (Figure 17) when associated with the histone chaperone Daxx (Elsässer, Huang et al. 2012; Liu, Xiong et al. 2012). Although the histone chaperone Daxx covers nearly 40% of the H3.3/H4 surface and no doubt contributes to conformational changes in H3.3, the fact that the αN helix extends C-terminally in a manner similar to that indicated by CD data (Section 3.2.1) a similar structural change may be exerted by K56 acetylation. Therefore distance measurements from V46R1 in the Daxx conformation were simulated to H4 positions from the Asf1-H3/H4 crystal structure. In this instance the correlation between distances measured and those simulated was even poorer than with the αN in an octameric conformation with an average RMSD of 1.75 nm per measured distance (Table 6). Clearly, in this case the acetyl lysine mimic K56Q does not cause the αN helix to fully adopt a Daxx like conformation. As none of the crystallographically determined orientations of the H3 αN were able to satisfy the EPR distance restraints an alternative approach to locate the position of the V46R1 spin label was pursued.

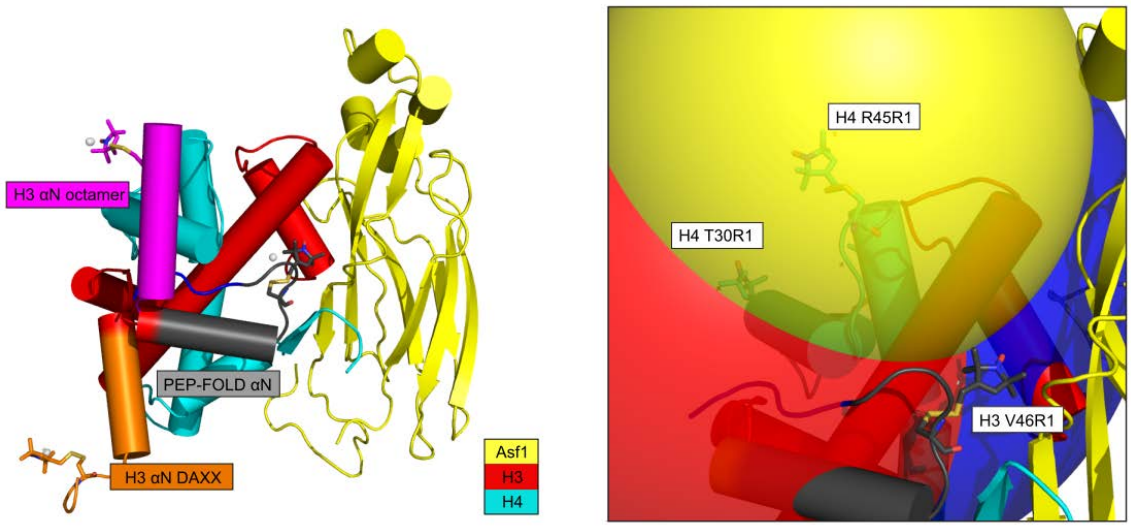

Figure 17 – Locating the αN helix from PELDOR distance measurements on the Asf1-H3/H4 complex. L*eft:* Crystal structure of Asf1 (yellow) in complex with the H3/H4 dimer (in red and cyan respectively) – pdb code 2HUE. The αN helix (P43-S57) modelled from: the histone octamer (pdb code 2HUE) in magenta, the Daxx H3.3/H4 structure (orange), and the PEP-FOLD predicted structure modelled in an orientation to satisfy EPR distance measurements (grey). The positions of V46R1 labels for the three models are show as sticks coloured by chain with the average nitroxide position of simulated side chains shown as a light grey sphere. *Right:* Spheres with radii equal to the respective modal distance from H3 V46R1 centred on the average position of H4 N25R1 (blue), T30R1 (red) and R45R1 (yellow) as modelled with pseudoatoms in PyMOL. Only the PEP-FOLD αN model is shown for clarity with the position of H3 V46R1 shown in stick representation coloured grey, H4 R45R1 and T30R1 can be seen within the semi-transparent spheres but H3 N25R1 is obscured.

Spheres with radii equal to the respective modal distance from H3 V46R1, as obtained from PELDOR measurements (Table 6), were placed at the average spin label location of H4 N25R1, T30R1 and R45R1. The intersection of the three spheres enabled an estimation of the modal location of the V46R1 spin label to be made. As can be seen the V46R1 spin label occupies a position which deviates significantly from its position in either the canonical octamer αN or the position occupied when in complex with the histone chaperone Daxx (Figure 17). In order to satisfy this positional restraint, the trajectory of αN helix would have rotate nearly 90^{o} towards Asf1, this motion would be incompatible with the canonical αN helix due to the number of steric clashes produced. However, using the representative PEP-FOLD predicted structure for the K56Q P38-I62 peptide (Figure 11) this motion is less sterically hindered as the N-terminus of the canonical αN helix folds down alongside a helical segment of the αN that starts at leucine 48. The precedence for the helical segment of the αN starting around L48 is also set by the structure of H3.3/H4 in complex with Daxx. Such a

90^{o} shift in trajectory of the αN helix may be initiated by the nucleation of alpha helical structure C-terminally to K56 as a result of the acetylation as describe previously (Section 3.2.1).

H3 V46 - H4 N25R1	Octamer	Daxx	PEP-FOLD
Average simulated distance / nm	2.53	4.33	2.93
Modal EPR distance / nm	2.90	2.90	2.90
Distance deviation / nm	-0.37	1.43	0.03
H3 V46 - H4 T30R1			
Average simulated distance / nm	1.62	3.50	2.83
Modal EPR distance / nm	2.85	2.85	2.85
Distance deviation / nm	-1.23	0.65	-0.02
H3 V46 - H4 R45R1			
Average simulated distance / nm	1.41	4.70	2.25
Modal EPR distance / nm	2.10	2.10	2.10
Distance deviation / nm	-0.69	2.60	0.15
Average RMSD of each distance / nm	0.84	1.75	0.09

Table 6 - Comparison of distance EPR distance measurements with those simulated with MtsslWizard for the αN helix in an octameric (pdb code – 1TZY), Daxx-like (pdb code – 4H9N) and PEP-FOLD

3.3 Discussion

The acetylation of lysine 56 of histone H3 has sparked a lot of interest in the chromatin field due to the location of the modification in the core of the histone octamer within the nucleosome. How the modification can be regulated within the context of the nucleosome is debateable as it is located underneath the gyres of the DNA. Indeed, Rtt109 has been shown to be inactive towards nucleosomal H3 (Han, Zhou et al. 2007). Whether the K56 histone deacetylases Hst3 or Hst4 are capable of acting on a nucleosomal substrate has yet to be deciphered. As the peak of K56 acetylation is during S-phase (Li, Zhou et al. 2008), a stage of the cell cycle with high levels of nucleosome turnover an alternative hypothesis is that K56 acetylation is exerting its effect on an intermediate of the assembly and disassembly process. This may be mediated by the enrichment of H3 acetylated at K56 acetylation in histone chaperones CAF-1 and Rtt106 complexes (Li, Zhou et al. 2008; Su, Hu et al. 2012). Lysine 56 acetylation has also be shown to promote nucleosome reassembly following double strand break repair (Chen, Carson et al. 2008).

The results described here show that K56 acetylation has a stabilising effect on the structure of histone H3 both in peptides and in biologically relevant full-length protein complexes. One intriguing possibility is that K56 acetylation propagates helical structure beyond the C-terminus of the canonical αN helix of the histone octamer and nucleosome. This could completely alter the trajectory of the αN helix in a manner similar to that observed in the case of the crystal structure of the H3.3 specific chaperone Daxx in complex with H3.3/H4 (Elsässer, Huang et al. 2012; Liu, Xiong et al. 2012). Such a change in trajectory of the helix may allow the handover from one chaperone to another, for example upon acetylation at K56 by Rtt109 the conformational change could stimulate the handover of H3/H4 dimers from Asf1 to Vps75. Additionally if the H3 tail was to fold down the side of the αN helix as per the PEP-FOLD predicted structure it may make the H3 tail residues K9 and K27 residues more amenable for acetylation in the Rtt109-Vps75 complex. Upon acetylation the charge neutralisation at K9 and K23, and to a lesser extent K14, K18 and K27 (Abshiru, Ippersiel et al. 2013), along with the structural transition exerted by K56 acetylation may act to prevent the tails interacting with DNA during the assembly of H3/H4 tetrasome in order to direct properly assembled nucleosomes.

It should be noted that the minor distance distributions observed experimentally at 3.55 nm for H3 V46R1 - H4 N25R1 (Figure 14), 3.55 nm for H3 V46R1 - T30R1 (Figure 15) and 3.90 nm for H3 V46R1 - H3R45R1 (Figure 16) may describe a small population of the H3 with the αN in an alternative conformation. Thus although K56Q has a stabilising effect on the structure of the H3 αN, there still remains a dynamic aspect to the region and to fully stabilise αN helix may require additional binding partners.

The full structural effect of K56 acetylation is only apparent when H3/H4 is present in a complex with Asf1. Competing structural effects in the histone octamer, such as stabilisation of the αN helix by the H2A C-terminal extensions and additional structural heterogeneity in the H3/H4 tetramer as a result of lateral movements across the tetramerisation interface and the presence of two copies of H3 may mask the true effect of K56 acetylation in these complexes. Nethertheless, structurally characterising K56 acetylation when in complex with Asf1 has significance in a biological context due to the requirement of Asf1 for K56 acetylation (Fillingham, Recht et al. 2008) and the fact that Asf1 co-immunoprecipitates with Rtt109 (Tsubota, Berndsen et al. 2007).

The advantage of the EPR approach taken here in assessing the structural effect of K56 acetylation on the structure of the H3 αN region is the techniques ability to identify conformational differences induced by acetylation and provide distance restraints for modelling purposes. The combined approaches of circular dichroism provide a good degree of confidence that the modification of K56 is having a stabilising effect on the H3 tail. However, identifying the final structure of the modified protein has inherent flaws as assumptions have to be made about secondary structure elements and that conformational changes are enacted by hinge type movements in loop regions. Nethertheless, this is the first documented case of a transition in tertiary structure of histone H3 promoted by the acetylation of a single lysine residue and raises an interesting mechanistic insight as to the effect of K56 acetylation. Of course higher resolutions approach such as X-ray crystallography or NMR may provide a more detailed picture of the structural effect of K56 acetylation. However these approaches are also not without their disadvantages.

4 The characterisation of Vps75 and Nap1 tetramers *in vitro*.

4.1 Introduction

Nucleosome Assembly Protein 1 (Nap1) was first identified from the cytoplasmic fraction of HeLa S3 cells and was found to bind all four core histones and facilitate nucleosome assembly reactions *in vitro* (Ishimi, Yasuda et al. 1983). The subsequent cloning of budding yeast Nap1 (Ishimi and Kikuchi 1991) allowed for further biochemical characterisation of the protein and ultimately the determination of its structure by x-ray crystallography (Park and Luger 2006). Another budding yeast protein Vacuolar protein sorting 75 (Vps75), named as a result of its identification in a genetic screen for factors affecting vacuolar protein sorting (Bonangelino, Chavez et al. 2002), was re-classified as a histone chaperone due to sequence homology to Nap1 (Selth and Svejstrup 2007). Like Nap1, Vps75 is capable of forming high affinity complexes with all core histones thus confirming the histone chaperone function of the protein (Selth and Svejstrup 2007; Tsubota, Berndsen et al. 2007; Andrews, Downing et al. 2008; Park, Sudhoff et al. 2008). Unsurprisingly the close functional relationship and sequence homology of Vps75 and Nap1 is mirrored in the homologous three dimensional fold of the proteins as determined by X-ray crystallography (Park and Luger 2006; Berndsen, Tsubota et al. 2008; Park, Sudhoff et al. 2008; Tang, Meeth et al. 2008).

NAP-1 fold proteins form homo-dimers in the confines of a crystal lattice with a characteristic headphone fold motif (Park and Luger 2006; Berndsen, Tsubota et al. 2008; Park, Sudhoff et al. 2008; Tang, Meeth et al. 2008). A long α-helical segment located towards the N-terminus contributes to the dimerisation of the polypeptide which self-associates in an antiparallel coiled-coil like configuration. The dimerisation domain is capped at the C-terminus by a globular domain consisting of a four strand antiparallel β-sheet which stacks upon alpha helical segments of the protein (Figure 18A and B). The surfaces of these proteins are highly hydrophilic and the relative orientation of the two globular domains in the dimer, thought to mediate protein-protein interactions, creates a concave acidic surface which may form the histone binding surface (Figure 18C). Nap1 contains additional features to Vps75 which are involved in the shuttling of histones in and out of the nucleus (Mosammaparast, Ewart et al. 2002; Mosammaparast, Del Rosario et al. 2005). The β-hairpin

extensions attached to the globular domain, which extend like wings of a plane from the globular domains and are highly basic in nature, contain an annotated nuclear localisation signal; and a short helical segment at the N-terminus of the protein which folds over the antiparallel helices in a manner obscuring an annotated nuclear export sequence in the protein (Figure 18A and B) (Park and Luger 2006; Zlatanova, Seebart et al. 2007). These accessory domains may have functional roles in addition to the nuclear trafficking of histones that are yet to be discerned. Vps75 also has an extra helical segment which is highly basic in nature and may overlap functionally with the Nap1 β-hairpin wings (Figure 18B).

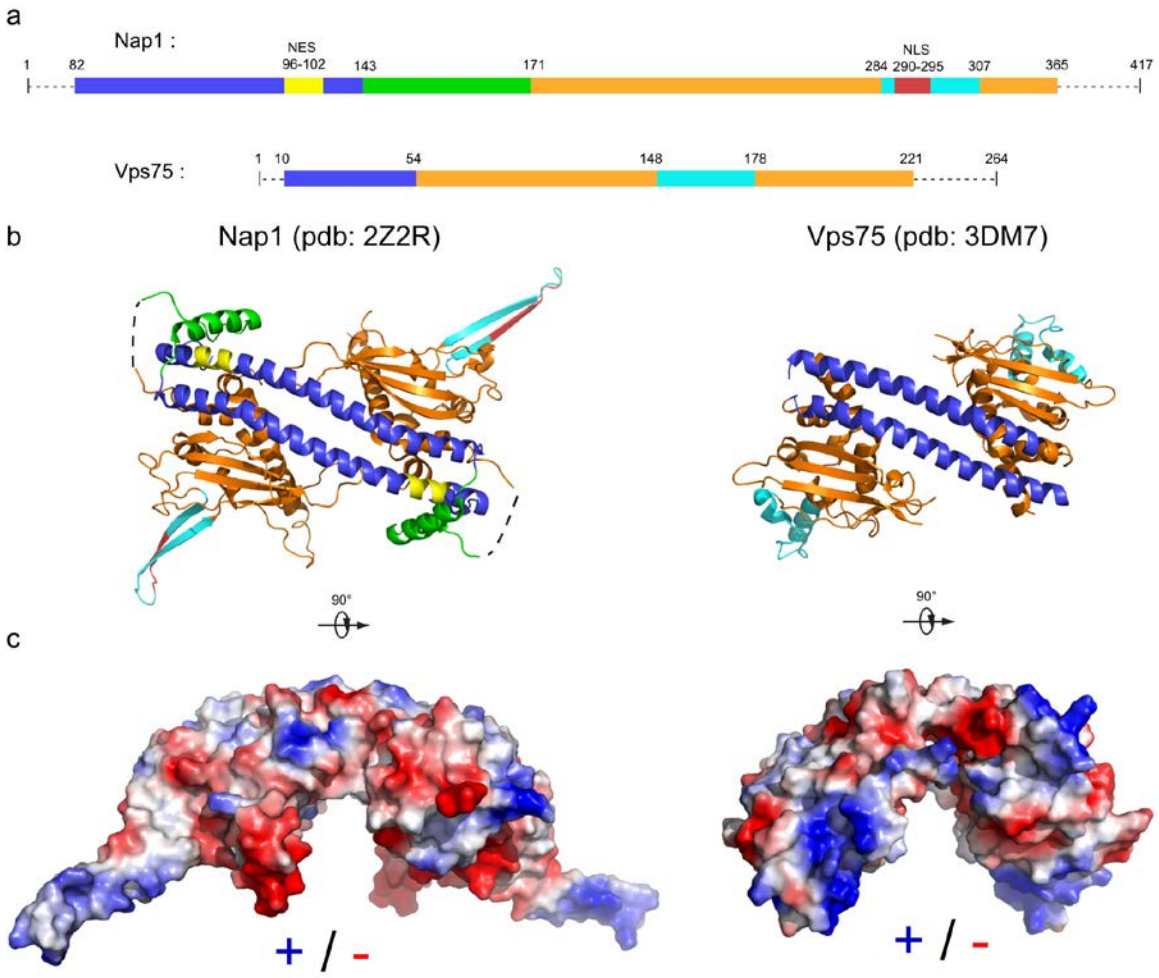

Figure 18 – A structural overview of the NAP-1 fold chaperones Nap1 and Vps75. (a) Colour coded features of Nap1 and Vps75 with residue locations noted. The antiparallel helices that form the dimerisation domain are seen in blue, the globular domains of the headphone fold in orange, secondary structural elements not conserved but highly basic in nature are indicated in cyan. In the case of Nap1 a nuclear localisation signal (red) is located in the β-hairpin extensions from the globular domains and a nuclear export signal (yellow) masked by an additional helical segment (green) not observed in Vps75. (b) the structure of Nap1 and Vps75 colour coded as in panel a. (c) Surface charge representation of Nap1 and Vps75 rotated 90^{o} from the representation in panel b. Figure adapted (Zlatanova, Seebart et al. 2007).

In addition to binding histones, Vps75 is also found stably associated with the histone acetyl-transferase Rtt109 (Krogan, Cagney et al. 2006; Selth and Svejstrup 2007) and stimulates the HAT activity of Rtt109 over 250 fold (Kolonko, Albaugh et al. 2010). Fluorescent anisotropy experiments (Park, Sudhoff et al. 2008) have been used to show that the interaction of Vps75 with Rtt109 is much weaker (~ 5 μM) than the interaction of either component in isolation with histones H3/H4 (~25 nM and 150 nM respectively). The fact that the full length Vps75 stimulates Rtt109 activity ~30 fold over the truncated form (Vps75 1-222) which

has a higher affinity for H3/H4 (13 nM) suggests that the stimulation of HAT activity by Vps75 is not solely a result of increasing the affinity of Rtt109 for histones. The same study found that although Nap1 can bind Rtt109, the chaperone does not stimulate the HAT activity of Rtt109 towards histone H3/H4. Another difference in activity between the two chaperones highlighted was the ability of Nap1 to remove H2A/H2B from nucleosomes in vitro which is not paralleled by Vps75.

Structural analyses of Vps75/Rtt109 complexes have revealed two distinct configurations with one or two copies of Rtt109 (Kolonko, Albaugh et al. 2010; Su, Hu et al. 2011; Tang, Holbert et al. 2011). Despite differing stoichiometries, the surface of Vps75 to which Rtt109 binds is similar in both structures (Figure 19). Rtt109 is an acetyl coenzyme A dependent acetyl transferase which requires auto acetylation at residue K190 for catalytic activity (Stavropoulos, Nagy et al. 2008). As can be seen by the superimposition of the Rtt109 structure in complex with acetyl-CoA with K190 acetylated (Stavropoulos, Nagy et al. 2008) with the 2:2 and 2:1 complexes, the active site of Rtt109 is buried in the core of the enzyme. Thus stable binding of H3/H4 to a histone chaperone may be a requirement for the acetylation of H3 tail residues, which are thought to be fairly dynamic in solution. Due to the lack of information regarding the stoichiometry of the Vps75-Rtt109 complex *in vivo*, the physiological relevance of the two alternate structures has yet to be addressed (reviewed by (D'Arcy and Luger 2011)).

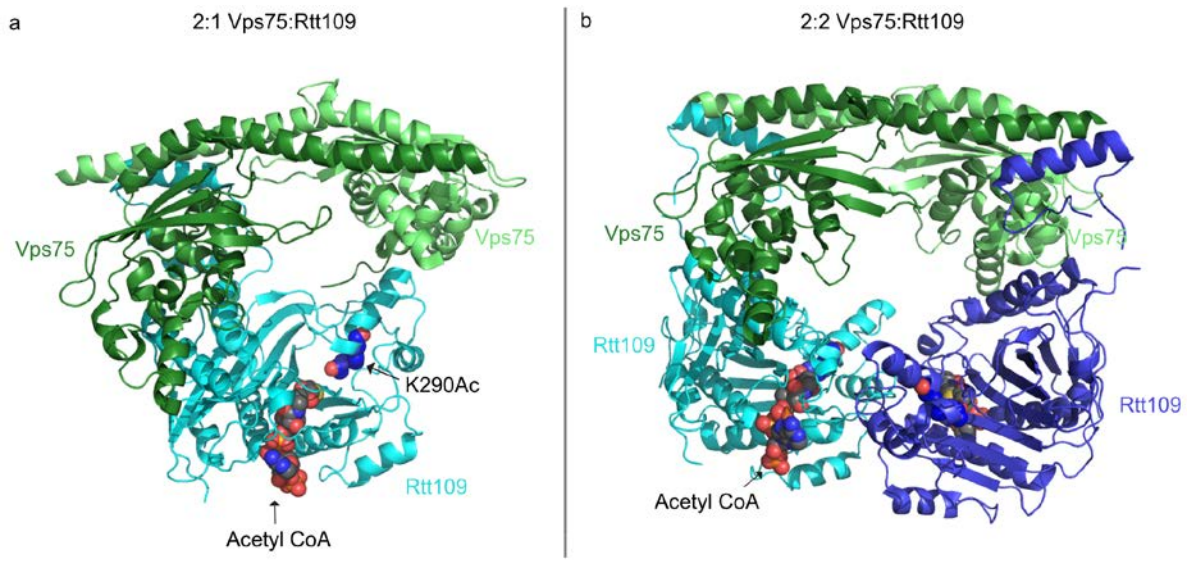

Figure 19 – Stoichiometric assemblies of Vps75 and Rtt109 with Acetyl CoA and the auto acetylated Rtt109 residue lysine 290 highlighted which define the Rtt109 active site. (a) The crystal structure of Vps75 with Rtt109 in a 2:1 stoichiometry (pdb: 3Q66 - Su, Hu et al. 2011), the auto acetylated residue K290 and Acetyl CoA binding site are highlighted by alignment to a separate crystal structure (pdb: 3CZ7 – Stavropoulos, Nagy et al. 2008). (b) The crystal structure of the 2:2 complex of Vps75 and Rtt109 (pdb: 3Q68 Tang, Holbert et al. 2011), the auto acetylated residue K290 and acetyl-CoA binding site are highlighted by alignment to a separate crystal structure (pdb: 3CZ7 - Stavropoulos, Nagy et al. 2008).

Vps75 is transcribed throughout the cell-cycle whereas Rtt109 transcripts peak during S-phase in a similar manner to histone expression and H3 K56 acetylation levels (Pramila, Wu et al. 2006; Driscoll, Hudson et al. 2007; Li, Zhou et al. 2008; Selth, Lorch et al. 2009; Kolonko, Albaugh et al. 2010). The *in vivo* expression profiles of Vps75 and Rtt109 suggests a role for Vps75 that is independent of Rtt109. It is possible that when in complex with Rtt109, Vps75 functions in DNA replication and repair pathways however an Rtt109 free pool of Vps75 may be present outside of S-phase with distinct functions in processes such as transcription.

Although dimeric under high salt conditions Nap1 has been shown to form soluble aggregates in a concentration dependent manner under physiological conditions (McBryant and Peersen 2004; Toth, Mazurkiewicz et al. 2005; Newman, Kneale et al. 2012). The exact nature of these self-associated states of Nap1 and their physiological relevance remains unclear, although they can be disrupted by mutations which likely disrupt secondary structure in the β-hairpin wings of Nap1 which form an extended antiparallel β-sheet in the crystal lattice (Park, McBryant et al. 2008).

4.2 Results

In the following section all samples relating to Vps75 pulsed EPR experiments were prepared by Dr Andrew Bowman, Dept. Physiological Chemistry, Adolf Butenandt Institute, Butenandtstr., 581377 Munich, Germany. Modelling of the Vps75 tetramer from EPR distance measurements was performed by Dr David Norman, College of Life Sciences, 5 Dow Street, University of Dundee, Dundee, DD3 5EH, United Kingdom. All EPR data was acquired by Dr Hassane El Mkami, College of Life Sciences, School of Physics and Astronomy, University of St-Andrews, KY16 9SS, United Kingdom. This section was prepared alongside a manuscript submitted for publication by Bowman and Hammond et. al. 2013

4.2.1 Vps75 forms tetramers under physiological conditions

Vps75 has previously been characterised as a homo-dimer in solution and by x-ray crystallography. However the elution profile of Vps75 varies during size exclusion chromatography (SEC) in a salt concentration dependent manner. At 500 mM NaCl (high salt) Vps75 elutes from an S200 10/300 column (GE Healthcare) at 13.2 ml, however upon reducing the salt concentration to 150 mM NaCl (low salt) the elution volume shifted to 11.3 ml. This suggested the presence of oligomers of Vps75 beyond the dimer, the formation of which is governed by electrostatic interactions which are effectively screened out at high salt. Indeed size exclusion chromatography coupled to inline multi angle light scattering (SEC-MALS) confirmed that at high salt Vps75 was a dimer with a molecular weight of 66.7 kDa (*cf.* 61.2 kDa) which upon reducing the salt concentration produced a species with a mass of 122.6 kDa consistent with a Vps75 tetramer (*cf.* 122.4 kDa) (Figure 20). As the crystal structure of the Vps75 dimer had been previously solved insight into the tetrameric assembly of Vps75 was sought from the relative position of Vps75 dimers within the crystallographic lattice. Although contacts between adjacent Vps75 dimers were observed in the crystal lattice no tetrameric assembly was observed that would eliminate further oligomerisation (not shown).

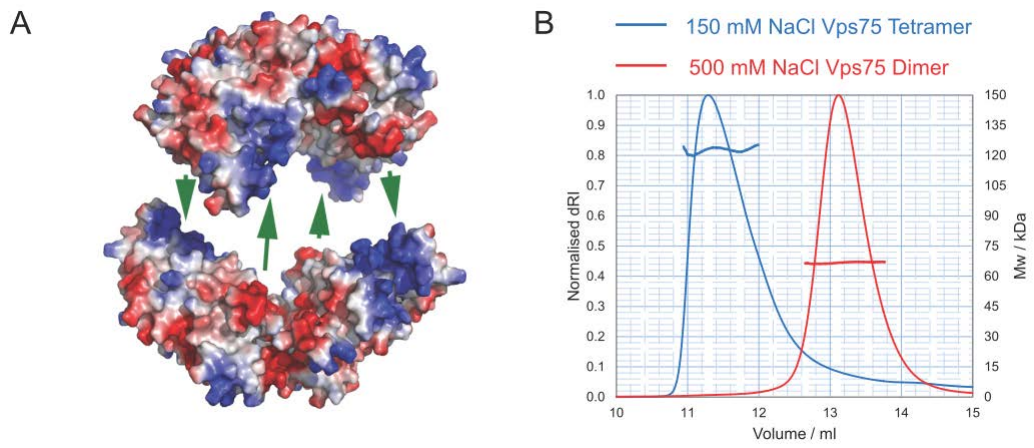

Figure 20 - (A) The basis of the charge complementarity of Vps75 (B) SEC-MALS elution profiles of Vps75 under tetramerising (500 mM NaCl, blue trace) and non-tetramerising conditions (500 mM NaCl, red trace).

As the tetramerisation of Vps75 was abolished at high salt the hypothesis that the tetramerisation interface is composed of complementary electrostatic surfaces was pursued. Indeed acidic and basic patched were observed on the earmuff domains of Vps75 which could interact if Vps75 was to form a ring like tetrameric structure (Figure 20). This type of tetrameric assembly would also provide a rationale for why the oligomerisation of Vps75 does not proceed beyond a tetrameric assembly.

4.2.2 Analysis of the tetrameric structure of Vps75 in solution by SDXSL and PELDOR

A PELDOR EPR approach was taken to further investigate the organisation of the Vps75 tetramer. In order to confirm whether or not the Vps75 tetramer was forming a ring-like structure in solution a distance measurement was sought from one Vps75 dimer to the other to test this hypothesis. In order to maintain a two spin system in the homo-tetrameric Vps75 complex, a site directed cross-link spin labelling (SDXSL) approach was taken to singly label a Vps75 dimer. A suitable site which comes in close proximity with itself on the opposing monomer was identified (Y35) which when mutated to cysteine could be cross-link labelled with the bifunctional cysteine reactive MTSL derived spin label (3,4-Bis-(methanethiosulfonylmethyl)-2,2,5,5-tetramethyl-2,5-dihydro-1H-pyrrol-1-yloxy Radical) to produce the spin labelled side chain Y35RX2 (Figure 21A).

Vps75 produced with the Y35C mutation was efficiently spin labelled with a cross-linking efficiency of ~ 80 % as determined by SDS-PAGE (Figure 21B). Subsequent PELDOR analysis of the Vps75 Y35RX2 sample under tetramerising conditions resulted in a stable oscillation in the raw dipolar evolution function (Figure 21C) which following background correction (Figure 21D) and Tikhonov transformation, produced a sharp distance distribution centred at 7.8 nm (Figure 21E). The modal distance observed could be satisfied by arranging the Vps75 dimers in a ring like conformation however the rotational relationship between the opposing dimers required further restraints to be acquired.

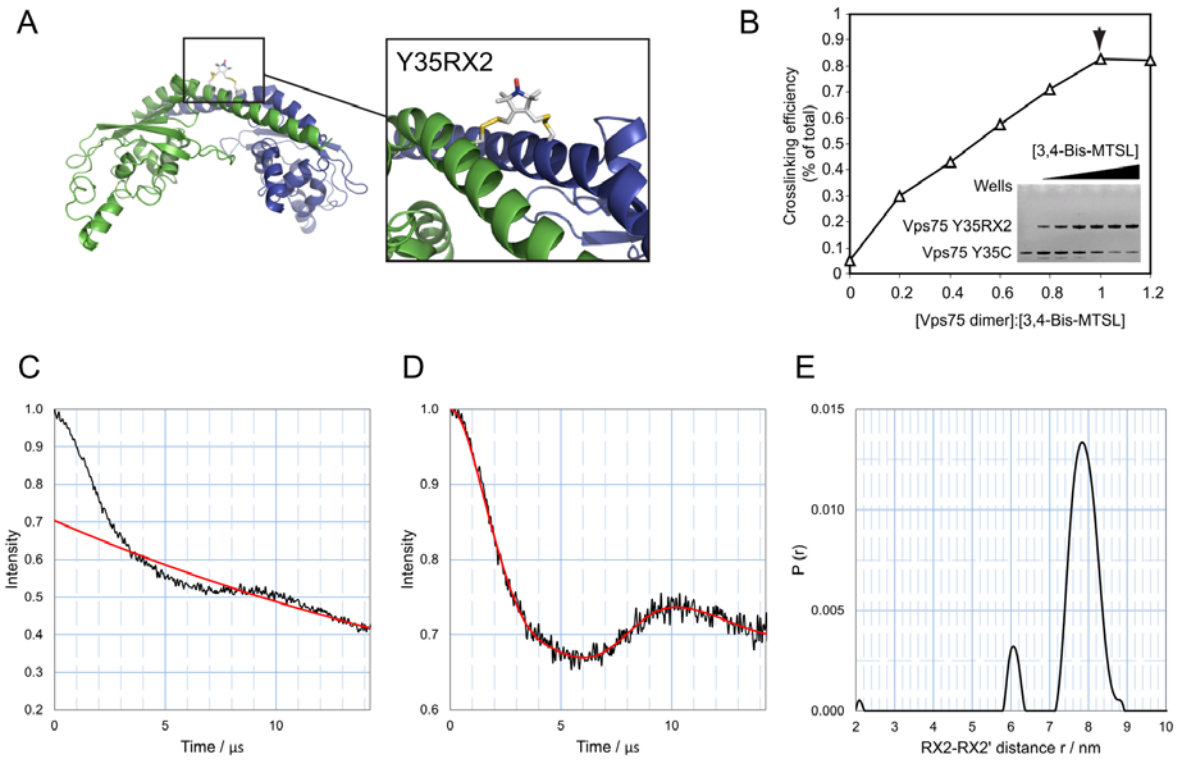

Figure 21 - Probing the structure of the Vps75 tetramer through site-directed cross-linking spin labelling. (A) The position of Y35RX2 in the Vps75 dimer. The boxed expansion shows a possible conformation of the cross-linked spin-labelled residue RX2 at position Y35 determined from molecular dynamic simulations. Monomers are differentially coloured blue and green for clarity. (B) Analysis of site-directed cross-link spin labelling. The compound 3,4-Bis-MTSL was titrated against a constant concentration of Vps75. Cross-linking efficiency was determined by resolving cross-linked from uncross-linked species through separation by SDS-PAGE and quantification of coomassie staining (gel shown in inset). An arrow head indicates a 1:1 ratio of cross-linker to Vps75 dimer. (C) PELDOR dipolar evolution function of Vps75 Y35RX2 at 150 mM NaCl, (D) background corrected dipolar evolution function, (E) Tikhonov distance distribution for Vps75 Y35RX2. The modal distance between Y35RX2 residues is 7.8 nm. *Experiments were performed by Andrew Bowman.

4.2.3 Refinement of the Vps75 tetramer structure using a four-spin system

In order to define the rotational relationship between Vps75 dimers in the tetrameric assembly a four spin EPR labelling approach was taken. In a four spin system one would expect to see, in addition to the intra-dimer labelled AB, two additional distances for the short distance and a longer diagonal distance across the tetramer - labelled AC and AD (Figure 22A). Labelling sites site were designed with a view to resolving the short AB distance in the Vps75 tetramer from other distances in a potentially complex four spin distance distribution. For this purpose the labelling sites E56R1 and K117R1 were chosen. As expected PELDOR analysis of Vps75 E56R1 and K117R1 at high salt resulted in a dipolar evolution function with an oscillation

depth consistent with a two spin dimeric system (Figure 22B – red trace), with respective modal distances of 7.09 nm and 8.47 nm (Figure 22C – red trace).

Upon reducing the salt concentration to 150 mM sodium chloride changes characteristic of tetramerisation were observed in the dipolar evolution functions of both Vps75 E56R1 and K117R1 samples. Firstly the oscillation depth of the dipolar evolution function was observed to drop compared to the same samples under dimeric conditions which indicates more than two spins are interacting in the system. Additionally the gradient of initial drop in the dipolar evolution function is steeper in the tetramer indicating a short distance is appearing which is not present in the comparative high salt dimeric sample (oscillation length is proportional to the distance between spin label). Consistent with these observations short distance were observed in the distance distribution of both Vps75 E56R1 and K117R1 which were assigned as the AC distance across the tetramerisation interface. Additional diagonal distances were observed in both spectra consistent with the expected diagonal AD distance. As the diagonal distances were close to the AB distances across the Vps75 dimer, and may be affected by the overlapping distributions, only the more distinct short AC distances were used as restraints for modelling purposes.

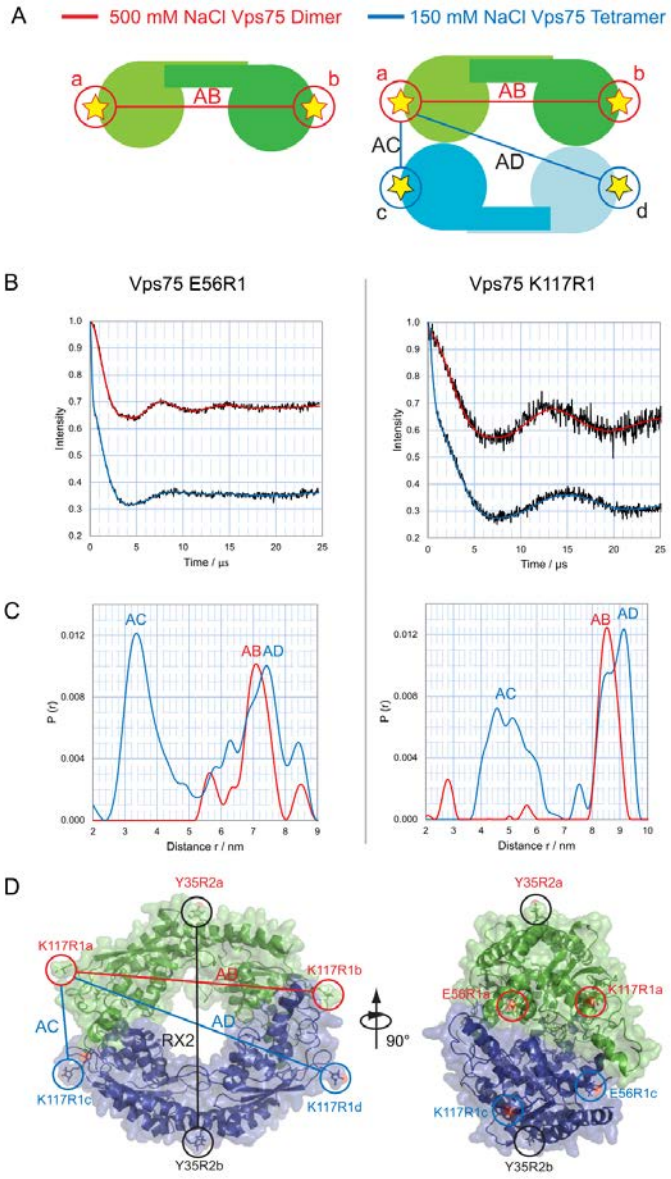

Figure 22 - Probing the structure of the Vps75 tetramer using quadruply labelled complex. (A) Schematic representation of the experimental approach for probing the Vps75 tetramer structure using a four spin label system. In the highly ionic environment of 500 mM sodium chloride the dimeric form of Vps75 is prevalent, giving a single distance AB (left). Under physiologically relevant ionic conditions of 150 mM sodium chloride the tetrameric form is prevalent, resulting in additional distances AC and AD (right). (B) Corrected dipolar evolution for Vps75 E56R1 (left) and Vps75 K117R1 (right) under dimeric (red) and tetrameric (blue) conditions. (C) Distance distributions for Vps75 E56R1 (left) and Vps75 K117R1 (right) under dimeric (red) and tetrameric (blue) conditions. (D) Molecular model of the Vps75 tetramer. The two Vps75 dimers are differentially coloured green and blue for clarity. Left: the 'Ring' model with Y35RX2 and K117R1 labelling sites circled (E56R1 is omitted for clarity). The RX2-RX2' distance is depicted as a black line, the AB distance is shown as a red line and AC and AD distances are shown as blue lines. Right: side view of the Vps75 tetramer with all labelling sites circled. *Experiments were performed by Andrew Bowman

4.2.4 Structure guided mutagenesis identifies residues at the tetramerisation interface.

Upon close inspection, our tetramer model revealed extensive charge complementarity between interacting earmuff domains. An acidic patch on one earmuff domain appeared to interact with a basic patch of another in an orthogonal fashion, providing a basis for the sensitivity of Vps75 to high ionic strengths. To further test our model we generated 8 charge reversal point mutations within this region and tested their ability to

tetramerise through gel filtration chromatography. A number of these mutants significantly affected the elution profile of Vps75 and were found to cluster in the 8th alpha helix of Vps75 and the preceding loop (R164D, K169E and K170E). These proteins were further subjected to SEC-MALS analysis under the tetramerising conditions of 150 mM sodium chloride (Figure 23A). The molecular weight of the aforementioned mutants suggested that the equilibrium of tetramerisation of Vps75 was significantly shifted towards the dimeric form. As such Vps75 R164D (73.2 kDa), K169E (67.8 kDa) and K170E (71.9 kDa) were termed non-tetramerising mutants.

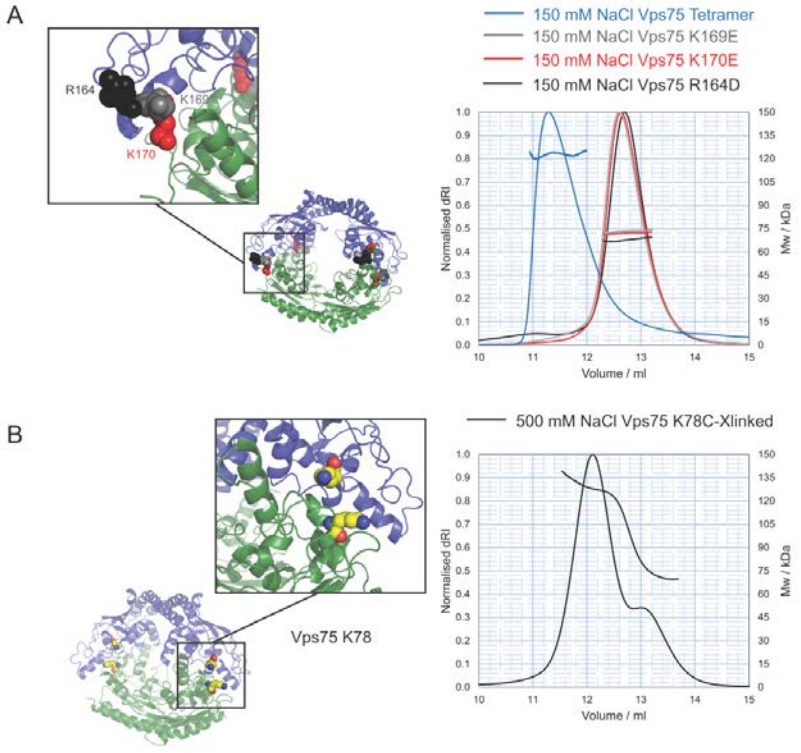

Figure 23 - Mutagenesis defines residues at the Vps75 tetramerisation interface (A) Model of Vps75 tetramer, opposing Vps75 dimers in blue and green, with the positions of non-tetramerising mutants shown as colour coded spheres (left) matching SEC-MALS elution profile colours of the corresponding mutant (right); K169E (grey), K170E (red) and R164D (black). (C) Identification of the cysteine cross-linking site K78 (left – yellow spheres) used to disulphide cross-link the Vps75 tetramer at 150 mM NaCl and the SEC-MALS elution profile of the cross-linked Vps75 K78C tetramer run at 500 mM NaCl (right).

Upon further inspection of the tetramer model derived from EPR measurements, the residue E209 appeared to come into close proximity with itself on the opposite dimer Vps75 within the ring-like tetramer. By mutating E209 to cysteine and using redox potential of Cu (II) Phenanthroline as a catalyst to oxidise the cysteine residues, a disulphide bond was formed at 150 mM sodium chloride across the tetramerisation interface demonstrating that indeed this residues does come into contact with itself in the opposing dimer. Furthermore, the presence of the induced disulphide effectively stabilised Vps75 in its ring-like form, eluting as a tetramer under the high salt conditions that previous resulted in a purely dimeric species (Figure 23B), further validating our molecular model.

4.2.5 The structurally related protein, Nap1, also adopts a tetrameric conformation under physiologically relevant ionic strength

SEC-MALS analysis of Nap1 at 150 mM sodium chloride was consistent with the dominant species in solution being tetrameric in equilibrium with a small proportion of Nap1 dimer with a weight averaged molecular mass of 187.7 kDa (theoretical tetramer 191.5 kDa). As predicted upon raising the salt concentration to 500 mM sodium chloride Nap1 reverts to its dimeric form with a mass of 97.8 kDa (theoretical dimer 95.7 kDa) obtained from SEC-MALS analysis (Figure 24A). The previously reported Nap1 PPP mutant (Park, McBryant et al. 2008), in which three residues within the β-hairpin domain which protrude from the Nap1 earmuff domain are mutated to proline to inhibit secondary structure formation in this region (R301P, T302P, K305P), gives a mass of 98.4 kDa at 150 mM sodium chloride, indicating a predominantly dimeric species (Figure 24B). This implies that indeed the β-hairpin region contributes to the stability of Nap1 tetramers.

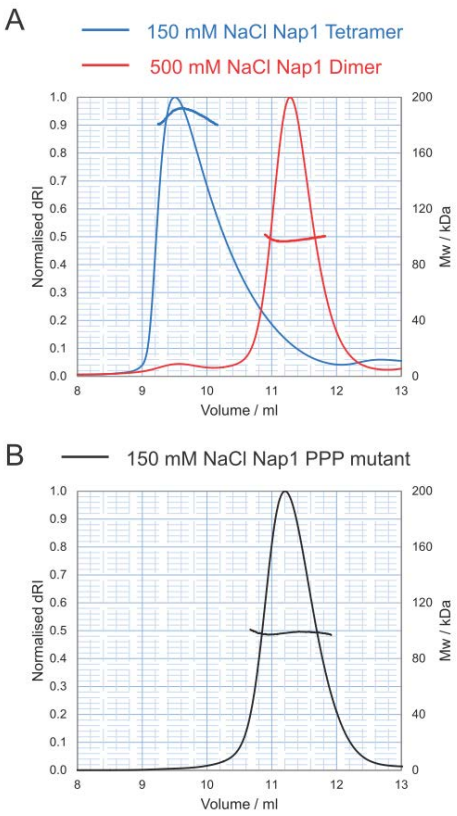

Figure 24 - SEC-MALS analysis of the structurally related protein Nap1 suggests it also adopts a stable tetramer under physiological conditions which maybe mediated by the β-hairpin. (A) SEC-MALS elution profiles of Nap1 at 150 mM (blue) and 500 mM NaCl (red). (B) SEC-MALS analysis of the Nap1 PPP mutant. The molar mass over elution peaks are shown in corresponding colours.

4.2.6 Probing the Nap1 tetramer structure using a four-spin system

The initial RX2 labelling strategy for labelling Nap1 at L120, the equivalent position to the Vps75 RX2 labelling site was unsuccessful. Upon further analysis of the Nap1 L120 site in the crystal structure (pdb: 2Z2R) the site appeared to be more buried than its Vps75 counterpart which may explain the poor labelling efficiency observed for this site.

Due to the lack of a suitable RX2 labelling site the refinement of the Nap1 tetramer model from 4 spin system was attempted. As the β-hairpins of opposing Nap1 dimers are implicated in the tetramerisation of Nap1, as deduced by SEC-MALS analysis of the PPP mutant, the sites T307 on the β-hairpin and E209 in close proximity to this region were chosen as labelling sites. In addition the more distal site T251 was chosen to acquire additional restraints to refine the model. PELDOR analysis of the three MTSL labelled cysteine mutants was performed under tetrameric (150 mM NaCl) and dimeric (500 mM NaCl) conditions.

Background corrected dipolar oscillations of all three labelling sites displayed the characteristic drop in oscillation depth which occurs as a result of the spin labels interacting in the system increasing from 2 at 500 mM sodium chloride to 4 upon tetramerisation at 150 mM sodium chloride (Figure 8B).

As expected, upon tetramerisation short AB distances across the tetramerisation interface were observed in both Nap1 E209R1 and T307R1 distance distributions (Figure 8C). This is also apparent from the initial gradient of the dipolar oscillation becoming steeper at 150 mM compared to 500 mM sodium chloride (Figure 8B). However in the case of Nap1 T251R1 the initial gradient in the dipolar oscillation (Figure 8B) is indistinguishable at both 150 mM and 500 mM sodium chloride. This implies that the shortest distance in the Nap1 T251R1 tetramer is identical to the AB distance in the Nap1 T251R1 dimer and is consistent with the observation of two longer distances in the Nap1 T251R1 150 mM distance distribution which were assigned as AC and AD (Figure 8C).

The complexities of the four spin PELDOR spectra make it difficult to quantify the magnitude of error associated with each interspin distance assigned. Initial modelling experiments suggest that the relative orientation of the Nap1 dimers is similar to that of Vps75. However, upon satisfying the modelling restraints obtained from the distance measurements assigned (Figure 8C) no significant contacts between Nap1 dimers were observed (Figure 8D). In the absence of a 2 spin RX2-RX2' distance measurement in Nap1 it is difficult to ascertain whether this is due to errors associated with each inter-spin distance assigned or whether there are conformational changes in Nap1 upon tetramerisation which may account for this difference. For example, it is foreseeable that the mechanism of tetramerisation is fundamentally different in Nap1 compared to Vps75 and that the positively charged Nap1 β-hairpins bind negative patches on the opposing dimer forming the charge based complementation required for tetramerisation of Nap1. This may account for gaps observed in the interaction surface between Nap1 dimers in the Nap1 tetramer model.

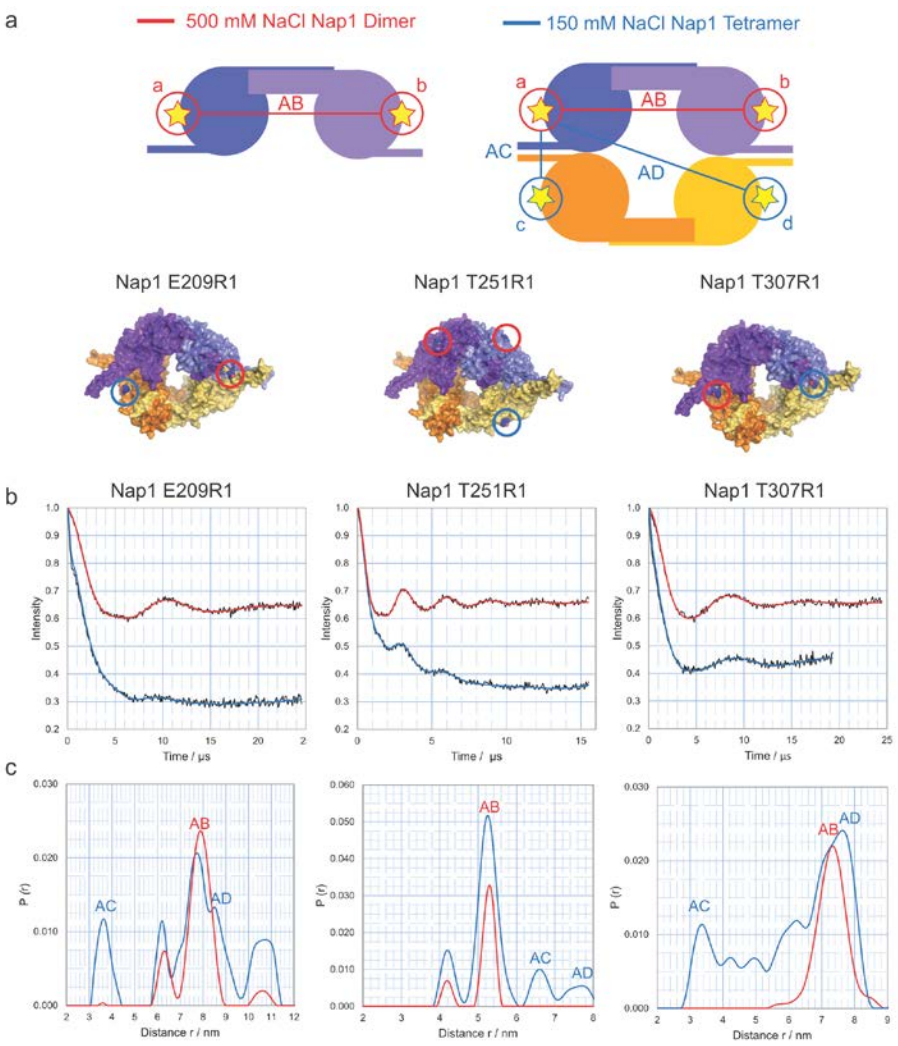

Figure 25 - Probing the structure of the Nap1 tetramer using a 4 spin system. (A) Schematic representation of the experimental approach for probing the Nap1 tetramer structure using a quadruply spin labelled system. In the highly ionic environment of 500 mM sodium chloride the dimeric form of Nap1 is prevalent, giving a single distance AB (left). Under physiologically relevant ionic conditions of 150 mM sodium chloride the tetrameric form is prevalent, resulting in additional distances AC and AD (right). The location of the spin labelling positions in the Nap1 tetramer derived from structural alignment with the Vps75 tetramer are indicated above the relevant PELDOR data. (B) Corrected dipolar evolution for Nap1 E209R1 (left), Nap1 T251R1 (middle) and Nap1 T307R1 (right) under dimeric (red) and tetrameric (blue) conditions. (C) Distance distributions for Nap1 E209R1 (left), Nap1 T251R1 (middle) and Nap1 T307R1 (right) under dimeric (red) and tetrameric (blue) conditions.

In concert, these observations suggest that Nap1, like Vps75, adopts a tetrameric configuration at low salt concentrations, making it possible that the formation of tetrameric ring-like structures is a common feature of Nap1 fold proteins.

4.2.7 Identification of an approach to test potential conformational changes in the β-hairpins of Nap1 induced by tetramerisation

As eluded to in section 4.2.6 there is potential for the β-hairpin extensions of the Nap1 protein to be critical for Nap1 tetramerisation. It is possible that the basic β-hairpin "wings" of Nap1 fold in towards the opposite Nap1 dimer and make electrostatic interactions with the opposite Nap1 dimer where an acidic patch is suitably located in the current Nap1 tetramer model (Figure 26A). Alternatively there is a possibility that the β-hairpins form an extended β-sheet in a similar fashion to that observed in the in the crystal lattice of Nap1 (Figure 26B). The extended β-sheet in the crystal lattice forms in an anti-parallel manner and this type of arrangement would also require the β-sheets to fold in towards the opposing dimer in order to curtail oligomerisation at the tetrameric level. Alternatively the β-hairpins may form an extended β-sheet in a parallel fashion and as such point away from the earmuff domains of Nap1 as seen in the crystal structure (Figure 26C). In order to test this hypothesis a cysteine labelling site was introduced on the Nap1 wings at position T302. The β carbons of T302 are 10.6 nm apart in the Nap1 crystal structure (pdb code = 2ayu) thus in order to measure such a large distance via PELDOR EPR the protein required deuteration.

The deuterated Nap1 protein was labelled with MTSL forming the spin labelled side chain T302R1 and PELDOR EPR measurements at 500 mM sodium chloride confirmed that the β-hairpins extend away from the Nap1 earmuff domains when Nap1 is dimeric, as observed in the crystal structure. The long modal distance of 10.2 nm (Figure 26E – red trace) observed in the Nap T302R1 dimer represents a current record distance measured by EPR and as can be seen in the dipolar evolution function a full oscillation from peak to peak requires a timing window in excess of ~20 us (Figure 26D - red trace).

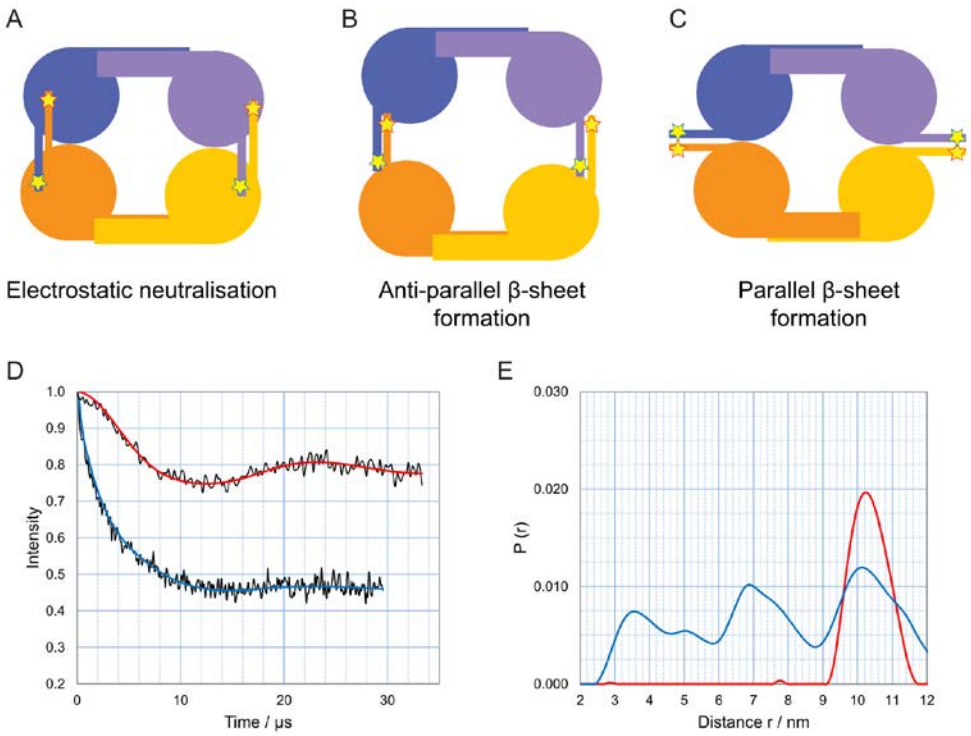

Figure 26 - Potential conformational changes in the Nap1 β-hairpins upon tetramerisation. *Top:* Schematic representation of the proposed Nap1 tetramer models with the β-hairpins (A) acting to neutralise an acidic patch on the Nap1 earmuff domain, (B) forming an extended anti-parallel β-sheet and (C) forming an extended parallel β-sheet. Nap1 dimers are differentially coloured in shades of orange and purple with the approximate location of the Nap1 T302R1 labelling sites depicted as stars. *Bottom:* (D) Corrected dipolar evolution for Nap1 T302R1 (D) at 500 mM NaCl (red) and 150 mM NaCl (blue). (E) Distance distributions for Nap1 T302R1 at 500 mM NaCl (red) and 150 mM NaCl (blue).

When the salt concentration of the sample was dropped to 150 mM NaCl the indicative drop in oscillation depth was observed consistent with tetramerisation of the sample (Figure 26D – blue trace) and upon Tikhonov regularisation a distance distribution with 3 obvious peaks was observed at 3.5, 6.9 and 10.1 nm (Figure 26E – blue trace). In models A and B the intra-dimer distance would shorten significantly upon tetramerisation and the diagonal distance could foreseeably be as long as the intra-dimer distance observed at high salt. However, if upon tetramerisation the β-hairpins form a parallel β-sheet as in model C then the diagonal distance would be almost equal to the intra-dimer distance. As such the distance distribution observed at low salt is most consistent with the β-hairpins folding in towards the earmuff domain of the opposing dimer as is the case in models A and B. Although one would expect three distances to be present in a four spin labelled Nap1 sample the oscillations of each distance in this instance are not easy to observe in

the dipolar evolution function (Figure 26E – blue trace). The initial drop in the dipolar evolutions function provides confidence that a short distance is appearing and evidence of a much longer oscillation is also observed in the data. However, due to the broad nature of the distribution it is hard to confidently assign each of the peaks as definitive distances.

One approach that would be worthwhile pursuing in order to delineate the position of the Nap1 β-hairpins within the Nap1 tetramer would be to mix the T302R1 labelled sample with an excess of unlabelled Nap1. This would allow the conformation of the β-hairpins in a dimer of Nap1 within a tetrameric assembly to be defined more easily reduceing the complexity of the PELDOR data by removing additional inter-dimer distances within the tetramer. This approach was attempted with a 10:1 excess of non-labelled Nap1 (data not shown). However, as the non-labelled Nap1 was non-deuterated the additional protons effectively quenched the signal from the dipolar interaction and the resultant timing window (~5 μs), over which the dipolar interaction could be measured, was insufficient for distance determination. Therefore by deuterating the non-labelled Nap1 in the same experiment conformational changes in the Nap1 β-hairpins upon tetramerisation may be elucidated in future experiments.

4.3 Discussion

Previous structural and functional studies of Vps75 have characterised the histone chaperone as a homo-dimer but did not report the presence of tetrameric assemblies of Vps75 (Selth and Svejstrup 2007; Tsubota, Berndsen et al. 2007; Berndsen, Tsubota et al. 2008; Park, Sudhoff et al. 2008; Tang, Meeth et al. 2008; Kolonko, Albaugh et al. 2010). These studies may not have noticed the tetrameric assembly of Vps75 due to the ionic conditions which were employed. In the case of yeast Nap1, self-association has been previously reported ranging from tetramers to hexadecamers which associate in a concentration dependent manner (McBryant and Peersen 2004; Toth, Mazurkiewicz et al. 2005; Park, McBryant et al. 2008; Newman, Kneale et al. 2012), a feature conserved in human Nap1 variants (Noda, Uchiyama et al. 2011). The oligomerisation of Nap1 is also sensitive to salt concentration and observations from this study suggest that Nap1 is predominantly tetrameric under conditions similar to those encountered within cells.

Vps75 associates with Rtt109 during S-phase and high resolution structural studies have reported two stoichiometries of the complex (Kolonko, Albaugh et al. 2010; Su, Hu et al. 2011; Tang, Holbert et al. 2011). The plasticity in Vps75 dimerisation interface seems to allow for one or two copies of Rtt109 to be accommodated by Vps75 (D'Arcy and Luger 2011) with both complexes form ring-like structures (Figure 19). The ring-like conformation of the Vps75 tetramer and Vps75-Rtt109 complexes suggests that histone may bind within the cavity of these protein complexes; however the size of the cavity would be too small to accommodate a H3/H4 tetramer. It is more probable that the cavity accommodates the partial insertion of a histone fold dimer or that histones associate on the lateral surface of the cavity, however the nature of the histone bound states of these complexes is yet to be discerned. The fact that Rtt109 occupies the Vps75 tetramerisation interface suggests that Rtt109 binding is incompatible with the tetrameric assembly of Vp75. Interestingly, mutation of both K169E and K170E does not affect Rtt109 binding (Tang, Holbert et al. 2011), while mutation of either residue individually does affect tetramerisation (Figure 23A). This provides scope for Rtt109 independent regulation of Vps75 tetramerisation.

The findings in this study raise the question of what role the tetramerisation of NAP-1 fold histone chaperones plays. One possibility is that tetramerisation is performing a self-chaperoning function required to shield the

acidic surface of the chaperones so as to prevent non-specific interactions with basic regions of histones exposed within chromatin. Another possibility is that the tetramerisation allows for the cooperative recognition of two histone fold dimers which may additionally drive the assembly of the H3/H4 tetramer prior to incorporation in chromatin. Further structural understanding of how these chaperones interact with histones is crucial for understanding the molecular mechanisms which underpin nucleosome assembly, disassembly and remodelling processes.

5 Investigating the mode of interaction of Vps75 and Nap1 with histones H3 and H4

5.1 Introduction

While there is excellent structural information for NAP-1 fold histone chaperones, less is known about their mode of interaction with histones. Both Vps75 and Nap1 interact with both H2A/H2B and H3/H4. Studies of the histone:chaperone stoichiometry within these complexes indicates that both Vps75 and Nap1 dimers associate with two histone H3/H4 or H2A/H2B dimers (Andrews, Downing et al. 2008; Park, Sudhoff et al. 2008). These studies did not distinguish whether or not histones H3/H4 were present in these complexes as two dimers or an intact tetramer. Subsequently it was shown that histones associate with Nap1 and Vps75 in a tetrameric configuration (Bowman, Ward et al. 2011). However, other studies have reported that a dimer of Nap1 binds a histone fold dimer (McBryant, Park et al. 2003; Newman, Kneale et al. 2012).

Further to these observations, the binding of Nap1 to histones H2A/H2B was found to be cooperative in nature under 150 mM sodium chloride conditions (Andrews, Downing et al. 2008) where Nap1 is now known to form tetrameric assemblies. The cooperative nature of histone binding to Nap1 may result from Nap1 effectively shielding histone interaction surfaces in its tetrameric configuration. Thus binding one dimer of histones may facilitate an additional binding event either by releasing a Nap1 dimer or through a reconfiguration of the Nap1 tetramer. Alternatively the tetrameric forms of NAP-1 fold chaperones may directly bind tetramers of H3/H4 without a reconfiguration of the chaperone, as such binding one dimer of H3/H4 would facilitate binding of an additional dimer through tetramerisation of the histone dimers. Whether Vps75 shows cooperativity when binding histones was not reported in these studies (Andrews, Downing et al. 2008; Park, Sudhoff et al. 2008).

Although Nap1 can form complexes with H2A/H2B the chaperone has a preference for histone H3/H4 *in vitro* as a result of the chaperones ability to bind the N-terminal tails of H3/H4 and not H2A/H2B (Su, Hu et al. 2012). The preferential interaction of Nap1 with histones H3/H4 was found to be mediated by the acidic C-

terminal tail of the chaperone which was found to not be required for the histone binding or nucleosome assembly activities of Nap1. Previous studies have suggested to the contrary that Nap1 has a higher affinity for H2A/H2B over H3/H4 (Ishimi, Kojima et al. 1987; McQuibban, Commisso-Cappelli et al. 1998).

The C-terminal tail of Vps75 is also dispensable for H3/H4 binding, in fact the truncated protein has marginally increased affinity for H3/H4 *in vitro* (Park, Sudhoff et al. 2008). Thus the ability of NAP-1 fold proteins to bind the histones is encoded in their structured domains which have been crystallographically determined. The same study found that Vps75 can also bind to histone H3 in the absence of H4 albeit with a significantly reduced affinity and that Vps75 binds H2A/H2B with a higher affinity than H3/H4. If Vps75 were to recognise the histone fold in a non-specific manner then it is unclear why the chaperone would have a preference for H2A/H2B over H3/H4. As these experiments were performed *in vitro* with recombinant histones there is a possibility that this specificity is encoded in the histone tails as is the case with Nap1. Furthermore as Vps75 is well characterised as directing the acetylation of H3 tail residues it seems counter intuitive that the chaperone would have a higher affinity for H2A/H2B dimers over H3/H4. The specificity for different histones *in vivo* may be modulated by histone PTMs. One attractive explanation is that acetylation of H3 K56 by Rtt109 would cause a conformational change in the αN helix of H3 that promotes association with Vps75. It is notable that regions of the histone fold to which Vps75 may bind could be obscured by the αN helix in H3/H4 (which is not present in H2A/H2B) and as such mask the specificity of Vps75 for H3/H4 over H2A/H2B. It is notable that Vps75 in contrast to Nap1 seems to display poor nucleosome assembly activity *in vitro* (Selth and Svejstrup 2007) however the assembly of nucleosomes by Vps75 is stimulated to a certain extent by Rtt109 in a manner not dependent on its acetyl transferase activity (Berndsen, Tsubota et al. 2008).

Structural studies on the mode of interaction of Nap1 and Vps75 with histones are limited. This may be due to the intractable nature of these large heterogeneous complexes. The surface of H3 (in complex with H4) to which Vps75 associates has been probed by hydrogen deuterium exchange experiments in the presence or absence of Rtt109. This study identified Vps75 dependent protection of backbone amide protons in the H3 tail and regions of the histone fold of H3 (Su, Hu et al. 2011). In the case of Nap1, another approach that has been used to characterise the interaction with histones utilises enzyme-linked immunosorbent assays (ELISA) to measure the binding of histone peptides to Nap1. This study identified regions of H2A, H2B, H3 and H4 that

interact with Nap1 of *Plasmodium falciparum*, the most significant binding was observed with two histone H3 peptides encapsulating residues 28-48 and 110-130 close to the nucleosomal dyad (Kumar, Kashyap et al. 2012). These results do however have to be interpreted with care due to the incomplete nature of the peptide array used with respect to sampling the entire length of each histone. Additionally interpretation of binding surfaces using this type of approach has the limitation that isolated peptides may not fold in a manner observed within the tertiary and quaternary structures of proteins. Thus the definition of the binding surface between Nap1 and histones requires further study.

As mentioned previously, structural studies on the mode of interaction of NAP-1 fold chaperones with histones may have been hindered by the ability of the chaperones to form large heterogenous complexes with histones. This is illustrated in a recent study of *Xenopus laevis* Nap1 with histones (Newman, Kneale et al. 2012). Cryo-Electron Microscopy analysis of these complexes showed spherical particles organised in disc like structures with overall radii on the order of 250 Å. The smaller spherical particles observed are similar in scale to a Nap-1 tetramer.

From the discussion above, it can be seen that little is known about how histones interact with NAP-1 fold histone chaperones. There is even some controversy regarding the stoichiometry of the complexes these proteins form with histones. As a result the aims of this chapter were to further characterise the complexes formed between NAP-1 fold histone chaperones and their cargo proteins. Special interest was played to investigating how the tetrameric configuration of NAP-1 fold histone chaperones relates to the complexes they form with histones.

5.2 Results

5.2.1 Assessing the stoichiometry of Vps75 with histones H3/H4

Initial experiments to assess the molecular weight of the Vps75 H3/H4 oligomeric assembly using SEC-MALS were unsuccessful for several reasons. Firstly the complex was found to regularly precipitate when the complex was concentrated above ~ 5 µM. Secondly at analytical levels histone H3/H4 has a tendency to stick to the S200 resin and thirdly SEC-MALS analysis showed that the mass of the complex decreased across the chromatogram peak (Figure 27A). This suggests that dissociation of the complex occurs during the timescale of the SEC-MALS analysis or that histones are stripped from the complex by non-specific interactions with the column resin. Despite these limitations, these complexes are much smaller (< 200 kDa) than those previously described for Nap1 (0.4-1.2 MDa) (Newman, Kneale et al. 2012).

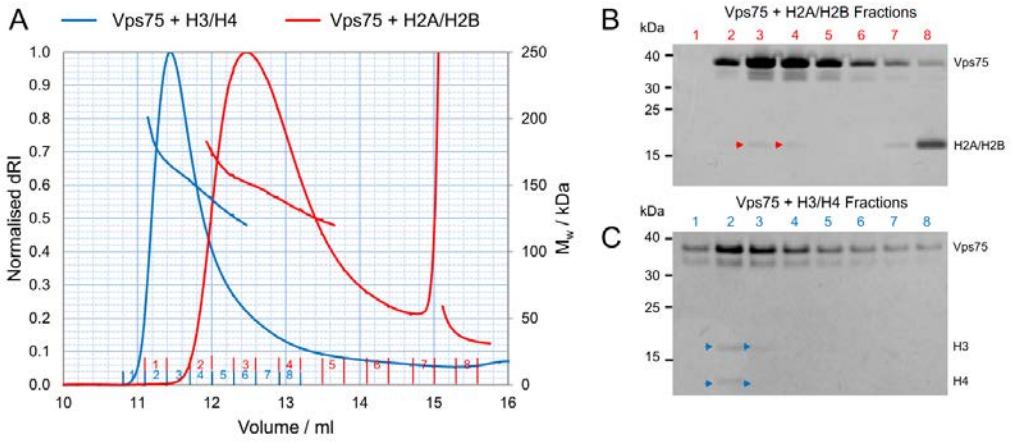

Figure 27 – SEC-MALS analysis of Vps75 and histones. (A) SEC-MALS elution profiles of Vps75 and H2A/H2B (red) or H3/H4 (blue) run at 150 mM NaCl, 5 mM $MgCl_2$, 20 mM HEPES-KOH and 5 mM β-mercaptoethanol. The second peak observed in the Vps75 + H2A/H2B is that of free histone dimers, no free histone peak was observed in the Vps75 + H3/H4 chromatogram despite evidence of dissociation of the complex. Chromatograms are normalised by the Vps75-histone peaks. SDS-PAGE analysis of fractions taken during SEC-MALS runs of Vps75 with H2A/H2B (B) and H3/H4 (C).

5.2.2 The cross-linking pattern of Vps75 titrated with histones H3/H4

The precipitation regularly observed when mixing histones with Vps75 may be avoided by optimising the stoichiometry and buffer conditions in which the components are mixed. In order to optimise these parameters, prior to subsequent SEC-MALS analysis, cross-linking reactions were performed on Vps75 titrated with H3/H4 at protein concentrations below the precipitation threshold. The extent of cross-linking was assessed by subjecting the samples to SDS-PAGE analysis which also gives information about the mass and likely composition of the cross-linked complex. As there was potential for the tetrameric form of Vps75 to be involved in binding histones the extent of cross-linking was assessed both under conditions that favour tetramerisation and conditions that favour the dimeric form of Vps75. To simplify the experimental approach conditions of 200 mM and 400 mM sodium chloride were chosen for this purpose and SEC-MALS analysis of Vps75 under these conditions confirmed the presence of tetrameric and dimeric assemblies of Vps75 respectively (data not shown).

Although these experiments were designed to optimise the conditions in which the components were mixed to produce homogeneously cross-linked complexes for subsequent SEC-MALS analysis additional strengths of the cross-linking approach quickly became apparent. The amine reactive cross-linker Bis(sulfosuccinimidyl) glutarate (BS_2G) was utilised to covalently link the subunits of the Vps75 H3/H4 complex. The cross-linker was applied in a large excess as to avoid limiting the extent of cross-linking, however, only partial cross-linking was observed in the SDS-PAGE analysis. This may reflect the modest 7.7 Å cross-linking radius of BS_2G compared to other available amine bifunctional cross-linkers. The benefit of choosing this cross-linker is the minimisation of species cross-linked in a non-specific manner (which may be more prevalent with longer cross-linkers) which simplifies the interpretation of the pattern observed in the SDS-PAGE analysis.

At 200 mM sodium chloride, in the absence of histones, cross-linked Vps75 forms four distinct bands which migrate at molecular weights consistent with monomeric, dimeric (★), trimeric and tetrameric (►) cross-linked species of Vps75 during SDS-PAGE analysis (Figure 28A). The reduced cross-linking efficiency of the Vps75 tetramer compared to that of the dimer at 200 mM sodium chloride is likely a result of a smaller

interface across the tetramer than across the Vps75 dimer.[2] As such the proximity of primary amines across the tetramerisation interface may limit the efficiency with which the tetramer is cross-linked. Additionally cross-linking the Vps75 tetramer requires a minimum of four simultaneous cross-links to be formed between the four Vps75 chains. Nevertheless the cross-linked tetramer is greatly reduced at 400 mM sodium chloride (Figure 28B) as expected.

In the same vein H3/H4 dimers are efficiently cross-linked (★) under the conditions employed whereas H3/H4 tetramers are not (Figure 28). This is likely a reflection of the smaller more dynamic H3/H4 tetramerisation interface compared to the larger more stable histone fold dimer interface. As no bands indicative of free histones H3 or H4 were observed in any of the titration points one can assume that the bands which appear in the cross-linking pattern when H3/H4 is titrated onto Vps75 are likely to contain one or more H3/H4 dimers. Consistent with this the band that migrates above the Vps75 dimer (▶) can be assigned as a Vps75 dimer plus a H3/H4 dimer. The next band above this species can then be assigned as a Vps75 dimer plus a H3/H4 tetramer (▶).

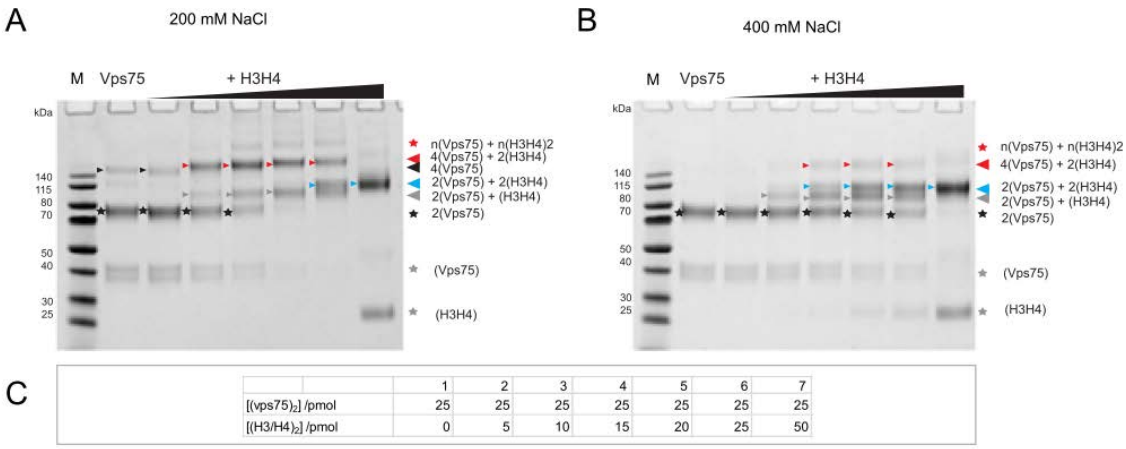

	1	2	3	4	5	6	7
$[(vps75)_2]$ /pmol	25	25	25	25	25	25	25
$[(H3/H4)_2]$ /pmol	0	5	10	15	20	25	50

Figure 28 - A species consistent with a Vps75 tetramer in complex with H3/H4 is observed in the BS2G cross-linking pattern of Vps75. (A) SDS-PAGE analysis of wild type Vps75 incubated with increasing concentrations of H3/H4 at (B) 200 mM NaCl and (C) 400 mM NaCl with 20 mM HEPES pH 7.5, cross-linked for 1 hour with 2 mM BS2G and run on 4-12% Bis –Tris SDS-PAGE gels (Invitrogen). Bands are marked with arrows and stars as referred to in the text. (D) Table summarising the amounts of H3/H4 incubated with Vps75 in each lane.

[2] Lower levels of the high molecular weight cross-linked species do not necessarily mean they are of low abundance in solution. In the absence of histones the cross-linked tetramer of Vps75 is not the major cross-linked species observed, but it is the major species observed by SEC-MALS.

The cross-linking pattern of Vps75 incubated with increasing concentrations of H3/H4 varies dependent on whether the reaction is performed at 200 mM or 400 mM sodium chloride (Figure 28). At early titration points when Vps75 is in excess of H3/H4 the most prominent cross-linked species (▶) observed at 200 mM NaCl is larger than the Vps75 tetramer and consistent with H3/H4 binding to the Vps75 tetramer[3] (Figure 28A). This species is also observed at 400 mM sodium chloride but is less prominent (Figure 28B). At higher histone ratios the most prominent species drops down in molecular weight to a Vps75 dimer plus a H3/H4 tetramer (▶). If both Vps75 dimers and tetramer can bind histone tetramers then a reasonable explanation would be that a Vps75 dimer binds a H3/H4 dimer and that a H3/H4 tetramer can accommodate two Vps75 dimers. Thus, at low salt the two dimers of Vps75 in the tetramer would be able to cooperatively assemble or recognise a H3/H4 tetramer (Figure 29).

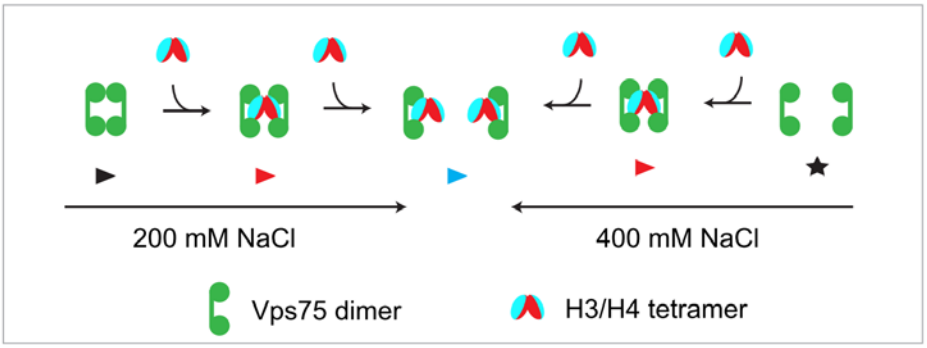

Figure 29 - Schematic representation of Vps75 H3/H4 complexes observed in cross-linking titration points

The intermediate Vps75 dimer to H3/H4 dimer species (▶) may only be present due to partial cross-linking of the Vps75 tetramer to H3/H4 tetramer species (▶). This would explain why the latter species is less abundantly cross-linked at 400 mM NaCl which disfavours Vps75 tetramerisation (Figure 28B). Although 400 mM salt would disfavour Vps75 tetramerisation it would have the opposite effect on H3/H4. As the H3/H4 tetramerisation interface is predominantly hydrophobic in nature, tetramerisation of H3/H4 is favoured at higher salt due to the increased hydrophobic effect. Thus the fact that the Vps75 dimer to H3/H4 tetramer

[3] Although the mass of two H3/H4 tetramers to one Vps75 dimer is similar to a Vps75 tetramer cross-linked with a H3/H4 tetramer the latter stoichiometry is more probable given the presence of excess Vps75.

species (▶) appears earlier in the titration at 400 mM NaCl than at 200 mM NaCl may simply be a result of more favourable H3/H4 tetramerisation conditions. Nevertheless, this observation is still compatible with a Vps75 dimer binding a H3/H4 dimer in a manner which does not obscure H3/H4 tetramerisation (Figure 29). Additional cross-linked species beyond the Vps75 tetramer to H3/H4 tetramer band (★) were observed at low salt which could be higher order oligomers which may or may not be non-specific in nature.

Thus it appears that the tetrameric form of Vps75 preferentially binds H3/H4 tetramers at low levels of H3/H4 and Vps75 reverts to a dimer binding a H3/H4 tetramer at high levels of H3/H4 (Figure 29). This would be made possible if a dimer of Vps75 were to bind a dimer of H3/H4 in a manner that does not compete with the tetramerisation of H3/H4. These experiments suggest that Vps75 has a buffering capacity for binding histones H3/H4 in different stoichiometries.

5.2.3 The cross-linking pattern of non-tetramerising mutants of Vps75 titrated with histones H3/H4

To help delineate the nature of the cross-linked assemblies of Vps75 and H3/H4 the BS_2G cross-linking experiment was repeated with the non-tetramerising mutants (K169E, K170E and R164D) identified in section 4.2.4. As expected no cross-linked bands were observed above the Vps75 dimer (★) in the absence of histones in tetramerising conditions (Figure 30A). Otherwise, the cross-linking pattern observed was highly similar to that for the wild-type Vps75 cross-linking pattern (Figure 30). In particular, a species consistent with a Vps75 tetramer bound to a H3/H4 tetramer was observed (▶) at 200 mM sodium chloride (Figure 30A) despite the absence of a cross-linked Vps75 tetramer species when no histones are present. At later titration points, at 200 mM and 400 mM sodium chloride, the most prominent cross-linked species had a lower molecular weight consistent with a Vps75 dimer bound to a H3/H4 tetramer (▶) (Figure 30). One observable difference in the cross-linking pattern between the Vps75 and non-tetramerising mutants of Vps75 with H3/H4 is the reduction in the abundance of higher molecular weight oligomers which were observed in the wild type Vps75 cross-linking pattern at 200 mM sodium chloride (★). This suggests that further oligomerisation of the Vps75 H3/H4 complexes may be governed by the same interface of Vps75 which governs tetramerisation.

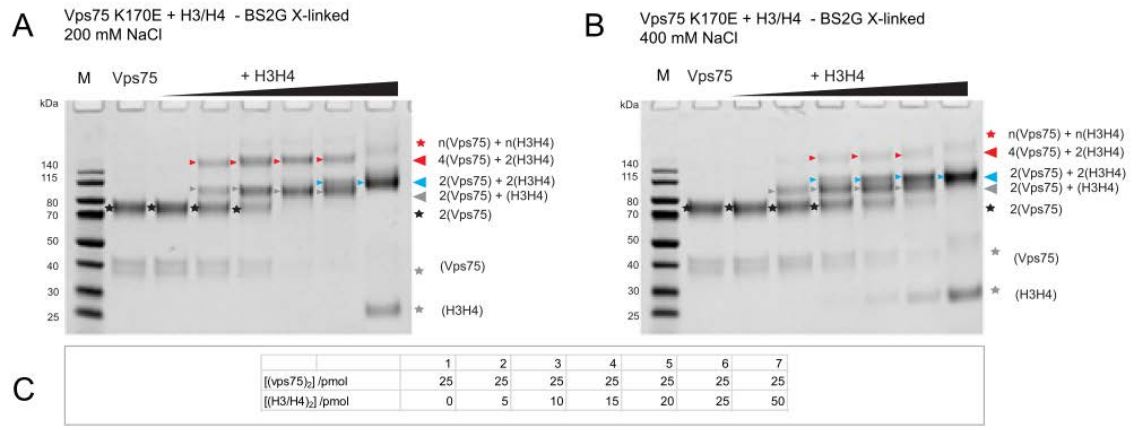

Figure 30 – Non-tetramerising mutants of Vps75 produce a similar BS2G cross-linking pattern with histones H3/H4 as wild type Vps75. SDS-PAGE analysis of the Vps75 K170E non-tetramerising mutant incubated with increasing concentrations of H3/H4 at (A) 200 mM NaCl and (B) 400 mM NaCl with 20 mM HEPES pH 7.5, cross-linked for 1 hour with 2 mM BS2G and run on 4-12% Bis – Tris SDS-PAGE gels (Invitrogen). (C) Table summarising the amounts of H3/H4 incubated with Vps75 in each lane.

The data presented here suggests that the binding of a H3/H4 tetramer stabilises the Vps75 tetramer and as such allow for the re-tetramerisation of non-tetramerising mutants of Vps75. This is reminiscent of previous observations indicating that non-tetramerising mutants of histones are forced to tetramerise in the presence of Vps75 (Bowman, Ward et al. 2011). Thus, the association of histones with Vps75 appears to stabilise both the chaperone and the histones in tetrameric conformations, until excess levels of histones are reached - at which point Vps75 reverts to its dimeric form.

5.2.4 The cross-linking pattern of Vps75 titrated with histone H3/H4 trapped in a tetrameric conformation

Although bands that are clearly dependent on the presence of H3/H4 were observed in the SDS-PAGE analysis of cross-linking reactions of Vps75 and Vps75 non-tetramerising mutants the exact composition of these bands could only be tentatively assigned. To unambiguously identify bands containing the H3/H4 tetramer the BS_2G cross-linking reaction was repeated with H3/H4 trapped in a tetrameric conformation. The dissociation of histone H3/H4 tetramer into obligate dimers was prevented by cross-linking a cysteine mutant of histone H3 (K115C) with the cysteine reactive cross-linker Bismaleimidoethane (BMOE). The fully cross-linked tetramer of H3H4 ($[H3(K115X)/H4]_2$) was purified from uncross-linked tetramer by gel filtration.

Upon performing the BS_2G cross-linking titration with 100% cross-linked H3/H4 tetramers the bands previously identified as a H3/H4 tetramer cross-linked with one (▶) or two Vps75 dimers (▶) were again observed with a similar cross-linking pattern observed at 400 mM sodium chloride to that described previously (Figure 31B). This confirmed the identity of these previously assigned species as a Vps75 dimer (▶) and a Vps75 tetramer (▶) bound to a H3/H4 tetramer.

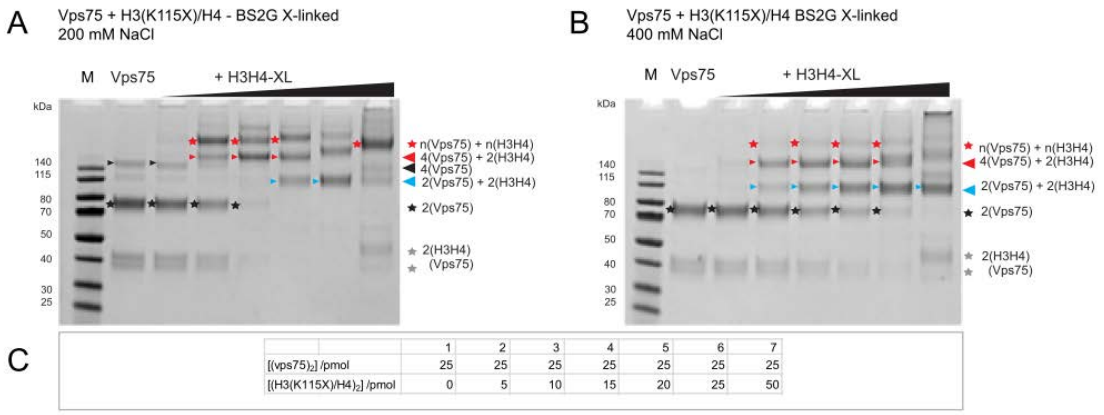

	1	2	3	4	5	6	7
$[(vps75)_2]$ /pmol	25	25	25	25	25	25	25
$[(H3(K115X)/H4)_2]$ /pmol	0	5	10	15	20	25	50

Figure 31 – The BS2G cross-linking pattern of Vps75 incubated with site directed cross-linked tetramers of H3/H4 confirm Vps75 histone complexes which contain the H3/H4 tetramer. SDS-PAGE analysis of Vps75 incubated with increasing concentration of H3/H4 tetramers cross-linked at K115C with BMOE (H3(K115X)H4) at 200 mM NaCl (A) or 400 mM NaCl (B) with 20 mM HEPES pH 7.5, and cross-linked for 1 hour with 2 mM BS2G then run on 4-12% Bis –Tris SDS-PAGE gels (Invitrogen). Predicted species are indicated by black arrows with (Vps75)2:(H3/H4)2 and 2(Vps75)2:(H3/H4)2 bands highlighted by blue and red arrows respectively for reference. The additional prominent species predicted to be 2(Vps75)2:(H3/H4)2 is highlighted in green. Bottom: Table summarising the amounts of H3(K115X)H4 incubated with Vps75 in each lane.

The cross-linking pattern at 200 mM sodium chloride was more complicated than anticipated with additional bands significantly larger (★) than Vps75 tetramer to H3/H4 tetramer (▶) band observed (Figure 31A). At 400 mM sodium chloride these species (★) migrated more consistently (Figure 31B) but were cross-linked to a lower efficiency. The nature of this species is hard to assign but it could be consistent with two H3/H4 tetramers binding to the Vps75 tetramer.

5.2.5 Estimation of the mass of cross-linked Vps75 H3/H4 complexes by SEC-MALS

Clearly Vps75 is capable of associating with histones in multiple stoichiometric assemblies, however the cross-linking pattern observed in the SDS-PAGE analysis does not necessarily describe the system fully as cross-linked sub complexes of Vps75 and H3H4 can be observed. Additionally the amine bifunctional cross-linker BS_2G, with a 7.7 Å range, may not capture all interactions between the polypeptide chains present in the Vps75 H3/H4 complex. Therefore a combination of cross-linking and SEC-MALS analysis was utilised in order to estimate the total molecular weight of the complexes within the cross-linked material.[4] For this approach the amine bifunctional cross-linker 3,3'-dithiobis[sulfosuccinimidylpropionate] (DTSSP - Figure 32D) which has a larger range of 12 Å was used. In addition to the increased cross-linking radius, compared to BS_2G, DTSSP also contains a disulphide bond which allows any cross-links formed to be reversed under reducing conditions.

Vps75 was partially cross-linked with DTSSP under the tetramerising conditions of 200 mM sodium chloride and SEC-MALS analysis was performed at 400 mM allowing separation of the cross-linked Vps75 tetramer from Vps75 cross-linked dimers. The SEC-MALS analysis of DTSSP cross-linked Vps75 resulted in major peak eluting at 11.53 ml with a mass of 130.7 kDa and a minor peak eluting at 12.87 ml with a mass of 65.3 kDa (Figure 32A) consistent with that of a Vps75 tetramer (125.3 kDa) and Vps75 dimer (62.6 kDa) respectively (Table 7). The difference in the observed mass and the theoretical for the Vps75 dimer of 2.7

[4] A related approach GraFix has been widely used to stabilise protein complexes for study by electron microscopy (Stark, H. (2010). "GraFix: stabilization of fragile macromolecular complexes for single particle cryo-EM." Methods Enzymol **481**: 109-126.

kDa equates to the presence of approximately 15 cross-links (174 Da) in addition to the two polypeptide chains of Vps75, in the case of the Vps75 tetramer this difference is 5.4 kDa which equates to approximately 31 cross-links. As there are 26 lysine residues in each chain of Vps75 it is reasonable that this level of cross-linking accounts contributes to the difference between the observed mass of Vps75 complexes and their theoretical values.

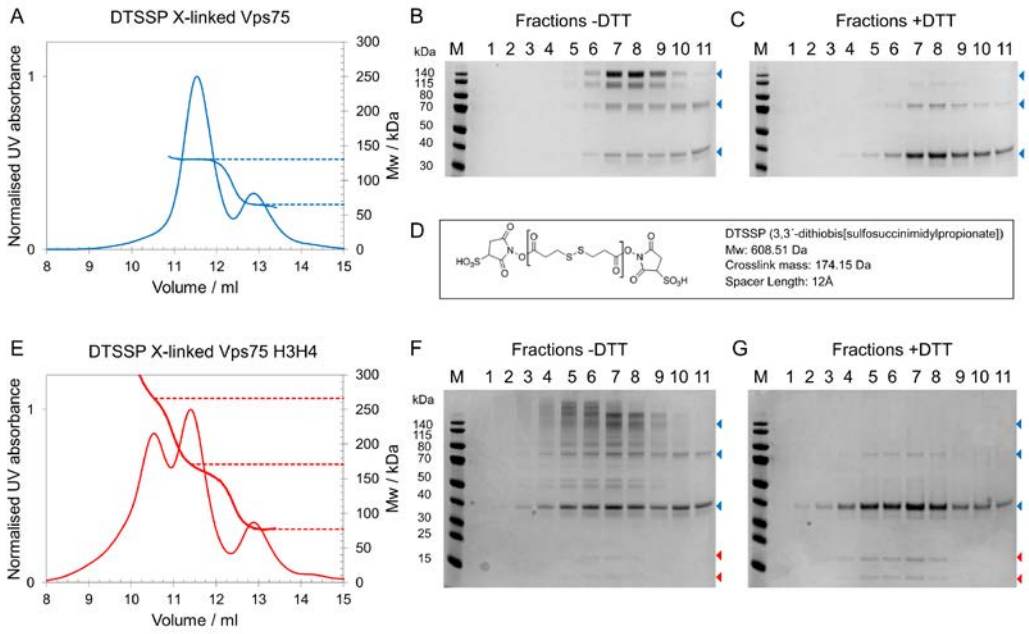

Figure 32 – SEC-MALS analysis of DTSSP cross-linked Vps75 and Vps75 with histones H3/H4. (A) SEC-MALS analysis of Vps75 cross-linked with DTSSP at 200 mM NaCl, 20 mM HEPES pH 7.5 and eluted from Superdex 200 10/300 GL column (GE Healthcare) at 400 mM NaCl, 20 mM HEPES. Dashed line indicates the molecular weights at the peak elution volume peak elution volume. SDS-PAGE analysis (4-12% Bis –Tris NuPAGE gels) of fractions from the SEC-MALS analysis of cross-linked Vps75 (B) and fractions treated with DTT (C). (D) Details of DTSSP cross-linker. (E-G) Analysis of Vps75 cross-linked with H3/H4 as described in A-C.

Next, Vps75 was mixed with histone H3/H4 in a 1:1 dimer to dimer stoichiometry and partial DTSSP cross-linking was performed at 200 mM sodium chloride (Figure 32E). The resultant SEC-MALS analysis at 400 mM sodium chloride resulted in three main peaks in the chromatogram. The species eluting at 12.9 ml was confidently assigned as that of the Vps75 dimer. Although this species has an apparent molecular weight of ~77 kDa the difference in mass compared to the Vps75 dimer cross-linked peak can be explained by insufficient separation form the adjacent peak at 11.40 ml. As can be seen in fractions 10 and 11 the major bands are that of Vps75 monomers and dimers (Figure 32F) with higher molecular weight bands above the Vps75 dimer contributing to the molar mass estimate of the species. This highlights the limitations of this

approach, as the SEC-MALS profile reports a running average molar mass of the cross-linked species across the elution profile. The mass at the peak centred at 11.4 ml is 170 kDa and the mass at the peak centred at 10.54 ml is 266 kDa. The masses of both species are likely to be affected by higher and lower molecular weight species eluting either side of the peak. As the mass decreases across each peak it is likely that some dissociation occurs during the course of separation on the column. Taking these effects on the accuracy of the mass estimate from SEC-MALS into account these species are consistent with a Vps75 tetramer plus one (178.2 kDa) or two H3/H4 tetramers (231 kDa). In principle the larger species could also be explained by the presence of an octamer of Vps75 (250.6 kDa), though this is somewhat unlikely as an octamer of Vps75 has not been observed in the absence of histones.

Vps75	H3/H4	H2A/H2B	Mass / kDa
2	-	-	62.6
4	-	-	125.3
-	1	-	26.4
-	2	-	52.9
4	1	-	151.7
4	2	-	178.2
4	4	-	231.0
-	-	1	28.0
-	-	2	55.9
2	-	1	90.6
2	-	2	118.6
4	-	2	181.2
4	-	1	153.2
4	-	4	237.1

Table 7 – Theoretical molar mass of complexes composed of different stoichiometries of Vps75, H3H4 and H2A/H2B. The molar masses of individual chains are for wild type *S. cerevisiae* proteins. *The mass of Vps75 represents the full length protein plus additional residues at the N-terminus which remain following the TEV cleavage of the six histidine N-terminal tag.

5.2.6 Estimation of the mass of cross-linked Vps75 H2A/H2B complexes by SEC-MALS

To investigate the size of Vps75-H2A/H2B complexes, Vps75 was mixed with histone H2A/H2B in a one dimer to one dimer stoichiometry and partial DTSSP cross-linking was performed at 200 mM sodium chloride. The resultant SEC-MALS analysis at 400 mM sodium chloride resulted in two main peaks in the chromatogram at 11.08 ml and 12.57 ml (Figure 33A). The mass at the centre of the peak at 12.7 ml is 107 kDa and the mass at the centre of the peak at 11.08 ml is 210 kDa. The cross-linked species of the peak centred at 12.7 ml are seen in fractions 9-11 and two prominent bands above the Vps75 dimer cross-linked species are observed (Figure 33B), the top band of which is likely to be a Vps75 dimer plus a H2A/H2B dimer. As the molecular weight at the peak centred at 11.2 ml is double that of the peak at 12.7 ml one may speculate that the larger species is a Vps75 tetramer plus two dimers of H2A/H2B.

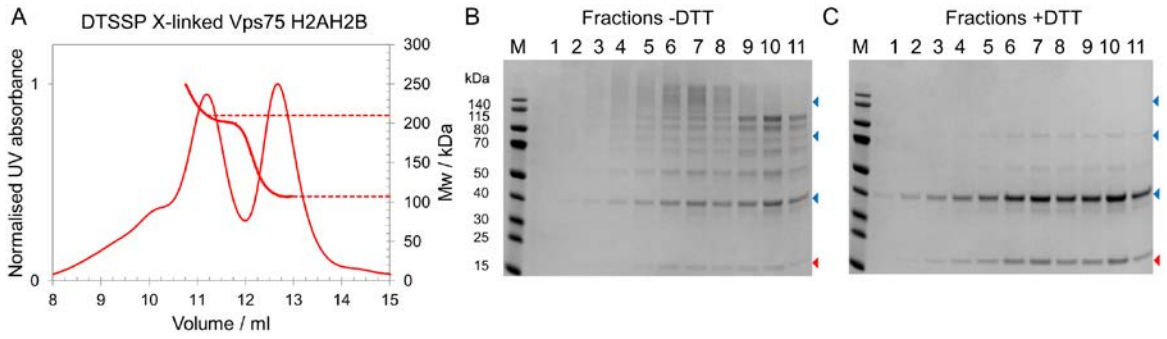

Figure 33 - SEC-MALS analysis of DTSSP cross-linked Vps75 with histones H2A/H2B. (A) SEC-MALS analysis of Vps75 cross-linked with DTSSP at 200 mM NaCl, 20 mM HEPES pH 7.5 and eluted from Superdex 200 10/300 GL column (GE Healthcare) at 400 mM NaCl, 20 mM HEPES. Dashed line indicates the molecular weights at the peak elution volume peak elution volume. SDS-PAGE analysis (4-12% Bis –Tris NuPAGE gels) of fractions from the SEC-MALS analysis of cross-linked Vps75 and H2A/H2B (B) and fractions treated with DTT (C).

5.2.7 Attempts at accurately defining the mass of Vps75 histone complexes by MALDI mass spectrometry

The combined observations from cross-linking experiments suggest that a dimer of Vps75 recognises a histone fold dimer and, in the case of H3/H4, Vps75 binds in a manner that does not interfere with H3/H4 tetramerisation. However, as the SEC-MALS approach was unable to confidently assign the stoichiometry of

Vps75 histone complexes, the cross-linking approach was coupled with MALDI mass spectrometry for more accurate quantification of the molecular weight of individual cross-linked bands observed in the SDS-PAGE analysis of cross-linked materials. Unfortunately, although the mass of the Vps75 tetramer could be observed by this approach (Figure 34), cross-linked Vps75 histone complexes did not yield additional higher molecular weight peaks in the MALDI spectrum. This may be a result of the broadening of the mass envelope at molecular weights species beyond the Vps75 tetramer leading to insufficient signal to noise or that the larger complex does not ionise well.

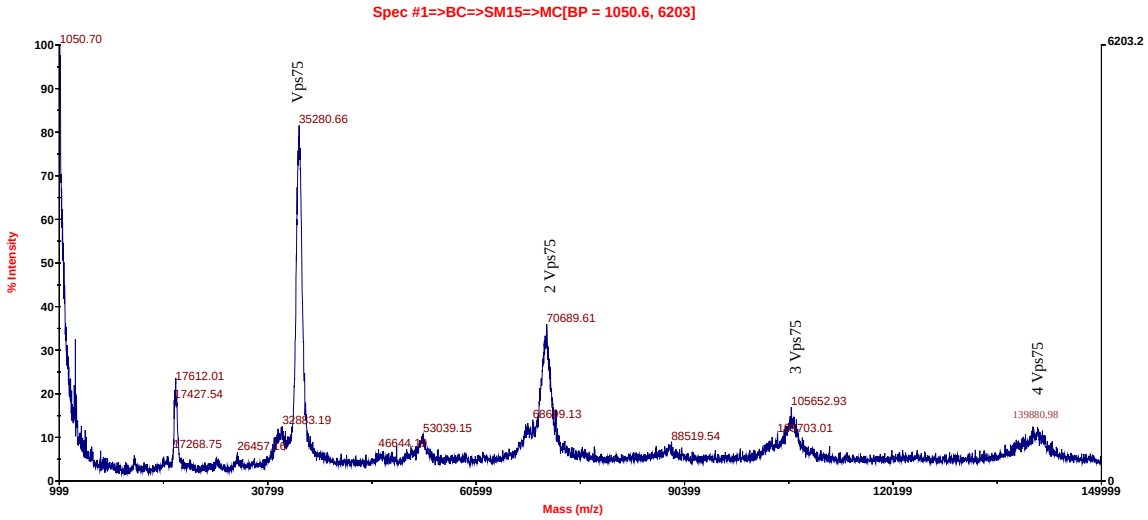

Figure 34 – MALDI mass spectrum of Vps75 cross-linked with DTSSP with annotation of Vps75 multimers. *The monomeric mass of the Vps75 construct used in this experiment is 34.3 kDa.

5.2.8 Potential reconfiguration of the Vps75 tetramer upon binding of histone H3/H4

As the residue K78 was found to come into close proximity with itself across the Vps75 tetramerisation interface the cysteine mutant Vps75 K78C was labelled with N1-(pyrene)maleimide (Figure 35A), a fluorescent label whose emission spectra exhibits a characteristic excimer when two of the pyrene labels come into close proximity. This potentially provides an independent means of monitoring tetramerisation. Upon labelling Vps75 K78C with the pyrene label (forming the side chain K78Py) the characteristic pyrene excimer peak was observed in the emission spectra at ~470 nm (Figure 35B), this proved that, in addition to the fact that K78 comes into close proximity with itself, the pyrene labels do not inhibit the tetramerisation of Vps75.

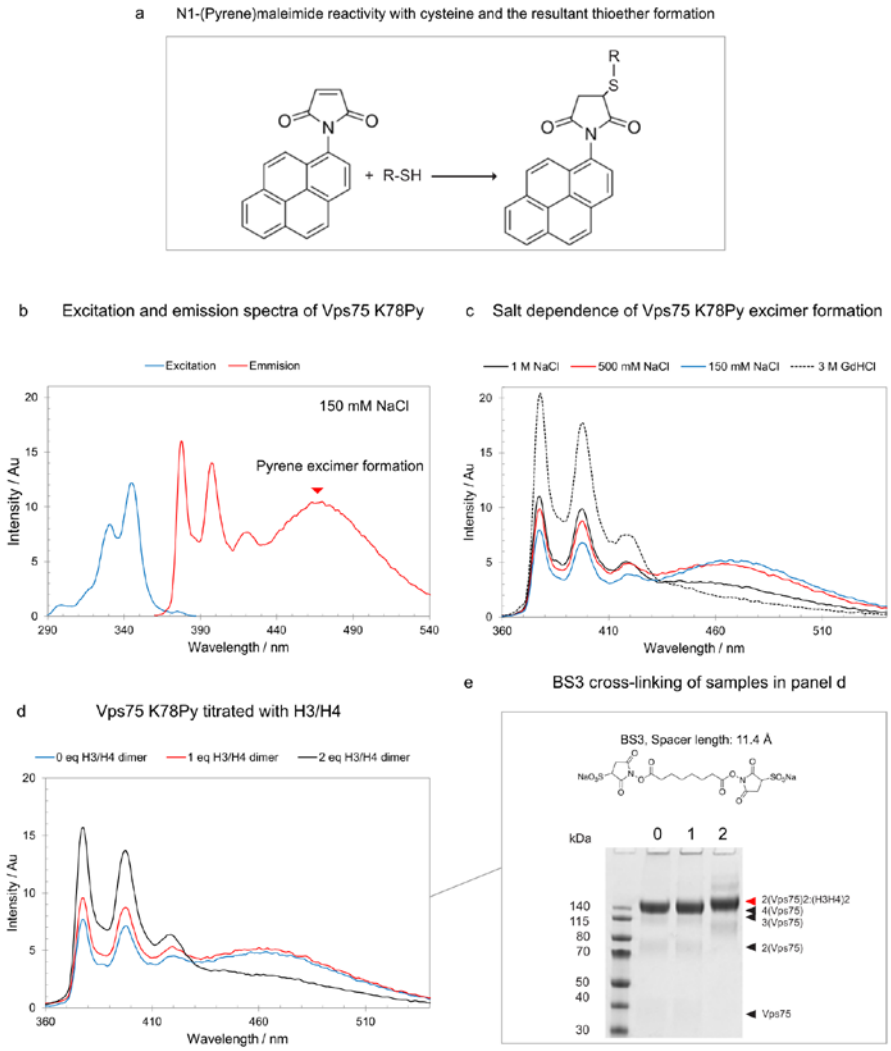

Figure 35 – Pyrene excimer formation upon tetramerisation of Vps75 K78C labelled with N1-(Pyrene)maleimide is quenched by histones H3/H4 but histones remain associated with the Vps75 tetramer. (a) Reaction scheme of N1-(Pyrene)maleimide reacting with a reduced cysteine side chain. (b) The excitation and emission spectra of Vps75 pyrene labelled at K78C forming the side chain K78Py ([$(Vps75)_2$] = 8 μM). Pyrene excimer formation at 470 nm is a result of two pyrene labels coming into close proximity across the Vps75 tetramerisation interface at 150 mM sodium chloride. (c) The salt dependence of pyrene excimer formation ([$(Vps75)_2$] = 4 μM) and total loss upon treatment with guanidine hydrochloride (GdHCl). (d) The addition of histones results in the loss of the Vps75 K78Py excimer at 400 mM sodium chloride ([$(Vps75)_2$] = 4 μM). (e) SDS-PAGE analysis of samples (4-12% Bis –Tris NuPAGE gels) in panel d cross-linked with Bis[sulfosuccinimidyl] suberate (BS3), the number above each lane represents the number of equivalents of H3/H4 dimers added to 1 equivalent of Vps75 K78Py dimer.

When the salt concentration was increased to 500 mM NaCl, conditions that favour the Vps75 dimer, the excimer peak at 470 nm persisted and although each dimer of Vps75 contains two pyrene molecules the distance between them would be much larger than that for efficient pyrene excimer formation (Bains, Kim et al. 2012). The explanation for this anomalous result is that the pyrene labels can form π-stacking interactions

which would stabilise the Vps75 tetramer at higher salt concentrations than usual. Indeed when the salt was increased to 1 M NaCl the loss of the peak at 470 nm indicated that the equilibrium is significantly shifted towards the Vps75 dimer. As a control the emission spectra under denaturing conditions (3M Guanidine HCl) is shown (Figure 35C).

When histones H3/H4 were titrated into the pyrene labelled Vps75 tetramer, two equivalents of H3H4 dimers to one equivalent of Vps75 dimer were sufficient to quench the pyrene excimer (Figure 35D). Initially this pointed to H3/H4 binding to Vps75 splitting the Vps75 tetramer, however, upon cross-linking the titration points with the amine bifunctional cross-linker Bis[sulfosuccinimidyl] suberate (BS3) the species previously assigned as a Vps75 tetramer bound to a H3/H4 tetramer was observed. This result points to a potential re-configuration of the Vps75 tetramer upon histone binding or quenching of the pyrene excimer by some other means.

Due to the limited time available for further experiments at this point of the project analogous experiments with Vps75 and histones H2A/H2B could not be performed. It is also notable that the complex forms a more homogeneously cross-linked species during the BS3 cross-linking than in previous experiments and as such SEC-MALS analysis of the BS3 cross-linked species is worthy of future investigation. A pyrene labelling approach should be feasible with Nap1 and may also resolve the questions about the involvement of the β-hairpins of Nap1 during tetramerisation, which were raised in section 4.2.7.

5.2.9 Vps75 binds histones H3/H4 in the presence of Asf1

Although not definitive, the initial BS_2G cross-linking studies identified cross-linked bands consistent with a Vps75 dimer and a Vps75 tetramer cross-linked to H3/H4 tetramer which suggests that a H3/H4 tetramer can accommodate two Vps75 dimers. Thus it appeared logical that a Vps75 dimer binds to a H3/H4 dimer in a manner which does not obscure the H3/H4 tetramerisation interface and as such Vps75 binding to H3/H4 may be compatible with Asf1 binding.

To test this hypothesis analytical gel filtration experiments were performed. Initially Vps75 was mixed with Asf1, in a 1:1 dimer to monomer ratio, to see if the chaperones interact independently of H3/H4 binding and analytical gel filtration was performed. As can be seen in the chromatogram (Figure 36) Asf1 and Vps75 elute separately when mixed together and SDS-PAGE analysis confirmed that the proteins do not co-fractionate. Thus Vps75 does not interact with the globular core of Asf1 in the absence of histone H3/H4. However when a dimer of histones H3/H4 was added to a dimer Vps75 and a monomer of Asf1 the elution profile peak shifted to 1.41 ml compared to the peak elution profile of Vps75 (1.44 ml) and SDS page analysis of the peak fractions confirmed the presence of all components at the peak elution volume.

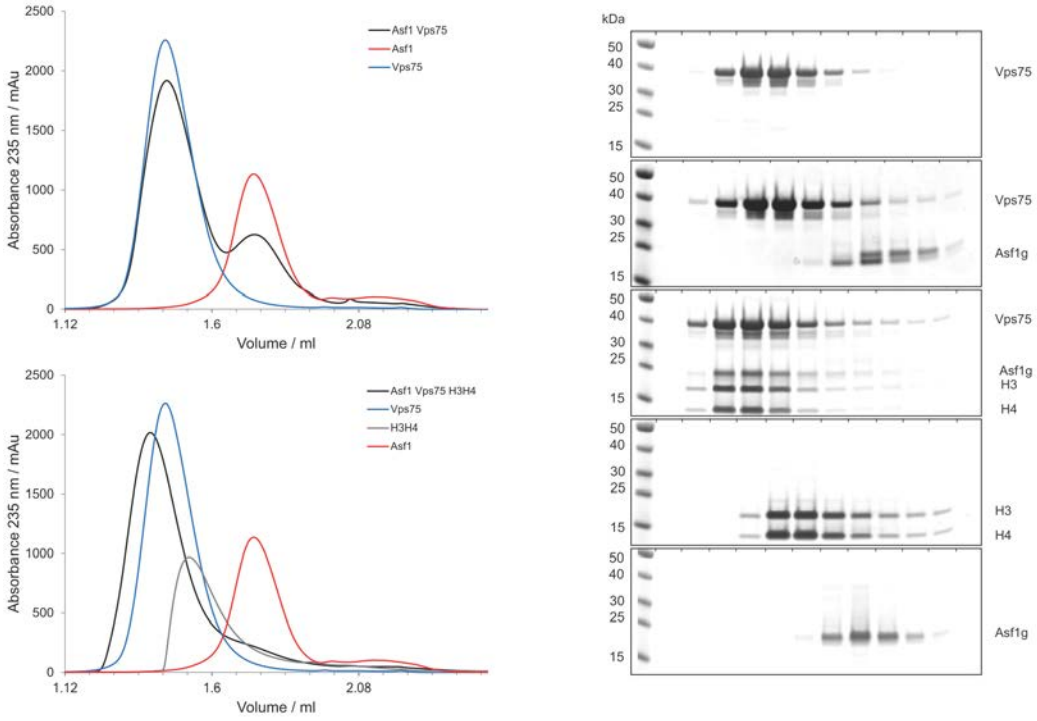

Figure 36 - Analytical gel filtration shows that Vps75 forms a complex with H3/H4 and the globular domain of Asf1 (Asf1g - residues 1-164). *Left:* Elution profiles from a Superdex 200 PC 3.2/30 column (GE Healthcare) at 400 mM NaCl, 30 % glycerol and 20 mM Tris pH 7.5. *Top Left:* Vps75 does not interact with Asf1 globular domain (Asf1g residues 1-164) in the absence of histones. Elution profiles of Vps75 dimer, Asf1g and Vps75+Asf1 (in 1:1 stoichiometry). *Bottom Left:* Vps75 binds H3/H4 in complex with Asf1. Equimolar elution profiles of Asf1g, H3/H4 tetramer, Vps75 dimer and Vps75+Asf1+H3/H4 (in a 2:1:1 stoichiometry. *Rig*ht: Aligned fractions from gel filtration, 20 µl of 80 µl fractions run on 4-12% Bis –Tris SDS-PAGE gels (Invitrogen).

As the elution buffer used during these analytical gel filtration experiments contained 30% glycerol SEC-MALS analysis could not be performed as the local concentration of glycerol in the elution buffer fluctuates during the chromatographic separation. This prevents an accurate baseline determination for the differential

refractive index signal and in turn prevents accurate concentration determination required to estimate the molecular weight of a substance from light scattered at multiple angles. Glycerol was required to prevent non-specific interactions of the histones with the Superdex 200 column, therefore a more traditional approach to estimating the molecular weight of the Vps75-H3/H4-Asf1 complex was undertaken using the molecular weight standard bovine serum albumin (BSA).

Under identical conditions, BSA was seen to elute from the column as mixture of monomer and dimer as expected, with the monomer peak eluting at 1.55 ml (66.5 kDa) and the dimer peak eluting at 1.36 ml (132.9 kDa) – data not shown. The Vps75-H3/H4-Asf1 complex elutes at 1.41 ml consistent with the anticipated 2:1:1 stoichiometry (116.1 kDa).

Protein	Mass kDa
$(Vps75^*)_2$	68.6
Asf1g*	21.1
H3	15.2
H4	11.2
Total	116.1

Table 8 - Theoretical molar mass of Vps75, H3H4 and H2A/H2B. The molar masses of individual chains are for wild type *S. cerevisiae* proteins. *The mass of Vps75 represents a dimer of the full length protein plus additional N-terminal six histidine tag and the TEV cleavage site. The mass of Asf1g is that of residues 1-164 plus the additional N-terminal six histidine tag and PreScission protease cleavage site.

5.2.10 Probing the structure of the Vps75-H3/H4-Asf1 complex

The Vps75-H3/H4-Asf1 complex eluted during analytical gel filtration in a single symmetrical peak when the components were mixed in a 2:1:1 ratio, this suggested that the complex would be a good candidate to probe using PELDOR EPR distance measurements. As such EPR samples were prepared in which deuterated cross-link labelled Vps75 (Y35RX2) was mixed with non-deuterated Asf1g and H3/H4 R1 labelled at either H3 Q125 or H4 R45 in the aforementioned stoichiometry (Figure 37A). Oscillations consistent with a structurally homogeneous complex were observed in the raw dipolar evolution functions for both the Asf1 + H3(Q125R1)/H4 – Vps75 Y35RX2 and the Asf1 + H3/H4(R45R1) – Vps75 Y35RX2 (Figure 37B and C respectively). Tikhonov transformation of the background corrected dipolar evolution function results in distance distributions with modal distances of 6.65 nm and 6.13 nm for Vps75 Y35RX2 to H3 Q125R1 (Figure 37B) and H4 R45R1 (Figure 37C) respectively.

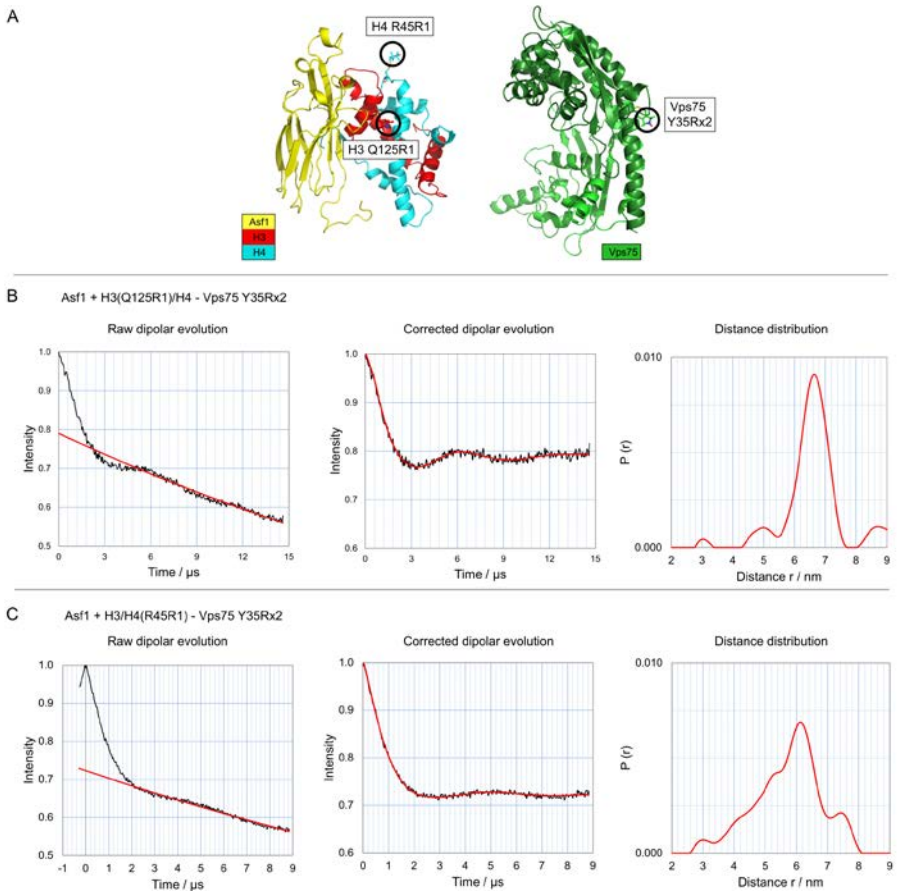

Figure 37 – The complex of Vps75-H3/H4-Asf1 shows a level of structural homogeneity not observed EPR measurements between Vps75 and histones in the absence of Asf1. (A) The location of spin labelling sites H3 Q125R1 and H4 R45R1 depicted in the crystal structure of H3/H4 in complex with Asf1 (pdb code: 2hue) and the location of the Vps75 labelling site Y35Rx2 in the respective crystal structure (pdb code: 2zd7). (B) PELDOR data for the Vps75-H3/H4-Asf1 complex spin labelled on H3 at Q125R1 and cross-link spin labelled on Vps75 at Y35Rx2. (C) PELDOR data for the Vps75-H3/H4-Asf1 complex spin labelled on H4 at R45R1 and cross-link spin labelled on Vps75 at Y35Rx2.

The partial deuteration of the system along with the deuteration of the exchangeable protons and solvent in the sample was sufficient to measure the raw dipolar evolution function for ~9-15 µs (Figure 37B and C). In general one full oscillation is required in the raw dipolar evolution function in order to reliably fit the background correction function to the raw dipolar evolution function. As the time to one full oscillation is proportional to the cube of the distance between spin labels (Figure 38) data measured up to 9 and 15 µs is theoretically sufficient to measure distances up to 7.8 and 9.2 nm respectively. Although further distance measurements are required in order to define how Vps75 interacts with histones H3/H4 in complex with Asf1,

including direct measurements from Asf1 to Vps75, the partial deuteration of the system should be sufficient to cover most distances within the structural limits of the complex.

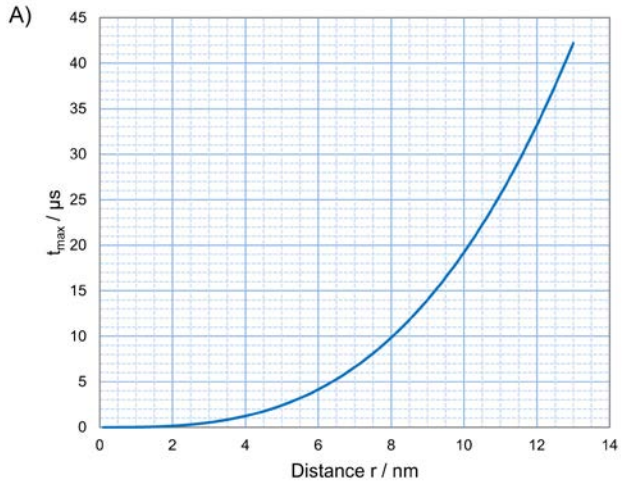

Figure 38 – The relationship between the timing window required to observe one full oscillation for a given distance measurement. (A) Plot of the relationship between the timing window required for one full oscillation (t_{max}) required to observe one full oscillation in the dipolar evolution function for a given distance (r). (B) The time to record one full oscillation t_{max} is proportional to the cube of the distance multiplied by constant parameters which can simplified to a single constant allowing the convenient calculation of t_{max} in micro seconds for a predicted distance in nanometres or vice versa. For the derivation of this formula see Jeschke, Polyhak *et al.* 2007.

5.2.11 Nap1 also binds histones H3/H4 in the presence of Asf1

As Vps75 was seen to bind H3/H4 in the presence of Asf1 analogous analytical gel filtration experiments were performed with Nap1. Again, when Nap1 was mixed with Asf1 and H3/H4 in a 2:1:1 ratio the elution peak super shifted to a higher molecular weight (1.24 ml) compared to that of the Nap1 dimer (1.26 ml) and all four proteins were observed in the SDS-PAGE analysis of the fractions spanning the peak elution volume. The super-shift of the Nap1-H3/H4-Asf1 species of 20 µl to 1.24 ml compared to Nap1 is in line with the super shift of 30 µl to 1.41 ml observed for Vps75-H3/H4-Asf1 suggesting that the stoichiometry of both complexes is the same. Thus a Nap1 dimer binds a H3/H4 dimer in the presence of Asf1.

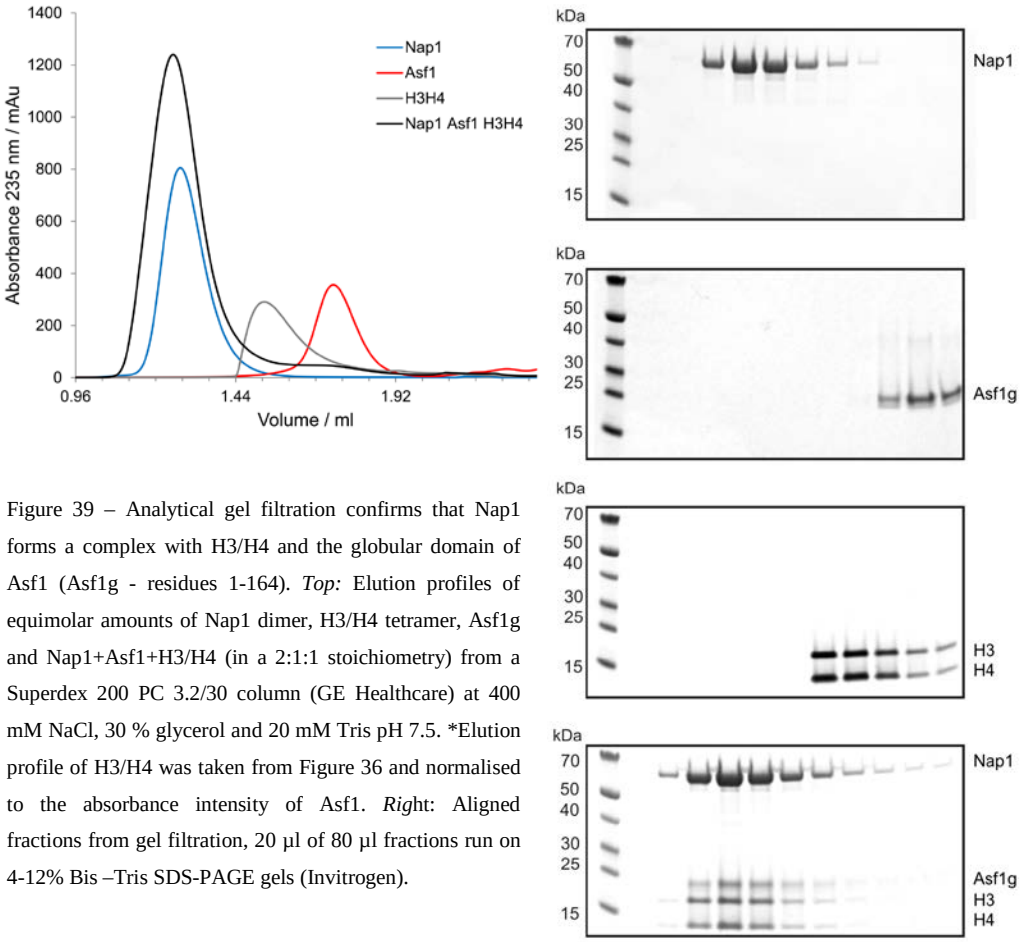

Figure 39 – Analytical gel filtration confirms that Nap1 forms a complex with H3/H4 and the globular domain of Asf1 (Asf1g - residues 1-164). *Top:* Elution profiles of equimolar amounts of Nap1 dimer, H3/H4 tetramer, Asf1g and Nap1+Asf1+H3/H4 (in a 2:1:1 stoichiometry) from a Superdex 200 PC 3.2/30 column (GE Healthcare) at 400 mM NaCl, 30 % glycerol and 20 mM Tris pH 7.5. *Elution profile of H3/H4 was taken from Figure 36 and normalised to the absorbance intensity of Asf1. *Rig*ht: Aligned fractions from gel filtration, 20 µl of 80 µl fractions run on 4-12% Bis –Tris SDS-PAGE gels (Invitrogen).

5.3 Discussion

Cross-linking analysis of Vps75 with histones shows that the histone chaperone is capable of forming multiple stoichiometric assemblies with histones. This may be a useful property of a histone chaperone as the amount of free histones in the cell varies during the cell cycle. The two major species encountered in the cross-linking titrations of histone H3/H4 with Vps75 are consistent with both a Vps75 dimer and a tetramer bound to a H3/H4 tetramer with the possibility of further oligomerisation of these species. When combined with the observation that Vps75 and Nap1 can bind to histone H3/H4 bound to the globular domain of Asf1, this data supports a model where a NAP-1 fold dimer binds a H3/H4 dimer in a manner which does not preclude H3/H4 tetramerisation in the absence of Asf1. Additionally, it appears that a Vps75 dimer is capable of binding a H2A/H2B dimer and through tetramerisation of Vps75 is able to form a complex of a Vps75 tetramer bound to two dimers of H2A/H2B.

Although evidence suggests that a Vps75 tetramer can bind a H3/H4 tetramer, the cavity of the Vps75 tetramer is too small to accommodate a H3/H4 tetramer. At most the cavity could accommodate a H3/H4 dimer. However, it is unlikely that a H3/H4 dimer could be recognised asymmetrically by four separate Vps75 chains and it is therefore unlikely that the intact Vps75 tetramer binds a H3/H4 dimer in its central cavity. Thus it would appear feasible that either the Vps75 tetramer binds a H3/H4 tetramer via the external surface or there is a reconfiguration of the Vps75 tetramer upon binding histones. The potential for a reconfiguration of the Vps75 tetramer upon H3/H4 binding has been highlighted in the pyrene excimer studies described here. Understanding of the nature of this reconfiguration is likely to be extrapolated from the structural analysis of the mode of interaction of Vps75 with H3/H4 when in complex with Asf1.

The recognition of histone fold dimers by NAP-1 fold histone chaperones may account for how both Vps75 and Nap1 can form high affinity complexes with both H3/H4 and H2A/H2B (Andrews, Downing et al. 2008; Park, Sudhoff et al. 2008). Furthermore, the Vps75 tetramer appears to have the ability to bind or promote the assembly of H3/H4 tetramers. It will be interesting to find out if the same holds true for Nap1. The ability of NAP-1 fold chaperones to assemble intermediates of the nucleosome such as the H3/H4 tetramer would place them down stream of Asf1 in *de novo* nucleosome assembly pathways, however they could also be involved in recycling chromatin bound histone tetramers - as such bypassing the need for Asf1 in parental histone

deposition. In both of these scenarios, NAP-1 fold chaperones could act to maintain the integrity of histone tetramers during dilution with new histones in S-phase - consistent with previous reports that new and old copies of H3 and H4 do not mix (Prior, Cantor et al. 1980; Radman-Livaja, Verzijlbergen et al. 2011). As both Nap1 and Vps75 are linked to transcription (Selth, Lorch et al. 2009; Xue, Kowalska et al. 2013), they may also have an important role in recycling chromatin bound H3/H4 tetramers in the wake of RNA polymerases transcribing the DNA template.

With NAP-1 fold chaperones having the ability to bind all four core histones the question as to whether they can bind a histone octamer has been suggested previously in the literature. Analytical ultracentrifugation studies where Nap1 bound to H2A/H2B was mixed with Nap1 bound to H3/H4 showed that the complexes do not combine (Ishimi, Kojima et al. 1987). However when H3/H4 was added to Nap1 bound to H2A/H2B a larger complex than either the Nap1 H2A/H2B or Nap1 H3/H4 complexes were observed which contained stoichiometric amounts of all core histones. When the reverse experiment was performed, i.e. H2A/H2B was added to Nap1 bound by H3/H4, the larger complex was observed but to a lower level with the concomitant appearance of the Nap1 H2A/H2B complex. This implies that Nap1 binds H2A/H2B more tightly and that Nap1 bound by H2A/H2B can combine with H3/H4 to form octamers. This function of Nap1 may be important in passage of chromatin bound nucleosomes behind a passing polymerase. Consistent with this idea Nap1 has been shown to be able to disengage H2A/H2B from DNA (Andrews, Chen et al. 2010), maybe in cooperation with nucleosome remodelling enzymes (Nakagawa, Bulger et al. 2001; Andrews, Chen et al. 2010).

Vps75 can bind one or two copies of Rtt109 (Kolonko, Albaugh et al. 2010; Su, Hu et al. 2011; Tang, Holbert et al. 2011) , the question as to which complex is the more physiologically relevant has implications for how many H3/H4 dimers the complex accommodates. Like the Vps75 tetramer, the cavity formed in these complexes could at most accommodate a dimer of H3/H4. If the physiologically relevant complex had two copies of Rtt109 one would expect it to bind two H3/H4 dimers. Due to the lack of space to accommodate a H3/H4 tetramer in this complex this would require two independent binding sites for H3/H4 dimers on a Vps75 dimer. As such a Vps75 dimer bound to two dimers of H3/H4 could oligomerise to form two tetramers of H3/H4 sandwiched between two Vps75 dimers (Figure 40A). A species consistent with this complex was

observed in the cross-linking analysis of Vps75 and histones which became more prominent when H3/H4 was trapped in its tetrameric conformation. In the case of the 2:1 Vps75:Rtt109 complex the fact that a dimer of Vps75 can bind asymmetrically to Rtt109 could potentially allow for asymmetry in H3/H4 binding. For example one globular domain of Vps75 could be bound by Rtt109 causing conformational changes which propagate in an allosteric manner to the other globular domain to support H3/H4 binding or *vice versa*. In a similar manner one could imagine that a dimer of H3/H4 could be asymmetrically recognised by a dimer of Vps75. In this instance a Vps75 dimer bound to a H3/H4 dimer could self-associate forming a tetramer plus a tetramer (Figure 40B).

From the initial distance measurements between from Vps75 Y35RX2 to H3 (Q125R1) and H4 (R45R1) it is not possible to accurately predict the mode of interaction between Vps75 and H3/H4. Although the most logical manner for Vps75 to assemble a H3/H4 tetramer, from a symmetry perspective, would be to accommodate the dyad of the H3/H4 tetramer within the acidic cavity of the Vps75 dimer, as has been suggested previously (Bowman, Ward et al. 2011). However, this orientation does not fit the initial measurements from Vps75 to positions on H3/H4 (which are close to the dyad) in complex with Asf1. This would also conflict with evidence presented here that the Vps75 tetramer seems to be able to recognise a H3/H4 tetramer. However, two models that could potentially satisfy the distance restraints are shown in Figure 40.

In the first model Vps75 is bound to H3/H4 via the globular domain of one Vps75 monomer which would allow the other monomer to be bound to either Rtt109 or another dimer of H3/H4 (Figure 40A). If both monomers of Vps75 were occupied by H3/H4 dimers, the orientation of the dimers of H3/H4 would not suitable for H3/H4 tetramerisation. Thus for H3/H4 tetramerisation in this model, the dimers of Vps75 bound to two dimers of H3/H4 would have to further oligomerise forming two tetramers of H3/H4 sandwiched between two Vps75 dimers. In the second model H3/H4 makes contacts with both monomers of the Vps75 dimer in an asymmetric manner (Figure 40B). In the absence of Asf1 binding the dimerisation of this complex would form a tetramer of H3/H4 bound to two dimers of Vps75. It is difficult to rule out either model based on the preliminary distance measurements.

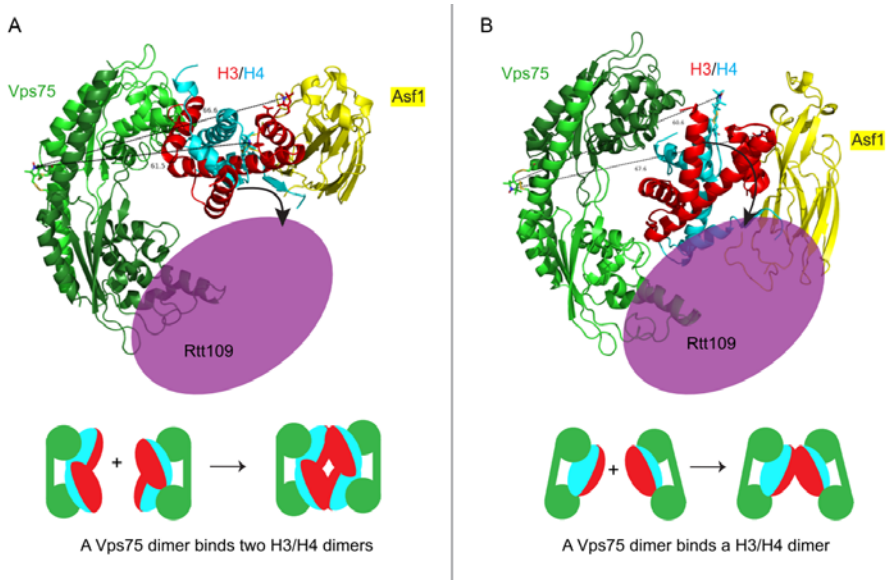

Figure 40 - Possible structural models of how H3/H4 interacts with Vps75 and mechanistic implications. (A) A H3/H4 dimer binds to a monomer of Vps75 allowing the other monomer of Vps75 to bind Rtt109. In the absence of Rtt109 Vps75 binding two independent H3/H4 dimers would be possible but not in a tetrameric conformation. (B) Both monomers of Vps75 bind to H3/H4 with each monomer making different contacts on the H3/H4 dimer thus recognising the histone fold in a non-specific manner.

Both Vps75 and Asf1 are known to stimulate the histone acetyl transferase activity of Rtt109 towards residues in histone H3, and both are capable of forming complexes with Rtt109. However, Asf1 is the chaperone which provides the specificity of Rtt109 acetylation towards H3 lysine 56. Results in section 3 show histone H3 K56 acetylation has a structural effect on the H3 tail, this may act as the trigger for the handover of histones from Asf1 to Vps75 allowing residues in the H3 tail, predominantly H3 K9 and K23 (Abshiru, Ippersiel et al. 2013), to be acetylated by Rtt109. If this is the case the Vps75-Asf1-H3/H4 (VAH) complex identified here may represent an important intermediate in this process. Probing the αN helix in this complex via PELDOR may provide a means as to whether the conformational change dependent on K56 acetylation would enhance or reduce the affinity of H3/H4 for Vps75. The sequential order of acetylation marks on newly synthesised H3 is currently unknown. However, quantitative proteomic profiling experiments, similar to those described in Abshiru, Ippersiel et al. 2013, using substrate H3/H4 pre-acetylated by either the Asf1-Rtt109 HAT complex or the Vps75-Rtt109 HAT complex may provide insights into this pathway. Outstanding questions as to whether Vps75 can bind histone H3/H4 in complex with full-length Asf1 and whether Rtt109 can bind this complex are subjects of future investigation.

6 Conclusions

This study has identified the ability of NAP-1 fold chaperones to tetramerise under physiological like conditions. The structural analysis of the tetrameric assemblies shows that the putative histone binding surface is sequestered in the cavity of ring like assemblies. The tetrameric assembly of Vps75 was shown to bind a H3/H4 tetramer. In the presence of excess histones Vps75 reverts to a dimer binding a H3/H4 tetramer. This histone buffering type capacity is a valuable attribute for a chaperone which has not been reported previously. As such NAP-1 fold histone chaperones may be important in the assembly of *de novo* H3/H4 tetramers, and/or the cooperative recognition and re-deposition of H3/H4 tetramers evicted from chromatin.

Dimers of Vps75 and Nap1 can also bind to a H3/H4 dimer in the presence of Asf1. The homogeneous nature of these complexes provides a means of mapping the interaction of histones with NAP-1 fold chaperones for the first time. Furthermore, there is precedence of Vps75 and Asf1 to be involved in the same pathway of acetylation histone H3 by Rtt109. Thus, the Vps75-Asf1-H3/H4 complex represents a potential intermediate in this pathway. This study has also demonstrated that a conformational change occurs in histone H3 upon acetylation at K56. As the acetylation of H3 K56 by Rtt109 is stimulated by Asf1, the resultant conformational change of histone H3 could trigger subsequent acetylation events in the H3 tail which are promoted by Vps75.

7 References

Abshiru, N., K. Ippersiel, et al. (2013). "Chaperone-mediated acetylation of histones by Rtt109 identified by quantitative proteomics." Journal of proteomics **81**: 80-90.

Alberts, B., A. Johnson, et al. (2002). Molecular Biology of the Cell. New York, Garland Science.

Albright, S., P. Nelson, et al. (1979). "Histone molar ratios among different electrophoretic forms of mono- and dinucleosomes." The Journal of biological chemistry **254**(4): 1065-1073.

Allard, S., R. T. Utley, et al. (1999). "NuA4, an essential transcription adaptor/histone H4 acetyltransferase complex containing Esa1p and the ATM-related cofactor Tra1p." EMBO J **18**(18): 5108-5119.

Allfrey, V., R. Faulkner, et al. (1964). "ACETYLATION AND METHYLATION OF HISTONES AND THEIR POSSIBLE ROLE IN THE REGULATION OF RNA SYNTHESIS." Proceedings of the National Academy of Sciences of the United States of America **51**: 786-794.

Andrews, A., X. Chen, et al. (2010). "The histone chaperone Nap1 promotes nucleosome assembly by eliminating nonnucleosomal histone DNA interactions." Molecular cell **37**(6): 834-842.

Andrews, A., G. Downing, et al. (2008). "A thermodynamic model for Nap1-histone interactions." The Journal of biological chemistry **283**(47): 32412-32418.

Arents, G., R. Burlingame, et al. (1991). "The nucleosomal core histone octamer at 3.1 A resolution: a tripartite protein assembly and a left-handed superhelix." Proceedings of the National Academy of Sciences of the United States of America **88**(22): 10148-10152.

Awad, S., D. Ryan, et al. (2010). "The Snf2 homolog Fun30 acts as a homodimeric ATP-dependent chromatin-remodeling enzyme." The Journal of biological chemistry **285**(13): 9477-9484.

Bains, G., S. Kim, et al. (2012). "The extent of pyrene excimer fluorescence emission is a reflector of distance and flexibility: analysis of the segment linking the LDL receptor-binding and tetramerization domains of apolipoprotein E3." Biochemistry **51**(31): 6207-6219.

Balasubramanian, R., M. G. Pray-Grant, et al. (2002). "Role of the Ada2 and Ada3 transcriptional coactivators in histone acetylation." J Biol Chem **277**(10): 7989-7995.

Baxevanis, A. D., G. Arents, et al. (1995). "A variety of DNA-binding and multimeric proteins contain the histone fold motif." Nucleic Acids Res **23**(14): 2685-2691.

Berndsen, C. and J. Denu (2008). "Catalysis and substrate selection by histone/protein lysine acetyltransferases." Current opinion in structural biology **18**(6): 682-689.

Berndsen, C., T. Tsubota, et al. (2008). "Molecular functions of the histone acetyltransferase chaperone complex Rtt109-Vps75." Nature structural & molecular biology **15**(9): 948-956.

Berndsen, C. E., T. Tsubota, et al. (2008). "Molecular functions of the histone acetyltransferase chaperone complex Rtt109-Vps75." Nature Structural and Molecular Biology **15**(9): 948-956.

Bian, C., C. Xu, et al. (2011). "Sgf29 binds histone H3K4me2/3 and is required for SAGA complex recruitment and histone H3 acetylation." EMBO J **30**(14): 2829-2842.

Bonangelino, C. J., E. M. Chavez, et al. (2002). "Genomic screen for vacuolar protein sorting genes in Saccharomyces cerevisiae." Mol Biol Cell **13**(7): 2486-2501.

Bowman, A., R. Ward, et al. (2010). "Probing the (H3-H4)2 histone tetramer structure using pulsed EPR spectroscopy combined with site-directed spin labelling." Nucleic acids research **38**(2): 695-707.

Bowman, A., R. Ward, et al. (2011). "The histone chaperones Nap1 and Vps75 bind histones H3 and H4 in a tetrameric conformation." Molecular cell **41**(4): 398-408.

Brownell, J. E., J. Zhou, et al. (1996). "Tetrahymena histone acetyltransferase A: a homolog to yeast Gcn5p linking histone acetylation to gene activation." Cell **84**(6): 843-851.

Bryan, P., E. Wright, et al. (1979). "Core nucleosomes by digestion of reconstructed histone-DNA complexes." Nucleic acids research **6**(4): 1449-1465.

Burgess, R., H. Zhou, et al. (2010). "A role for Gcn5 in replication-coupled nucleosome assembly." Molecular cell **37**(4): 469-480.

Burma, S., B. P. Chen, et al. (2001). "ATM phosphorylates histone H2AX in response to DNA double-strand breaks." J Biol Chem **276**(45): 42462-42467.

Chen, C.-C., J. Carson, et al. (2008). "Acetylated lysine 56 on histone H3 drives chromatin assembly after repair and signals for the completion of repair." Cell **134**(2): 231-243.

Chen, H. and L. Symington (2013). "Overcoming the chromatin barrier to end resection." Cell research **23**(3): 317-319.

Chen, X., D. Cui, et al. (2012). "The Fun30 nucleosome remodeller promotes resection of DNA double-strand break ends." Nature **489**(7417): 576-580.

Cho, U. S. and S. C. Harrison (2011). "Recognition of the centromere-specific histone Cse4 by the chaperone Scm3." Proc Natl Acad Sci U S A **108**(23): 9367-9371.

Costanzi, C. and J. R. Pehrson (1998). "Histone macroH2A1 is concentrated in the inactive X chromosome of female mammals." Nature **393**(6685): 599-601.

Costelloe, T., R. Louge, et al. (2012). "The yeast Fun30 and human SMARCAD1 chromatin remodellers promote DNA end resection." Nature **489**(7417): 581-584.

D'Anna, J. and I. Isenberg (1974). "A histone cross-complexing pattern." Biochemistry **13**(24): 4992-4997.

D'Arcy, S. and K. Luger (2011). "Understanding histone acetyltransferase Rtt109 structure and function: how many chaperones does it take?" Curr Opin Struct Biol.

Das, C., M. Lucia, et al. (2009). "CBP/p300-mediated acetylation of histone H3 on lysine 56." Nature **459**(7243): 113-117.

Donham, D., J. Scorgie, et al. (2011). "The activity of the histone chaperone yeast Asf1 in the assembly and disassembly of histone H3/H4-DNA complexes." Nucleic acids research **39**(13): 5449-5458.

Dover, J., J. Schneider, et al. (2002). "Methylation of histone H3 by COMPASS requires ubiquitination of histone H2B by Rad6." J Biol Chem **277**(32): 28368-28371.

Downs, J. (2008). "Histone H3 K56 acetylation, chromatin assembly, and the DNA damage checkpoint." DNA repair **7**(12): 2020-2024.

Driscoll, R., A. Hudson, et al. (2007). "Yeast Rtt109 promotes genome stability by acetylating histone H3 on lysine 56." Science (New York, N.Y.) **315**(5812): 649-652.

Driscoll, R., A. Hudson, et al. (2007). "Yeast Rtt109 promotes genome stability by acetylating histone H3 on lysine 56." Science **315**(5812): 649-652.

Dudas, A. and M. Chovanec (2004). "DNA double-strand break repair by homologous recombination." Mutat Res **566**(2): 131-167.

Durand-Dubief, M., J. Svensson, et al. (2011). "Topoisomerases, chromatin and transcription termination." Transcription **2**(2): 66-70.

Elsässer, S., H. Huang, et al. (2012). "DAXX envelops a histone H3.3-H4 dimer for H3.3-specific recognition." Nature **491**(7425): 560-565.

English, C., M. Adkins, et al. (2006). "Structural basis for the histone chaperone activity of Asf1." Cell **127**(3): 495-508.

Ferreira, H., J. Somers, et al. (2007). "Histone tails and the H3 alphaN helix regulate nucleosome mobility and stability." Molecular and cellular biology **27**(11): 4037-4048.

Fillingham, J., J. Recht, et al. (2008). "Chaperone control of the activity and specificity of the histone H3 acetyltransferase Rtt109." Molecular and cellular biology **28**(13): 4342-4353.

Garcia-Ramirez, M., C. Rocchini, et al. (1995). "Modulation of chromatin folding by histone acetylation." The Journal of biological chemistry **270**(30): 17923-17928.

Gill, J., A. Kumar, et al. (2010). "Structure, localization and histone binding properties of nuclear-associated nucleosome assembly protein from Plasmodium falciparum." Malar J **9**: 90.

Green, E., A. Antczak, et al. (2005). "Replication-independent histone deposition by the HIR complex and Asf1." Current biology : CB **15**(22): 2044-2049.

Gunjan, A., J. Paik, et al. (2005). "Regulation of histone synthesis and nucleosome assembly." Biochimie **87**(7): 625-635.

Hagelueken, G., R. Ward, et al. (2012). "MtsslWizard: In Silico Spin-Labeling and Generation of Distance Distributions in PyMOL." Applied magnetic resonance **42**(3): 377-391.

Han, J., H. Zhou, et al. (2007). "The Rtt109-Vps75 histone acetyltransferase complex acetylates non-nucleosomal histone H3." The Journal of biological chemistry **282**(19): 14158-14164.

Hebbes, T., A. Clayton, et al. (1994). "Core histone hyperacetylation co-maps with generalized DNase I sensitivity in the chicken beta-globin chromosomal domain." The EMBO journal **13**(8): 1823-1830.

Hebbes, T., A. Thorne, et al. (1988). "A direct link between core histone acetylation and transcriptionally active chromatin." The EMBO journal **7**(5): 1395-1402.

Hereford, L. M., M. A. Osley, et al. (1981). "Cell-cycle regulation of yeast histone mRNA." Cell **24**(2): 367-375.

Hondele, M., T. Stuwe, et al. (2013). "Structural basis of histone H2A-H2B recognition by the essential chaperone FACT." Nature **499**(7456): 111-114.

Hoppe, G., J. Tanny, et al. (2002). "Steps in assembly of silent chromatin in yeast: Sir3-independent binding of a Sir2/Sir4 complex to silencers and role for Sir2-dependent deacetylation." Molecular and cellular biology **22**(12): 4167-4180.

Hu, H., Y. Liu, et al. (2011). "Structure of a CENP-A-histone H4 heterodimer in complex with chaperone HJURP." Genes Dev **25**(9): 901-906.

Huang, S., H. Zhou, et al. (2005). "Rtt106p is a histone chaperone involved in heterochromatin-mediated silencing." Proceedings of the National Academy of Sciences of the United States of America **102**(38): 13410-13415.

Hyland, E., M. Cosgrove, et al. (2005). "Insights into the role of histone H3 and histone H4 core modifiable residues in Saccharomyces cerevisiae." Molecular and cellular biology **25**(22): 10060-10070.

Ishimi, Y. and A. Kikuchi (1991). "Identification and molecular cloning of yeast homolog of nucleosome assembly protein I which facilitates nucleosome assembly in vitro." The Journal of biological chemistry **266**(11): 7025-7029.

Ishimi, Y., M. Kojima, et al. (1987). "Binding mode of nucleosome-assembly protein (AP-I) and histones." European journal of biochemistry / FEBS **162**(1): 19-24.

Ishimi, Y., H. Yasuda, et al. (1983). "A protein which facilitates assembly of nucleosome-like structures in vitro in mammalian cells." Journal of biochemistry **94**(3): 735-744.

Jeschke, G., V. Chechik, et al. (2006). "DeerAnalysis2006—a comprehensive software package for analyzing pulsed ELDOR data." Applied Magnetic Resonance **30**(3-4): 473-498.

Joshi, A. and K. Struhl (2005). "Eaf3 chromodomain interaction with methylated H3-K36 links histone deacetylation to Pol II elongation." Molecular cell **20**(6): 971-978.

Kaufman, P., R. Kobayashi, et al. (1995). "The p150 and p60 subunits of chromatin assembly factor I: a molecular link between newly synthesized histones and DNA replication." Cell **81**(7): 1105-1114.

Kolonko, E., B. Albaugh, et al. (2010). "Catalytic activation of histone acetyltransferase Rtt109 by a histone chaperone." Proceedings of the National Academy of Sciences of the United States of America **107**(47): 20275-20280.

Kolonko, E. M., B. N. Albaugh, et al. (2010). "Catalytic activation of histone acetyltransferase Rtt109 by a histone chaperone." Proceedings of the National Academy of Sciences of the United States of America **107**(47): 20275-20280.

Kolonko, E. M., B. N. Albaugh, et al. (2010). "Catalytic activation of histone acetyltransferase Rtt109 by a histone chaperone." Proc Natl Acad Sci U S A **107**(47): 20275-20280.

Krogan, N. J., G. Cagney, et al. (2006). "Global landscape of protein complexes in the yeast Saccharomyces cerevisiae." Nature **440**(7084): 637-643.

Kulaeva, O., F.-K. Hsieh, et al. (2013). "Mechanism of transcription through a nucleosome by RNA polymerase II." Biochimica et biophysica acta **1829**(1): 76-83.

Kumar, A., M. Kashyap, et al. (2012). "Structural delineation of histone post-translation modifications in histone-nucleosome assembly protein complex." Journal of structural biology **180**(1): 1-9.

Laskey, R., B. Honda, et al. (1978). "Nucleosomes are assembled by an acidic protein which binds histones and transfers them to DNA." Nature **275**(5679): 416-420.

Lee, K. K., L. Florens, et al. (2005). "The deubiquitylation activity of Ubp8 is dependent upon Sgf11 and its association with the SAGA complex." Mol Cell Biol **25**(3): 1173-1182.

Li, Q., H. Zhou, et al. (2008). "Acetylation of histone H3 lysine 56 regulates replication-coupled nucleosome assembly." Cell **134**(2): 244-255.

Liu, C.-P., C. Xiong, et al. (2012). "Structure of the variant histone H3.3-H4 heterodimer in complex with its chaperone DAXX." Nature structural & molecular biology **19**(12): 1287-1292.

Liu, W. H., S. C. Roemer, et al. (2012). "CAF-1-induced oligomerization of histones H3/H4 and mutually exclusive interactions with Asf1 guide H3/H4 transitions among histone chaperones and DNA." Nucleic Acids Res **40**(22): 11229-11239.

Liu, Y., H. Huang, et al. (2010). "Structural analysis of Rtt106p reveals a DNA binding role required for heterochromatin silencing." The Journal of biological chemistry **285**(6): 4251-4262.

Luger, K., A. Mäder, et al. (1997). "Crystal structure of the nucleosome core particle at 2.8 A resolution." Nature **389**(6648): 251-260.

Luger, K., T. J. Rechsteiner, et al. (1999). "Expression and purification of recombinant histones and nucleosome reconstitution." Methods Mol Biol **119**: 1-16.

Lutter, L. (1979). "Precise location of DNase I cutting sites in the nucleosome core determined by high resolution gel electrophoresis." Nucleic acids research **6**(1): 41-56.

Malay, A., T. Umehara, et al. (2008). "Crystal structures of fission yeast histone chaperone Asf1 complexed with the Hip1 B-domain or the Cac2 C terminus." The Journal of biological chemistry **283**(20): 14022-14031.

Masumoto, H., D. Hawke, et al. (2005). "A role for cell-cycle-regulated histone H3 lysine 56 acetylation in the DNA damage response." Nature **436**(7048): 294-298.

Maupetit, J., P. Derreumaux, et al. (2009). "PEP-FOLD: an online resource for de novo peptide structure prediction." Nucleic Acids Res **37**(Web Server issue): W498-503.

McBryant, S., Y.-J. Park, et al. (2003). "Preferential binding of the histone (H3-H4)2 tetramer by NAP1 is mediated by the amino-terminal histone tails." The Journal of biological chemistry **278**(45): 44574-44583.

McBryant, S. J. and O. B. Peersen (2004). "Self-association of the yeast nucleosome assembly protein 1." Biochemistry **43**(32): 10592-10599.

McKittrick, E., P. Gafken, et al. (2004). "Histone H3.3 is enriched in covalent modifications associated with active chromatin." Proceedings of the National Academy of Sciences of the United States of America **101**(6): 1525-1530.

McQuibban, G., C. Commisso-Cappelli, et al. (1998). "Assembly, remodeling, and histone binding capabilities of yeast nucleosome assembly protein 1." The Journal of biological chemistry **273**(11): 6582-6590.

Meneghini, M., M. Wu, et al. (2003). "Conserved histone variant H2A.Z protects euchromatin from the ectopic spread of silent heterochromatin." Cell **112**(5): 725-736.

Mizuguchi, G., X. Shen, et al. (2004). "ATP-driven exchange of histone H2AZ variant catalyzed by SWR1 chromatin remodeling complex." Science (New York, N.Y.) **303**(5656): 343-348.

Moggs, J., P. Grandi, et al. (2000). "A CAF-1-PCNA-mediated chromatin assembly pathway triggered by sensing DNA damage." Molecular and cellular biology **20**(4): 1206-1218.

Moriniere, J., S. Rousseaux, et al. (2009). "Cooperative binding of two acetylation marks on a histone tail by a single bromodomain." Nature **461**(7264): 664-668.

Mosammaparast, N., B. Del Rosario, et al. (2005). "Modulation of histone deposition by the karyopherin kap114." Molecular and cellular biology **25**(5): 1764-1778.

Mosammaparast, N., C. Ewart, et al. (2002). "A role for nucleosome assembly protein 1 in the nuclear transport of histones H2A and H2B." The EMBO journal **21**(23): 6527-6538.

Murray, K. (1964). "THE OCCURRENCE OF EPSILON-N-METHYL LYSINE IN HISTONES." Biochemistry **3**: 10-15.

Murzina, N. V., X. Y. Pei, et al. (2008). "Structural basis for the recognition of histone H4 by the histone-chaperone RbAp46." Structure **16**(7): 1077-1085.

Muto, S., M. Senda, et al. (2007). "Relationship between the structure of SET/TAF-Ibeta/INHAT and its histone chaperone activity." Proceedings of the National Academy of Sciences of the United States of America **104**(11): 4285-4290.

Nakagawa, T., M. Bulger, et al. (2001). "Multistep chromatin assembly on supercoiled plasmid DNA by nucleosome assembly protein-1 and ATP-utilizing chromatin assembly and remodeling factor." The Journal of biological chemistry **276**(29): 27384-27391.

Neumann, H., S. Hancock, et al. (2009). "A method for genetically installing site-specific acetylation in recombinant histones defines the effects of H3 K56 acetylation." Molecular cell **36**(1): 153-163.

Newman, E., G. Kneale, et al. (2012). "Large multimeric assemblies of nucleosome assembly protein and histones revealed by small-angle X-ray scattering and electron microscopy." The Journal of biological chemistry **287**(32): 26657-26665.

Newman, E. R., G. G. Kneale, et al. (2012). "Large Multimeric Assemblies of Nucleosome Assembly Protein and Histones Revealed by Small-angle X-ray Scattering and Electron Microscopy." Journal of Biological Chemistry **287**(32): 26657-26665.

Noda, M., S. Uchiyama, et al. (2011). "Assembly states of the nucleosome assembly protein 1 (NAP-1) revealed by sedimentation velocity and non-denaturing MS." Biochem J **436**(1): 101-112.

Orphanides, G., G. LeRoy, et al. (1998). "FACT, a factor that facilitates transcript elongation through nucleosomes." Cell **92**(1): 105-116.

Owen-Hughes, T. and T. Gkikopoulos (2012). "Making sense of transcribing chromatin." Current opinion in cell biology **24**(3): 296-304.

Papamichos-Chronakis, M., S. Watanabe, et al. (2011). "Global regulation of H2A.Z localization by the INO80 chromatin-remodeling enzyme is essential for genome integrity." Cell **144**(2): 200-213.

Park, Y.-J. and K. Luger (2006). "The structure of nucleosome assembly protein 1." Proceedings of the National Academy of Sciences of the United States of America **103**(5): 1248-1253.

Park, Y.-J., K. Sudhoff, et al. (2008). "Histone chaperone specificity in Rtt109 activation." Nature structural & molecular biology **15**(9): 957-964.

Park, Y. J., S. J. McBryant, et al. (2008). "A beta-hairpin Comprising the Nuclear Localization Sequence Sustains the Self-associated States of Nucleosome Assembly Protein 1." Journal of Molecular Biology **375**(4): 1076-1085.

Park, Y. J., K. B. Sudhoff, et al. (2008). "Histone chaperone specificity in Rtt109 activation." Nature Structural & Molecular Biology **15**(9): 957-964.

Park, Y. J., K. B. Sudhoff, et al. (2008). "Histone chaperone specificity in Rtt109 activation." Nature Structural and Molecular Biology **15**(9): 957-964.

Pehrson, J. R. and V. A. Fried (1992). "MacroH2A, a core histone containing a large nonhistone region." Science **257**(5075): 1398-1400.

Pramila, T., W. Wu, et al. (2006). "The Forkhead transcription factor Hcm1 regulates chromosome segregation genes and fills the S-phase gap in the transcriptional circuitry of the cell cycle." Genes Dev **20**(16): 2266-2278.

Prior, C., C. Cantor, et al. (1980). "Incorporation of exogenous pyrene-labeled histone into Physarum chromatin: a system for studying changes in nucleosomes assembled in vivo." Cell **20**(3): 597-608.

Prisner, T., M. Rohrer, et al. (2001). "Pulsed EPR spectroscopy: biological applications." Annu Rev Phys Chem **52**: 279-313.

Radman-Livaja, M., K. F. Verzijlbergen, et al. (2011). "Patterns and mechanisms of ancestral histone protein inheritance in budding yeast." PLoS Biol **9**(6): e1001075.

Rangasamy, D., I. Greaves, et al. (2004). "RNA interference demonstrates a novel role for H2A.Z in chromosome segregation." Nature structural & molecular biology **11**(7): 650-655.

Ray-Gallet, D., J.-P. Quivy, et al. (2002). "HIRA is critical for a nucleosome assembly pathway independent of DNA synthesis." Molecular cell **9**(5): 1091-1100.

Ridgway, P. and G. Almouzni (2000). "CAF-1 and the inheritance of chromatin states: at the crossroads of DNA replication and repair." Journal of cell science.

Roccatano, D., G. Colombo, et al. (2002). "Mechanism by which 2,2,2-trifluoroethanol/water mixtures stabilize secondary-structure formation in peptides: a molecular dynamics study." Proceedings of the National Academy of Sciences of the United States of America **99**(19): 12179-12184.

Rufiange, A., P.-E. Jacques, et al. (2007). "Genome-wide replication-independent histone H3 exchange occurs predominantly at promoters and implicates H3 K56 acetylation and Asf1." Molecular cell **27**(3): 393-405.

Schmitges, F. W., A. B. Prusty, et al. (2011). "Histone methylation by PRC2 is inhibited by active chromatin marks." Mol Cell **42**(3): 330-341.

Scholes, D. T., M. Banerjee, et al. (2001). "Multiple regulators of Ty1 transposition in Saccharomyces cerevisiae have conserved roles in genome maintenance." Genetics **159**(4): 1449-1465.

Schulze, J. M., A. Y. Wang, et al. (2009). "YEATS domain proteins: a diverse family with many links to chromatin modification and transcription." Biochem Cell Biol **87**(1): 65-75.

Sekulic, N., E. Bassett, et al. (2010). "The structure of (CENP-A-H4)(2) reveals physical features that mark centromeres." Nature **467**(7313): 347-351.

Selth, L., Y. Lorch, et al. (2009). "An rtt109-independent role for vps75 in transcription-associated nucleosome dynamics." Molecular and cellular biology **29**(15): 4220-4234.

Selth, L. and J. Svejstrup (2007). "Vps75, a new yeast member of the NAP histone chaperone family." The Journal of biological chemistry **282**(17): 12358-12362.

Selth, L. and J. Q. Svejstrup (2007). "Vps75, a new yeast member of the NAP histone chaperone." Journal of Biological Chemistry **282**(17): 12358-12362.

Selth, L. A., Y. Lorch, et al. (2009). "An rtt109-independent role for vps75 in transcription-associated nucleosome dynamics." Mol Cell Biol **29**(15): 4220-4234.

Sharp, J., E. Fouts, et al. (2001). "Yeast histone deposition protein Asf1p requires Hir proteins and PCNA for heterochromatic silencing." Current biology : CB **11**(7): 463-473.

Shibahara, K. and B. Stillman (1999). "Replication-dependent marking of DNA by PCNA facilitates CAF-1-coupled inheritance of chromatin." Cell **96**(4): 575-585.

Spellman, P. T., G. Sherlock, et al. (1998). "Comprehensive Identification of Cell Cycle-regulated Genes of the Yeast Saccharomyces cerevisiae by Microarray Hybridization." Molecular Biology of the Cell **9**.

Sreerama, N. and R. W. Woody (2000). "Estimation of protein secondary structure from circular dichroism spectra: comparison of CONTIN, SELCON, and CDSSTR methods with an expanded reference set." Anal Biochem **287**(2): 252-260.

Stark, H. (2010). "GraFix: stabilization of fragile macromolecular complexes for single particle cryo-EM." Methods Enzymol **481**: 109-126.

Stavropoulos, P., V. Nagy, et al. (2008). "Molecular basis for the autoregulation of the protein acetyl transferase Rtt109." Proceedings of the National Academy of Sciences of the United States of America **105**(34): 12236-12241.

Stillman, B. (1986). "Chromatin assembly during SV40 DNA replication in vitro." Cell **45**(4): 555-565.

Stillman, B. and Y. Gluzman (1985). "Replication and supercoiling of simian virus 40 DNA in cell extracts from human cells." Molecular and cellular biology **5**(8): 2051-2060.

Strahl, B. and C. Allis (2000). "The language of covalent histone modifications." Nature **403**(6765): 41-45.

Su, D., Q. Hu, et al. (2012). "Structural basis for recognition of H3K56-acetylated histone H3-H4 by the chaperone Rtt106." Nature **483**(7387): 104-107.

Su, D., Q. Hu, et al. (2011). "Structure and histone binding properties of the Vps75-Rtt109 chaperone-lysine acetyltransferase complex." The Journal of biological chemistry **286**(18): 15625-15629.

Su, D., Q. Hu, et al. (2011). "Structure and histone binding properties of the Vps75-Rtt109 chaperone-lysine acetyltransferase complex." The Journal of biological chemistry **286**(18): 15625-15629.

Sullivan, K., M. Hechenberger, et al. (1994). "Human CENP-A contains a histone H3 related histone fold domain that is required for targeting to the centromere." The Journal of cell biology.

Sun, Z. W. and C. D. Allis (2002). "Ubiquitination of histone H2B regulates H3 methylation and gene silencing in yeast." Nature **418**(6893): 104-108.

Tachiwana, H., W. Kagawa, et al. (2011). "Crystal structure of the human centromeric nucleosome containing CENP-A." Nature **476**(7359): 232-235.

Tagami, H., D. Ray-Gallet, et al. (2004). "Histone H3.1 and H3.3 complexes mediate nucleosome assembly pathways dependent or independent of DNA synthesis." Cell **116**(1): 51-61.

Tan, M., H. Luo, et al. (2011). "Identification of 67 histone marks and histone lysine crotonylation as a new type of histone modification." Cell **146**(6): 1016-1028.

Tang, Y., M. Holbert, et al. (2011). "Structure of the Rtt109-AcCoA/Vps75 complex and implications for chaperone-mediated histone acetylation." Structure (London, England : 1993) **19**(2): 221-231.

Tang, Y., M. A. Holbert, et al. (2011). "Structure of the Rtt109-AcCoA/Vps75 complex and implications for chaperone-mediated histone acetylation." Structure **19**(2): 221-231.

Tang, Y., K. Meeth, et al. (2008). "Structure of Vps75 and implications for histone chaperone function." Proceedings of the National Academy of Sciences of the United States of America **105**(34): 12206-12211.

Tang, Y., M. Poustovoitov, et al. (2006). "Structure of a human ASF1a-HIRA complex and insights into specificity of histone chaperone complex assembly." Nature structural & molecular biology **13**(10): 921-929.

Tjeertes, J., K. Miller, et al. (2009). "Screen for DNA-damage-responsive histone modifications identifies H3K9Ac and H3K56Ac in human cells." The EMBO journal **28**(13): 1878-1889.

Toth, K. F., J. Mazurkiewicz, et al. (2005). "Association states of nucleosome assembly protein 1 and its complexes with histones." Journal of Biological Chemistry **280**(16): 15690-15699.

Tsubota, T., C. Berndsen, et al. (2007). "Histone H3-K56 acetylation is catalyzed by histone chaperone-dependent complexes." Molecular cell **25**(5): 703-712.

Tsubota, T., C. E. Berndsen, et al. (2007). "Histone H3-K56 Acetylation Is Catalyzed by Histone Chaperone-Dependent Complexes." Molecular Cell **25**(5): 703-712.

VanDemark, A., M. Blanksma, et al. (2006). "The structure of the yFACT Pob3-M domain, its interaction with the DNA replication factor RPA, and a potential role in nucleosome deposition." Molecular cell **22**(3): 363-374.

Värv, S., K. Kristjuhan, et al. (2010). "Acetylation of H3 K56 is required for RNA polymerase II transcript elongation through heterochromatin in yeast." Molecular and cellular biology **30**(6): 1467-1477.

Wang, X., S. Moore, et al. (2000). "Acetylation increases the alpha-helical content of the histone tails of the nucleosome." The Journal of biological chemistry **275**(45): 35013-35020.

Ward, R., A. Bowman, et al. (2009). "Long distance PELDOR measurements on the histone core particle." Journal of the ...

Watanabe, S., M. Radman-Livaja, et al. (2013). "A histone acetylation switch regulates H2A.Z deposition by the SWR-C remodeling enzyme." Science (New York, N.Y.) **340**(6129): 195-199.

Whitmore, L. and B. A. Wallace (2004). "DICHROWEB, an online server for protein secondary structure analyses from circular dichroism spectroscopic data." Nucleic Acids Res **32**(Web Server issue): W668-673.

Winkler, D., H. Zhou, et al. (2012). "Yeast CAF-1 assembles histone (H3-H4)2 tetramers prior to DNA deposition." Nucleic acids research **40**(20): 10139-10149.

Wood, A., N. J. Krogan, et al. (2003). "Bre1, an E3 ubiquitin ligase required for recruitment and substrate selection of Rad6 at a promoter." Mol Cell **11**(1): 267-274.

Xie, X., T. Kokubo, et al. (1996). "Structural similarity between TAFs and the heterotetrameric core of the histone octamer." Nature **380**(6572): 316-322.

Xing, Z., Y. Zhe, et al. (2003). "Structural Basis for the Product Specificity of Histone Lysine Methyltransferases." Molecular cell **12**.

Xu, F., K. Zhang, et al. (2005). "Acetylation in histone H3 globular domain regulates gene expression in yeast." Cell **121**(3): 375-385.

Xue, Y.-M., A. Kowalska, et al. (2013). "Histone chaperones Nap1 and Vps75 regulate histone acetylation during transcription elongation." Molecular and cellular biology **33**(8): 1645-1656.

Zasadzinska, E., M. C. Barnhart-Dailey, et al. (2013). "Dimerization of the CENP-A assembly factor HJURP is required for centromeric nucleosome deposition." EMBO J **32**(15): 2113-2124.

Zhang, W., M. Tyl, et al. (2013). "Structural plasticity of histones H3-H4 facilitates their allosteric exchange between RbAp48 and ASF1." Nature structural & molecular biology **20**(1): 29-35.

Zhou, Z., H. Feng, et al. (2008). "NMR structure of chaperone Chz1 complexed with histones H2A.Z-H2B." Nat Struct Mol Biol **15**(8): 868-869.

Zlatanova, J., C. Seebart, et al. (2007). "Nap1: taking a closer look at a juggler protein of extraordinary skills." FASEB journal : official publication of the Federation of American Societies for Experimental Biology **21**(7): 1294-1310.